

Phototransduction in Vertebrate Rods and Cones: Molecular Mechanisms of Amplification, Recovery and Light Adaptation

E.N. PUGH Jr

*Department of Ophthalmology and
Institute of Neurological Sciences,
University of Pennsylvania,
Philadelphia*

T.D. LAMB

*Department of Physiology,
University of Cambridge*

Contents

1.	Introduction	186
1.1.	Phototransduction is a prototypical example of a G-protein signaling cascade	186
1.2.	Goals and organization of the chapter	188
2.	Structure and function of vertebrate photoreceptors	189
2.1.	Functional compartments: The inner and outer segment	189
2.2.	Photon capture and single-photon detection	189
2.3.	The circulating electrical current	191
2.4.	The photoresponse and its underlying molecular mechanism	191
2.5.	Outer segment free calcium concentration, $[Ca^{2+}]$	195
3.	Activation of phototransduction: The protein constituents and cGMP	196
3.1.	Rhodopsin: The G-protein coupled-receptor of rods	196
3.2.	Transducin: The heterotrimeric G-protein of rod and cone phototransduction	198
3.3.	The cGMP phosphodiesterase: The effector protein of vertebrate phototransduction . .	199
3.4.	cGMP: The cytoplasmic messenger of phototransduction	199
3.5.	The cGMP-gated channels of the plasma membrane	199
4.	Quantitative analysis of activation: Proteins at the disc membrane	200
4.1.	R^* production	201
4.2.	G^* production	201
4.3.	E^* production	204
5.	Quantitative analysis of activation: cGMP and the electrical response	206
5.1.	Buffering of cGMP in the cytoplasm	206
5.2.	Diffusion of cGMP in the cytoplasm	208
5.3.	Differential equation for hydrolysis of cGMP by PDE	208
5.4.	Combined synthesis and hydrolysis of cGMP	209
5.5.	Solution for the light-induced change in cGMP concentration	210
5.6.	Solution for the electrical response to a flash of light	211
5.7.	Significance of the equations: Amplification and response kinetics	213
5.8.	Comparison between experiment and theory	215
5.9.	Rate of activation of G-protein and PDE	218
5.10.	Validity of the solutions, and limitations	219
6.	Termination and modulation: The participating proteins and calcium	220
6.1.	R^* shut-off: Rhodopsin kinase (RK), arrestin (Arr), and recoverin (Rec)	221
6.2.	G^*-E^* shut-off: RGS9, G β 5 and phosducin	223
6.3.	Regulation of cGMP synthesis: Guanylyl cyclase (GC) and its activating proteins (GCAPs)	224
6.4.	Ca^{2+} efflux: The Na^+/Ca^{2+} , K^+ exchanger (NCKX)	226
6.5.	Regulation of the cyclic GMP gated channel by CM	227
7.	Recovery phase of the response: Predicted form of flash families	227
7.1.	Equations for the inactivation of R^* and of G^*-E^*	227

7.2. Equations for cGMP concentration	230
7.3. Equations for calcium fluxes and concentration	230
7.4. Equations for calcium-dependent activation of guanylyl cyclase	231
7.5. Solution for the flash response in the presence of inactivation reactions	231
7.6. Validity of the solutions, and limitations	233
8. Light adaptation: A composite of activation, termination and modulation	234
8.1. General characteristics of light adaptation: Response desensitization and acceleration, and calcium dependence	235
8.2. Role of calcium	237
8.3. Analysis of individual mechanisms underlying light adaptation	237
8.4. Summary	244
9. Single-photon responses: Implications of observed variability	244
9.1. Reproducibility: Ensemble behavior	245
9.2. Variability of the individual singletons	247
9.3. Implications of the observed variability	247
References	249

1. Introduction

1.1. Phototransduction is a prototypical example of a G-protein signaling cascade

Phototransduction is the process by which light, captured by a visual pigment molecule in a photoreceptor cell, generates an electrical response. In all vertebrate and invertebrate photoreceptor cells that have been investigated (including, of course, retinal rods and cones), phototransduction is effected by a 'G-protein cascade' – a sequence of reactions initiated by a G-protein-coupled receptor (GPCR) protein.

A generic G-protein cascade is illustrated in Fig. 1. In the first step of the cascade the binding of a specific ligand, L, induces the receptor, R, to undergo a conformational change to a state, R^* , in which it is enzymatically active. In the second step, R^* catalyzes the exchange of GTP for GDP on the α -subunit ($G\alpha$) of a specific heterotrimeric 'G-protein' – so-named because of its guanine nucleotide exchange function. In the third step the activated subunit of the G-protein, G^* ($\equiv G\alpha-GTP$) conveys the signal onward, by binding to a specific 'effector protein', E, which is thereby converted to its active form, E^* . A few examples of the vast variety of G-protein cascades are identified in Fig. 1.

The cascade of phototransduction may appear to be the 'odd man out', in the sense that the stimulus to activation is a photon of light rather than a chemical substance. Nevertheless, it does conform to the general pattern of ligand activation, because in the dark state the ligand (11-*cis* retinal) acts as a powerful antagonist, preventing activation. Absorption of a photon of light isomerizes the ligand to all-*trans* retinal, which acts instead as a powerful agonist to activation.

Receptor protein. Each GPCR is an integral membrane protein, comprising seven *trans*-membrane helices linked by six extra-membrane segments. GPCRs are members of a super-family of proteins which includes at least five main families, and GPCR genes are thought to constitute 3–5% of the human genome (cf. [12,13]). Numerically, the olfactory receptor proteins appear to comprise the largest group of GPCRs, with more than 1000 members [14,15]. To date the genes of several thousand GPCRs from many species have been sequenced, and characterized with respect to their ligand- and G-protein specificity, though many remain 'orphans'.

G-protein. In the second stage of the phototransduction cascade (Fig. 1), the signal (that a photon of light has been captured by the GPCR) is not simply transmitted, but is greatly amplified, by the catalytic activation of a heterotrimeric G-protein. Heterotrimeric G-proteins comprise one division of the super-family of G-proteins, all of which switch between two signaling states. The inactive state is that with a molecule of GDP bound; transition to the active state occurs upon

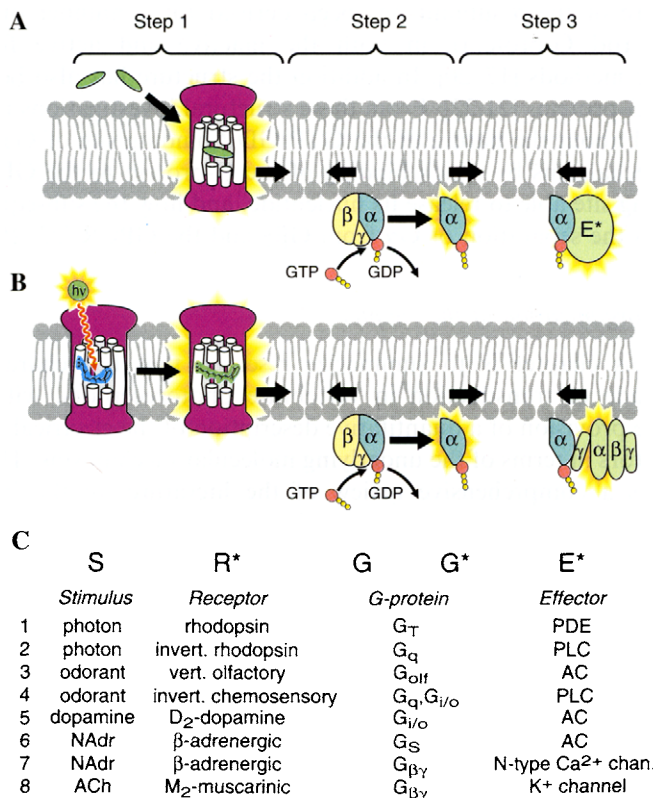


Fig. 1. Generic G-protein signal transduction cascade. (A) The cascade comprises three proteins, a G-protein-coupled receptor, R, a G-protein, G, and an effector protein, E, which are activated in three steps. In the first step, the receptor R is activated to R^* , and in most cases this is brought about by the binding of a ligand. In the second step, R^* activates a specific G-protein by catalyzing the release of GDP from the inactive form (G-GDP), and thereby permitting the binding of GTP, to create the active form G* (=G α -GTP). A single R^* can activate many molecules of G-protein, because it is released unaltered after the interaction. In the third step, the usual mechanism is that the G* binds to the effector protein E, causing it to switch states to an active form E*. (B) The G-protein transduction cascade of vertebrate photoreceptors follows the general pattern shown in A, except that activation of R to R^* is caused by the photoisomerization of a ligand, 11-cis retinal, that is already attached covalently to the receptor protein. (C) Identification of the components in a few examples of the many families of heterotrimeric G-protein signalling cascades, with sample references as follows. (1) Pugh and Lamb (this chapter); (2) [1]; (3) [2–4]; (4) [5]; (5) [6]; (6) [7,8]; (7) and (8) the G $\beta\gamma$ subunit serves to carry the signal modulating the conductance of subclasses of K⁺ channels and Ca²⁺ channels [9–11].

exchange of this GDP for a GTP; transition back to the inactive state results from hydrolysis of the terminal phosphate of the GTP, converting it back to GDP. Because of the nature of the state-switch, the super-family is also known as the GTPase super-family [16].

The structure of the α -subunit has been derived for a number of G-proteins (including the rod G-protein), in both the inactive and active forms, using crystallographic methods [17–20]. In addition the structure has also been reported for some holo-G-proteins [21,22]. From these structural investigations much insight has been gained about the nature of the GTP/GDP binding site of $G\alpha$, and about the physical mechanisms by which binding of the G-protein to the GPCR renders the GDP-binding site able to release its nucleotide, and how the subsequent binding of GTP triggers the separation of $G\alpha$ from $G\beta\gamma$ and the GPCR [23–25].

1.2. Goals and organization of the chapter

The goal of this chapter is to summarize research that has characterized the G-protein cascade of transduction in vertebrate photoreceptors, with particular emphasis on the provision of a quantitative description of the electrical responses of rod photoreceptors in terms of the underlying molecular mechanisms. The chapter is not intended as a comprehensive review of the literature on the biochemistry, molecular biology, or even the physiology of phototransduction, nor is it intended as a modern history of the field. Instead it is directed towards a synthesis of those results that appear most relevant to obtaining a quantitative understanding of the molecular events underlying the amplification, response kinetics, and adaptational behavior of rod and cone photoreceptor cells.

The quantitative basis of the extremely high amplification of the molecular reactions of phototransduction is now understood in detail [26,27], and will be developed here in abbreviated form by a journey through the individual reactions. This account of *amplification* automatically provides a description of the *kinetics* of activation of the light response. To account for the kinetics of recovery, it is necessary to examine the molecular reaction steps underlying inactivation of each of the activated products. Thereafter, to explain photoreceptor light adaptation, account must be taken of the modulatory mechanisms in the outer segment, where a change in cytoplasmic calcium concentration, $[Ca^{2+}]_i$, plays a central role.

The molecular reactions of phototransduction can be separated conceptually into three divisions: activation, termination, and modulation. By ‘activation’ we mean those steps that lead to the onset phase of the light response; by ‘termination’ we mean those steps that tend to shut-off each of the activated molecular species; and by ‘modulation’ we mean the overall regulation of the entire signaling system. However, the latter two aspects of photoresponses are so closely inter-linked (especially in time) that in practice it is most convenient to combine them, and to consider just two major divisions: (i) *activation*, and (ii) *termination and modulation*.

Accordingly, the layout of the chapter is as follows. Section 2 presents the basic structure and function of rods and cones, as a cellular-level backdrop for all that follows. Activation of the light response is dealt with in the subsequent two sections. Thus, Section 3 introduces the species mediating activation (rhodopsin, the G-protein, the phosphodiesterase, cGMP, and the cGMP-gated channel), with a description of their most important characteristics and a summary of their interactions. Sections 4 and 5 then derive a quantitative model of activation, and it is

here that the concept of amplification is given its precise meaning, and the kinetics of the rising-phase of the response are derived. Section 4 analyzes the reactions that occur at the disc membrane. Section 5 then analyzes the reactions involving cGMP and the cGMP-activated channels, and completes the derivation of the activation phase of the response. Here the predictions are compared with responses of individual rods and cones, and with the massed responses of rods and cones recorded as the electroretinogram.

Section 6 describes the proteins mediating response termination and modulation, as well as those mediating Ca^{2+} fluxes, and calcium-dependent modulation of the cascade components. The combined effects of the activation, termination and modulation reactions are then analyzed in three important cases: Section 7 presents the kinetic form of flash response families of dark-adapted rods; Section 8 provides an account of photoreceptor light adaptation; finally, Section 9 analyzes the features of the single-photon response (especially its variability). Where it seems helpful, we have listed relevant review articles at the ends of sections or sub-sections.

2. Structure and function of vertebrate photoreceptors

2.1. Functional compartments: The inner and outer segment

Vertebrate rods and cones are elongated and polarized cells that have closely similar structures. As illustrated in Fig. 2, the photoreceptor is divided into an outer segment region that contains the machinery of phototransduction, and an inner segment region that contains the mitochondria, nucleus, and endoplasmic reticulum, and that connects to the synaptic terminal. In addition to its function in providing energy and performing protein synthesis, the inner segment also acts as a miniature light guide, trapping light that propagates parallel to the cell's long axis, and guiding it to the outer segment where photon capture and transduction take place [28,29]. This funneling is much more pronounced in cones than in rods, with the consequence (discovered by Stiles and Crawford in 1933) that cones exhibit high directional sensitivity; thus, cones respond preferentially to light incident through the center of the pupil, in comparison with light incident near the edge of the dilated pupil [30,31].

2.2. Photon capture and single-photon detection

The outer segment comprises a stack of 'disc' membranes, spaced uniformly at intervals of about 28 nm. The visual pigment molecule is by far the most abundant protein constituent of the outer segment, with a concentration C of $\sim 3 \text{ mM}$ (referenced to the envelope volume of the outer segment), corresponding to a surface density in the disc membranes of about 25,000 pigment molecules μm^{-2} . The long stack of discs serves to increase the probability that a photon propagating axially down the outer segment will be captured. Thus, the probability p that a 500 nm photon propagating down a toad rod outer segment of length $L = 60 \mu\text{m}$ (2100 discs) will be captured by one of the rhodopsin molecules can be estimated from

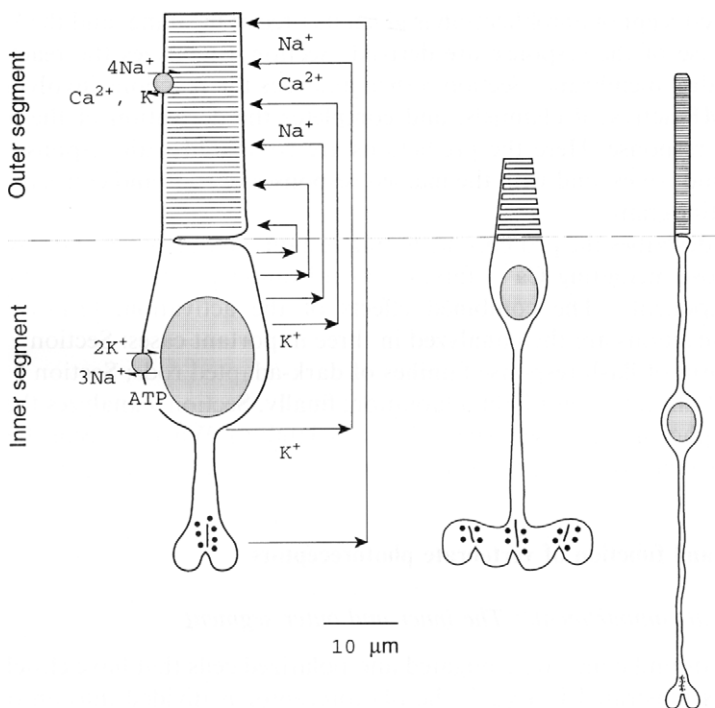


Fig. 2. Structure of rods and cones, and nature of the circulating current. A salamander rod, a salamander red-sensitive cone, and a mammalian rod are shown approximately to scale. The outer segment of each cell, which contains the lamellar membranes in which the visual pigment molecules are embedded, and where phototransduction occurs, is situated above the dotted line, while the inner segment, which contains the mitochondria, nucleus and synaptic region, is below the dotted line. The circulating current is illustrated for the salamander rod only (but applies to each cell).

Beer's Law to be $p = 1 - 10^{-\alpha L} \approx 89\%$. Here α is the axial pigment density, which has been measured as $0.016 \mu\text{m}^{-1}$ [32], and which can also be obtained as $\alpha = \epsilon_{\max} C$, where $\epsilon_{\max} \approx 60,000 \text{ cm}^2 \text{ mmole}^{-1}$ is the decadic molar absorbance coefficient of rhodopsin in the disc membrane for axially propagating light [33]. Were the outer segment only $1 \mu\text{m}$ in length (36 discs), the photon capture probability would be $p \approx 4\%$, drastically lower than the actual probability in a real photoreceptor.

Physiological recordings have established the remarkable finding that photoisomerization of any one of the 3×10^9 rhodopsin molecules assembled into the toad rod disc stack will generate a reliable electrical signal [34–36]. Consistent with this physiological finding, behavioral experiments have demonstrated that a toad can detect and capture prey with 100% accuracy, under illumination conditions that generate no more than 1 photoisomerization per rod every 10 s [37]. Single photon responses have also been recorded from primate rods [38], and from mouse rods [39,40]. Thus, a universal (and virtually defining) characteristic of vertebrate rods is their ability to provide reliable single-photon detection. Characterization of the

molecular mechanisms underlying this ability has long posed a central challenge to research in phototransduction.

2.3. The circulating electrical current

The protein composition of the surface membrane of photoreceptors differs greatly between the inner and outer segments. With regard to ion permeation, the outer segment membrane contains only two contributing classes of protein: the cGMP-gated channel (or cyclic-nucleotide gated channel, CNCC), and the electrogenic $\text{Na}^+/\text{Ca}^{2+}$, K^+ exchanger (NCKX) [41–46]. The membrane of the inner segment, on the other hand, contains K^+ channels of two main varieties (the so-called I_{Kx} and I_h channels) as well as channels permeable to other cations, including Ca^{2+} [46]. In addition, the inner segment membrane contains the Na^+/K^+ pump (or Na^+/K^+ -ATPase) that maintains the ionic concentration gradients between the inside and outside of the cell.

Under resting dark conditions the cytoplasmic concentration of free cGMP is several μM (see Section 3), so that a small proportion of the cGMP-gated channels are held open. Since these channels are relatively non-specific in their permeability for different monovalent cations, the net current flowing through them is inward (at the normal resting potential of vertebrate rods and cones, ca. -35 to -45 mV). About 85–90% of this inward current is carried by Na^+ , simply because Na^+ is the predominant external cation. And since the channels are highly permeable to Ca^{2+} ions, most of the remaining 10–15% of the current is carried by Ca^{2+} , with an additional contribution from Mg^{2+} that normally is quite small [47].

At rest, a balancing current flows outwards across the inner segment membrane, carried primarily by the I_{Kx} channels. Together, the influx of current into the outer segment and the balancing efflux of current from the inner segment create a loop (Fig. 2) known as the 'circulating current' – or, in darkness, as the 'dark current'. In different vertebrate rods, whether of the large amphibian variety or of the smaller mammalian type, the magnitude of the dark current ranges from 20 to 70 pA per rod. Table 1 summarizes the magnitude of the dark current, and gives other electrical properties, for rods and cones of a number of species that have been investigated extensively.

2.4. The photoresponse and its underlying molecular mechanism

The primary electrical event in vertebrate phototransduction is a transient suppression of the circulating current, that results from closure of cGMP-gated channels in the outer segment. Characteristic families of electrical responses are illustrated in Fig. 3, for both a salamander rod and a mammalian rod, exposed to brief flashes of progressively greater intensity. The ordinate of Fig. 3 is plotted in terms of the circulating current, $J(t)$, and the photocurrent response $r(t)$ is the change in current induced by the flash: for flashes presented in darkness the photocurrent response is simply $r(t) = J_{\text{dark}} - J(t)$.

The photocurrent families exhibit a number of well-known properties. For example: each response reflects a graded suppression of the circulating current; the peak amplitude increases monotonically as a function of flash intensity, until saturation

Table 1
Typical outer segment parameters, and dark resting electrical properties, of vertebrate rods and cones^a

Quantity	Symbol	Unit	Rods			Cones			Primate
			Salamander	Toad	Primate	Mouse	Salamander	Turtle	
<i>Outer segment parameters</i>									
Wavelength of maximum absorption	λ_{\max}	nm	500	500	500	500	610	650	565
Length	L	μm	22	60	25	20	8	15	13
Diameter (base, tip)	d	μm	11	6	2	~2	4, 2.5	2.5, ~1	3, ~1
Envelope volume	V_{tot}	μm ³	2000	1800	40	30	70	30	30
Cytoplasmic volume	V_{cyto}	μm ³	1000	900	20	15	35	30	15
Temperature	T	°C	22	22	37	37	22	22	37
cGMP-activated current (in dark)	J_{cg}^D	pA	-70	-40	-50	-20	-50		-40
Na ⁺ /Ca ²⁺ ,K ⁺ exchange current (in dark)	J_{ex}^D	pA	-4	-3	-2	-1	2		
<i>Typical whole-cell electrical properties</i>									
Resting potential (in dark)	V_m	mV	-40		-37		-40	-40	-45
Time-to-peak (dim flashes)	t_{peak}	ms	700	1500	200	240	170	100	50
Flash sensitivity (at t_{peak} , in darkness)	S_f^D	pA/Φ	0.2	1	0.7	0.4	0.03	0.025	0.005
Capacitance	C	pF	20	20		1	70	40	
Time constant (dark)	τ_m	ms	20	20	1	1	50	5	3
References			[48-50]	[34,51]	[38,52,53]	[39,40,54]	[50,55-57]	[58-60]	From [61] as cited in [62]; [63,64]

^a Notes: 1. Values given are representative of measurements in the literature.

2. Where whole-cell recording data are not available, we have used estimates based on suction-electrode recordings, and assumed a suction electrode collection efficiency of 2/3.

3. Primate cone anatomical properties are systematically dependent on distance from the fovea; the parameters given are applicable for the shorter but wider peripheral cones. The cited references illustrate and discuss this variation in cone anatomy.

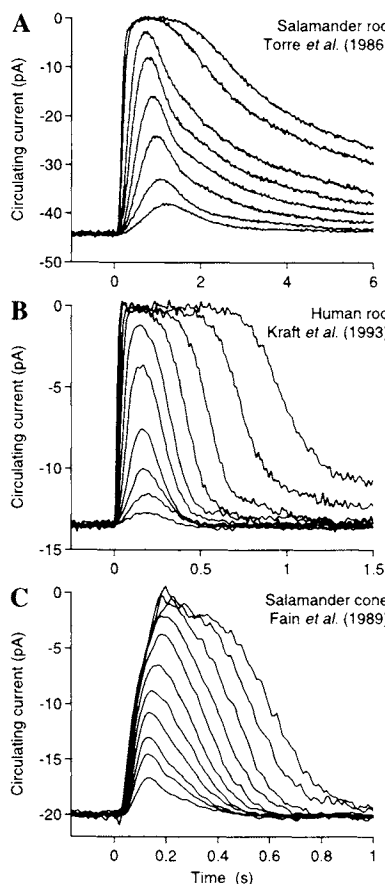


Fig. 3. Families of flash responses for three types of photoreceptor, recorded using the suction pipette method. In each experiment, flashes of progressively greater intensity were delivered at time zero. (A) Salamander rod, exposed to flashes estimated to deliver from 10 to 2000 photoisomerizations; ca. 22°C; data from Fig. 2A of Ref. [65]. (B) Human rod, for flashes delivering from 12 to 5200 photoisomerizations; 37°C; data from Fig. 1 of [53], kindly supplied by Dr. J.L. Schnapf. (C) Salamander red-sensitive cone; flashes delivering 1400 to 6×10^5 photoisomerizations; ca. 22°C; data from Fig. 6A of Ref. [56].

is reached, when the circulating current declines to zero; the dim-flash responses reach peak in roughly 1 s (at room temperature), or roughly 200 ms (at mammalian body temperature), while the bright-flash responses reach peak earlier.

The molecular mechanisms underlying activation of the electrical response (along with some of the termination reactions) are illustrated in Fig. 4A. Activation of the G-protein cascade causes stimulation of the cGMP phosphodiesterase and hence increased hydrolysis of cGMP, so that the cytoplasmic concentration of cGMP is reduced in the vicinity of the absorbed photon. As a result, the cGMP-gated channels in this region are no longer held open, and a localized reduction occurs in the influx of cations (primarily Na^+ and Ca^{2+}) into the outer segment.

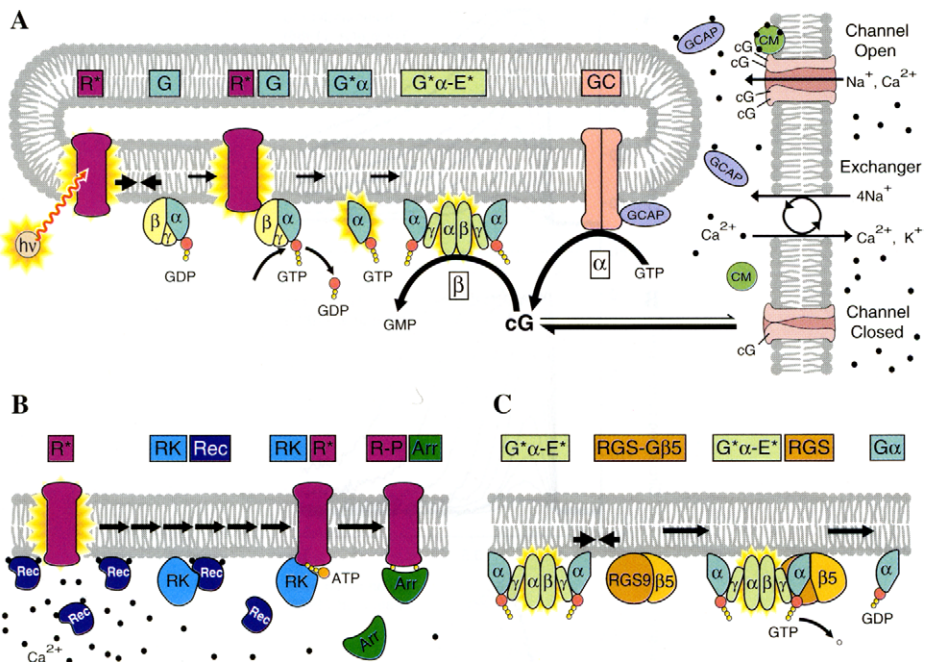


Fig. 4. Schematic of the phototransduction cascade in vertebrate photoreceptors. A. Activation steps of the cascade. Following absorption of a photon ($h\nu$), the activated rhodopsin (R^*) repeatedly contacts molecules of the G-protein, catalyzing the exchange of GDP for GTP, producing the active form G^* ($=G\alpha$ -GTP). Two G^* subunits bind to the two inhibitory γ subunits of the phosphodiesterase (E), thereby activating the corresponding α and β catalytic subunits, forming E^* which then catalyzes the hydrolysis of cGMP (cG). The consequent reduction in cytoplasmic concentration of cGMP leads to the closure of cyclic nucleotide gated channels, and blockage of the inward flux of Na^+ and Ca^{2+} ; i.e. to a reduction in the circulating electrical current. A Na^+ / Ca^{2+} , K^+ exchanger continues to pump Ca^{2+} out, so that the cytoplasmic Ca^{2+} concentration declines, activating at least three 'calcium feedback' mechanisms, of which two are illustrated in this panel. Release of Ca^{2+} from guanylyl cyclase activating protein (GCAP) allows the GCAP to bind to a cytoplasmic domain of the guanylyl cyclase (GC), increasing the cyclase activity; release of Ca^{2+} from calmodulin (CM) causes it to dissociate from the channels, lowering the $K_{1/2}$ of the channels for cGMP. The boxed symbols ' α ' and ' β ' are used throughout the text and in Table 4 to refer respectively to the rate of synthesis of cGMP by GC, and the rate constant of hydrolysis of cGMP by E^* , and should not be confused with the protein subunit labels. B. Inactivation of R^* . At the dark concentration of $[Ca^{2+}]_i$ (left side of diagram), most of the recoverin (Rec) is in the Ca^{2+} -bound form at the membrane; Rec- $2Ca$ forms a complex with rhodopsin kinase (RK), blocking its activity. Thus at the resting Ca^{2+} level, few molecules of RK are available to interact with R^* . When $[Ca^{2+}]_i$ drops during the light response (arrows indicate progression of time), Rec releases its Ca^{2+} , and dissociates from RK. The elevated concentration of free RK increases the frequency of interaction between R^* and RK, permitting more rapid phosphorylation of R^* . Arrestin (Arr) then binds, substantially quenching the R^* activity. C. Inactivation of G^* -E*. G^* is inactivated when the terminal phosphate of its bound GTP is hydrolyzed. Although the G-protein has intrinsic GTPase activity, this capacity is only enabled when the G^* is bound to PDE γ and when, in addition, the GTPase accelerator protein (or GAP factor) RGS9-G β 5 also binds. The resulting tetra-molecular complex, $G^*\alpha$ -PDE γ -RGS9-G β 5, rapidly hydrolyzes the GTP to GDP, returning the $G\alpha$ subunit to its inactive form. The inactive $G\alpha$ -GDP dissociates from the PDE, so that the E^* and G^* are inactivated simultaneously.

The reduced influx of positive charge causes the intracellular voltage to become more negative – thus the cell hyperpolarizes, toward the reversal potential of the I_{K_x} channels. This negative-going response is the opposite of the positive-going responses triggered by stimuli in most other sensory cells, and from this point of view it may be helpful to think of darkness as the excitatory stimulus for the photoreceptor. The unusual polarity of response may be beneficial to the organism, in balancing the consumption of energy by the photoreceptors over the diurnal cycle [66]. In darkness, high consumption of energy is required to maintain the ionic gradients supporting the dark current, but virtually none is required to regenerate visual pigment. Conversely, in daylight, when very little energy is expended in pumping ions, the re-synthesis of visual pigment consumes a great deal of energy.

The light-induced hyperpolarization is transmitted to the synaptic terminal with relatively little attenuation, because the cable ‘length constant’ of a vertebrate rod or cone is typically longer than the cell itself. At the synaptic terminal hyperpolarization decreases the rate of release of the neurotransmitter glutamate into the synaptic cleft. This reduction conforms to the general rule that neurotransmitter release from chemical synapses is greatest in the depolarized state.

2.5. Outer segment free calcium concentration, $[Ca^{2+}]_i$

As the cGMP-gated channels are highly permeable to Ca^{2+} , there is a continual influx of Ca^{2+} through open channels in darkness. This influx of Ca^{2+} must be matched by extrusion at a rate sufficient to maintain the free calcium concentration, $[Ca^{2+}]_i$, at the appropriate level – which, as in most cells, is sub-micromolar. As indicated in Fig. 4, the extrusion is mediated by $Na^+ - Ca^{2+}, K^+$ exchange. To appreciate the general requirements for an efflux mechanism, it is helpful to consider the normal range of Ca^{2+} concentrations experienced by the rod. Table 2 sum-

Table 2
Measurements of concentration of free calcium in rods and cones^a

Preparation	T (°C)	Method	$[Ca^{2+}]_o$ (mM)	Dark $[Ca^{2+}]_i$ (nM)	Light $[Ca^{2+}]_i$ (nM)	Ref.
Bullfrog retina	25	Fura-2	1.5	~220	~140	[67]
Bullfrog retina	22	Fura-2	1.5	200–400	<30	[68]
Toad retina	24	Quin2/AM	1	273 ± 129	<50	[69]
Salamander rods	22	Aequorin	1	~400	<50	[70]
Salamander rods	23	Fluo-3	1	670 ± 250	30 ± 10	[71]
Salamander cones	23	Fluo-3	1	410 ± 104	5.5 ± 6.7	[72]
Lizard rods	22	Indo-dextran	1	554 ± 25	~50	[73,74]

^a Notes: In the preparation column, the labels ‘rods’ and ‘cones’ signify that the investigators made the measurements in isolated cells or outer segments. Dark $[Ca^{2+}]_i$ is the concentration measured in the fully dark adapted state. Light $[Ca^{2+}]_i$ is the concentration measured after the cell had been held in saturation by a bright light for some time. Errors are SDs, as reported by the authors or computed from their data.

marizes different estimates of the extreme levels: in darkness (when $[Ca^{2+}]_i$ is highest), and during prolonged bright illumination (when it is lowest).

Regulation of $[Ca^{2+}]_i$ in the outer segment is of profound importance. As in most cells, high $[Ca^{2+}]_i$ in photoreceptors is harmful, and probably lethal if prolonged. But of greater functional significance to vision is the fact that phototransduction is delicately regulated by at least four calcium-binding proteins. The properties of these regulatory proteins will be discussed in Section 6, and their roles in response recovery and light adaptation will be analyzed in Sections 7 and 8.

3. Activation of phototransduction: The protein constituents and cGMP

The protein constituents of the phototransduction cascade are listed in Table 3. Values are given for the molecular weight, subunit structure, membrane density (i.e., concentration), and so on, for typical amphibian and mammalian rods.

In this section we shall discuss the properties of the principal proteins mediating activation – rhodopsin, the G-protein, the phosphodiesterase, and the cGMP-gated channels – as well as cGMP itself. The remaining constituents will be described in subsequent sections.

3.1. Rhodopsin: The G-protein-coupled receptor of rods

The structure of the visual pigment of rods, rhodopsin, is illustrated in Fig. 10 of the chapter by DeGrip and Rothschild [76] (see also Fig. 1 of the chapter by Mathies and Lugtenburg [77]). Although the rod opsin is usually taken as the prototypical visual pigment, it is worth noting that the cone opsins comprise a phylogenetically more ancient group, from which the rhodopsins subsequently separated [96]. All visual pigment molecules of vertebrate rods and cones are now known to be GPCRs, and all show close sequence homology to human rhodopsin, which comprises 348 amino acid residues. And for all vertebrate visual pigments the ‘ligand’ is the 11-*cis* isomer of the aldehyde of either vitamin A or its de-hydro analogue (i.e., 11-*cis* retinal or 11-*cis* dehydroretinal). This ‘chromophore’ (=color-bearing, Greek) is covalently bound via a Schiff-base linkage to a conserved lysine residue in the seventh trans-membrane helix (at position 296 in mammalian rhodopsin). On its own, or when bound in the unprotonated form, retinal absorbs maximally in the UV (at about 380 nm), but when the Schiff-base is protonated the absorption shifts into the visible part of the spectrum. In different visual pigments the wavelength of maximal absorption (λ_{max}) of the chromophore is ‘tuned’, through weak interactions with charged and polar residues of the opsin in which it is embedded [97,98].

Activation of quiescent visual pigment (R) to R* occurs by photoisomerization of the chromophore from its bent 11-*cis* conformation to the relatively straight all-*trans* form. This isomerization rapidly converts the ligand from a powerful antagonist to a powerful agonist. In simplistic terms, it seems that the straightening of the

Table 3
Physical properties of the principal proteins in the phototransduction cascade of rods^a

	Protein	Holoprotein structure	MW (kDa)	Salamander			MW (kDa)	Mammalian			Ref.
				Ratio of Rh per protein	Molecules per rod	Density or conc'n. (see Note 2)		Ratio of Rh per protein	Molecules per rod	Density or conc'n. (see Note 2)	
Rh G	Rhodopsin	7 TM helices	36	1	3×10^9	$25000 \mu\text{m}^{-2}$	36	1	10^8	$25000 \mu\text{m}^{-2}$	[75-77]
	G-protein	Heterotrimer (α , β , γ)	81 (39, 36, 6)	10	3×10^8	$2500 \mu\text{m}^{-2}$	81 (39, 36, 6)	10	10^7	$3000 \mu\text{m}^{-2}$	[18,22]
E	Phosphodiesterase	Heterotetramer (α , β , γ , γ)	194 (88, 84, 11, 11)	270	1.3×10^7	$100 \mu\text{m}^{-2}$	215 (95, 94, 13, 13)	50	2×10^6	$500 \mu\text{m}^{-2}$	[78,79]
GC	Guanylyl cyclase	Homodimer (α , α)	400	7	10^6	$60 \mu\text{m}^{-2}$	224 (112, 112)	400	2×10^5	$50 \mu\text{m}^{-2}$	[80,81]
CNGC	cGMP-gated channel	Heterotetramer (2α , 2β)	6000	5	10^5	$500 \mu\text{m}^{-2}$ (in PM)	606 (63, 240)	1700	6×10^4	$500 \mu\text{m}^{-2}$ (in PM)	[46,82]
NCKX	$\text{Na}^+/\text{Ca}^{2+}$, K^+ exchanger	Homodimer (α , α)		$>6 \times 10^3$	$>5 \times 10^5$	$>500 \mu\text{m}^{-2}$ (in PM)	410 (205, 205)	$>2 \times 10^3$	$>6 \times 10^4$	$>500 \mu\text{m}^{-2}$ (in PM)	[43,83,84]
RK	Rh kinase	monomer	65	800	4×10^6	7 μM	65	500	2×10^5	12 μM	[85]
Arr	Arrestin	monomer	48	10	3×10^8	600 μM	48	8	1.2×10^8	800 μM	[86,87]
Rec	Recoverin	2 EF hands functional	23	14-160	2×10^6 to 2×10^7	35-400 μM	23	11	10^7	600 μM	[88-90]
RGS	RGS9	G β 5 Heterodimer					57/44	1000	10^5	6 μM	[91,92]
GCAP1	GC activating protein	3 EF hands functional					24				[93]
GCAP2											
CM	Calmodulin	4 EF hands functional	26	800	4×10^6	8 μM	26	800	1.2×10^6	8 μM	[94]
PD	Phosducin	monomer					33	16	6×10^6	400 μM	[95]

^a Notes: 1. Entries are taken either from the cited references, or from two secondary sources, [27,44]; both of these reviews give additional information about methods employed in the primary papers, and general evaluation of the estimated numbers. Numbers for the salamander rod are assumed approximately equal to those for the toad, from which much of the information is derived. Empty cells in the table indicate that the relevant information is not available. 2. In the upper section of the Table, the quantity of protein is expressed as its density in the disc membrane (or plasma membrane, PM), in molecules μm^{-2} , while in the lower section the quantity of soluble proteins is expressed as cytoplasmic concentration in μM .

chromophore molecule extends its length slightly, so that it stresses the opsin protein molecule from the interior and thereby triggers the conformational changes that lead to initiation of its enzymatic activity.

The Schiff-base deprotonation that follows photoisomerization (with some delay) shifts the λ_{max} of light absorption from the visible back into the UV, so that the pigment appears to lose its color – a phenomenon known since the 19th century as pigment ‘bleaching’. In the pigment’s signaling state (R^*) the chromophore remains covalently attached to opsin, but later (after the activated state has been quenched by biochemical mechanisms, discussed below) the Schiff-base linkage is hydrolyzed and the chromophore detaches. A supply of 11-cis chromophore is then needed to reconstitute the opsin to rhodopsin, R, to restore its capacity for photon capture and signaling. This reconstitution is known as pigment regeneration.

3.2. *Transducin: The heterotrimeric G-protein of rod and cone phototransduction*

The second component of the G-protein cascade of rods and cones is the 80 kDa heterotrimeric G-protein, transducin, which will be symbolized as G in equations and figures. The G-protein, whose structure has been determined by crystallographic methods [17,18,22], is present in the disc membrane at a density typically about 10% that of rhodopsin (Table 3).

The holo-G-protein is firmly anchored to the disc membrane, the adhesion being achieved primarily by a farnesyl group attached to the carboxy-terminal of the γ -subunit [99,100], but also being assisted by acylation of the amino-terminal of the α -subunit [101,102]. This anchoring to the membrane dictates that contact between the G-protein and R^* must occur at the membrane surface, through lateral diffusion of the two protein species; indeed, absence of the farnesyl group causes failure of activation of G by R^* [103]. In a successful encounter between an R^* and a G–GDP, the two molecules bind, thereby increasing the accessibility of the nucleotide binding site to the aqueous environment, so that the GDP can dissociate [23–25]. Loss of the GDP results in even tighter binding of the G to R^* , until the complex encounters a GTP in the cytoplasm [103–105]. Binding of a GTP in place of the GDP triggers a conformational change that leads to separation of the G–GTP from R^* , and also to separation of the α - and $\beta\gamma$ -subunits (G α -GTP and G $\beta\gamma$).

G α -GTP represents the active form of the G-protein that carries the signal forward, and for brevity we shall denote it as G*. The entire sequence of steps – diffusional encounter, binding of G–GDP to R^* , release of GDP, binding of GTP, and separation of the subunits to form G* – takes no more than 5–10 ms at room temperature under cellular conditions. Furthermore, at the end of the sequence the R^* is released unaltered, and is therefore free to interact with further molecules of G, and thereby to catalyze their activation as well. As a result, a single activated molecule of R^* can trigger the activation of G* at a rate of the order of hundreds of molecules per second (reviewed in Refs. [27,103,106]).

3.3. The cGMP phosphodiesterase: The effector protein of vertebrate phototransduction

In vertebrate photoreceptors the third element of the cascade, the ‘effector protein’, is the cGMP phosphodiesterase (PDE) which will be symbolized as E in equations and figures. The PDE is tetrameric in structure, with nearly bilateral symmetry [79,107]. Thus the holo-enzyme comprises two nearly-identical (although distinct) catalytic α - and β -subunits ($E\alpha$ and $E\beta$), which are regulated by two identical inhibitory γ -subunits ($E\gamma$). The PDE is anchored to the disc membrane by isoprenylation and carboxymethylation of the C-terminals of both $E\alpha$ and $E\beta$ [108,109], and thus, as in the activation of G by R^* , the interaction between G^* and PDE requires lateral diffusion of the molecules at the membrane surface. The density of PDE in the disc membrane is only about 1–2% that of R, so that the three principal proteins are present in the approximate ratio of 100 R:10 G:1 PDE. A strong case can be made that the densities of the G-protein and the PDE have been selected to optimize the signal-to-noise ratio of phototransduction. On this view, the quantities of these proteins are the minimum needed for adequate amplification, permitting spontaneous activation in darkness to be kept very low [110]. As indicated schematically in Fig. 4A, the binding of G^* to a γ -subunit of PDE relieves the inhibition that the latter subunit imposes, thereby causing activation of the associated catalytic subunit; this activated state of the effector will be symbolized as E^* .

For further review, see Refs. [107,111].

3.4. cGMP: The cytoplasmic messenger of phototransduction

Research on photoreceptors in the 1970s and 1980s was motivated by the insight that (at least in rods) there had to be a soluble internal messenger that communicated between the disc membrane, where the photon was captured by rhodopsin, and the plasma membrane, where the light-regulated cationic channels resided [59,112–114]. For about a decade calcium and cGMP competed as candidates for internal messenger, until 1985 when the issue was finally resolved by the discovery of cGMP-activated channels (Section 3.5).

But for some years after its unequivocal identification as the cytoplasmic messenger of phototransduction, a number of fundamental issues about cGMP and its mode of action remained unresolved. Among these were: the identity and properties of cGMP binding sites in the outer segment (Section 5.1); quantification of the diffusion of cGMP in the cytoplasm (Section 5.2); precise details of the two enzymes, guanylyl cyclase and phosphodiesterase, that control cGMP synthesis and hydrolysis; and the molecular basis for the calcium-dependent regulation of these steps (Section 6.3).

For further review, see Refs. [81,93].

3.5. The cGMP-gated channels of the plasma membrane

The final element in activation of the cascade is the cGMP-gated channel (or, more generally, the cyclic nucleotide gated channel, CNGC), which translates the message

embodied in the cytoplasmic concentration of cGMP into an electrical signal. The existence of this ionic mechanism was discovered by Fesenko, Kolesnikov and Lyubarsky (1985) [115] in excised patches of outer segment membrane from frog rods. These investigators not only settled a major controversy in the theory of phototransduction – the identity of the internal messenger of activation – but in doing so they opened up an entirely new chapter in the history of ion channel research. Cyclic nucleotide gated channels are now known to be expressed in a wide variety of cells, including receptor cells for olfaction and taste, retinal Müller and bipolar cells, sperm, pinealocytes, kidney cells, lung epithelial cells, and in cells of the hippocampus and cerebellum [45,116]. Accordingly, they have become a major focus of ion channel research.

The native cyclic nucleotide gated channel is most likely a hetero-tetramer, probably comprising a combination of 2α - and 2β -subunits (see Figs. 4–6 in Ref. [46]). Like other ligand-gated cation channels (ionotropic receptors, such as the ACh-gated and glutamate-gated channels), CNGCs are relatively non-specific cation channels, being quite permeable to the two most common monovalent cations, Na^+ and K^+ , and also very permeable to the two most common divalent cations, Ca^{2+} and Mg^{2+} . The properties of cyclic nucleotide gated channels are discussed in detail in the chapter by Molday and Kaupp [46].

The cGMP-gated channels of the rod outer segment exhibit a number of features that are critical to phototransduction. (1) The opening of the channels is gated cooperatively by cGMP; this cooperative gating contributes importantly to the amplification of the photoresponse, as we shall see in Section 5.7. (2) The channels are highly permeable to Ca^{2+} ; this permeability is critical to the role that Ca^{2+} plays in the ‘feedback’ regulation of phototransduction (Sections 7–9). (3) The current–voltage relation of the channels is very shallow in the normal range of membrane potentials [48]. Thus the current through the cGMP-gated channels of the rod is only very weakly dependent on the transmembrane potential between -35 and -65 mV (the normal operating range of the rod membrane potential), so that the pathway serves effectively as a ‘current source’ which imposes almost no resistive load on the rod. The high resistance is crucial in establishing a long space constant for the cable properties of the outer segment, so that a single photon will generate a voltage response of nearly constant amplitude, irrespective of its position of absorption along the outer segment.

For further review, see Refs. [45,46,82,117].

4. Quantitative analysis of activation: Proteins at the disc membrane

This section and the next one present a quantitative analysis of the onset phase of the light response, i.e., the activation of phototransduction. First we consider activation of the proteins at the disc membrane, and then in the next section we consider the reactions in the cytoplasm – the change in cGMP concentration and the resultant channel closure and electrical response. The treatment in both sections is based on the more complete derivation given in our previous papers [26,27].

Analysis of the activation phase is greatly simplified by the assumption that the effects of all inactivation reactions can be ignored. This assumption turns out to be valid over the entire rising phase of the electrical response for sufficiently bright flashes, and at sufficiently early times in the response to dim flashes; the meaning of 'sufficiently' in these contexts was investigated in the papers cited above, and will be summarized as part of our analysis.

Table 4 lists the symbols that we will use to denote the variables of the transduction cascade (i.e., quantities and concentrations), and the parameters of the reactions involved (i.e., rate constants, etc.). The individual variables and parameters will also be introduced and defined in the text as the presentation proceeds. To avoid possible confusion, we mention here our convention for denoting substances and their concentrations: the name of a substance will be given in roman typeface, while the variable representing its concentration (or density) will be given in italic; for example, the quantity of R^* at time t will be denoted $R^*(t)$, and the concentration of cGMP at time t will be denoted $cG(t)$.

4.1. R^* production

Overwhelming evidence identifies R^* , the activated form of rhodopsin that catalyzes the activation of G^* , as the spectral photointermediate named metarhodopsin II (meta II) (reviewed in Refs. [103,104,123]). Although meta II and its precursor meta I are in a tautomeric equilibrium, the balance lies strongly towards meta II at cellular pH, and thus the production of R^* is predicted to occur approximately as a first-order process with time constant equal to that of the meta I \leftrightarrow meta II equilibrium, which is ca. 1 ms for amphibian rhodopsin at room temperature (22°C) [124], and ca. 0.1 ms at mammalian body temperature [125]. Thus, following a flash producing Φ photoisomerizations at time $t = 0$, the number of activated molecules of R^* in the rod will be

$$R^*(t) = \Phi(1 - \exp(-t/t_R)) \quad (1)$$

where t_R is the time constant of appearance of meta II. At times substantially longer than t_R , Eq. (1) closely approximates to a step increase, i.e., $R^*(t) \approx \Phi H(t - t_R)$, where $H(t)$ is the Heaviside step function, defined as zero for $t \leq 0$ and as unity for $t > 0$.

4.2. G^* production

A molecule of R^* must find its substrate, G-GDP, by lateral diffusion of the two species in (or at the surface of) the disc membrane. At the microscopic level of individual protein molecules, 'lateral diffusion' simply means Brownian motion, i.e., random walking of the molecules in the plane of the disc membrane. If each encounter of R^* with a G-GDP results in a successful GDP/GTP exchange (and thus the loss of the G-GDP from the original pool), and if the boundary condition posed by the finite extent of a disc can be neglected, then the rate v_{enc} of encounter between a single R^* and molecules of G-GDP may be predicted from diffusion theory [26,110,126] to be

Table 4
Definitions of variables and parameters of the modeling, with representative values^a

Symbol	Units	Value (in dark)	Refs.	Definition	Used in Eqs.
Φ	Isomerizations			A. Variables	
R^*	Molecules			Number of photoisomerizations per rod per flash	1, 4, 5, 19, 20, 25, 29
G^*	Molecules			Number of activated rhodopsin molecules per rod	1
E^*	Subunits			Number of activated G-protein molecules per rod	4
α	$\mu\text{M s}^{-1}$	1.2–2.4		Number of activated PDE subunits per rod	5, 29
β	s^{-1}	0.6–1.2	[118,119]	Rate of synthesis of cGMP by guanylyl cyclase	13–16, 33, 34
cG	μM	2	[46,82]	Rate constant of cGMP hydrolysis by PDE	13–16, 34
J_{cG}	pA	Table 1		Free concentration of cGMP in the outer segment	9, 10, 13, 14, 16–18, 20, 22
J_{ex}	pA	Table 1		Current carried by cGMP-gated channels	21, 31
J	pA			Electrogenic current carried by exchanger	31, 32
F	—			Total outer segment current; $J = J_{\text{cG}} + J_{\text{ex}}$	23, 25
Ca	μM	Table 2		Normalized circulating current; $F = J/J_0$	31
v_{RG}	s^{-1}	~150	[127]	Free concentration of Ca^{2+} in the outer segment	
v_{RE}	s^{-1}	~150	[127]	B. Activation parameters	
c_{GE}	—	< 1		Rate of G^* formation per fully activated R^*	6
k_{cat}	s^{-1}	4400	[78]	Rate of E^* formation per fully activated R^*	5, 6, 26, 29
K_m	μM	10	[127]	Coupling coefficient from G^* to E^* ; $c_{\text{GE}} = v_{\text{RE}}/v_{\text{RG}}$	6
V_{cyto}	Pl	1		Turnover rate of doubly-activated PDE holomer	9
B_{cG}	—	~2		Michaelis constant of cGMP hydrolysis by PDE	9
β_{sub}	s^{-1}	$2\text{--}4 \times 10^{-4}$	[127]	Cytoplasmic volume of the outer segment	9, 31
				Buffering power of the cytoplasm for cGMP	9
				Rate constant of cGMP hydrolysis per E^* subunit	11, 26

Table 4 (continuation)

Symbol	Units	Value (in dark)	Refs	Definition	Used in Eqs
K_{cG}	μM	20		cGMP conc. for half-maximal channel opening	21
n_{cG}	—	2–3	[82, 115]	Hill coefficient of the cGMP channel activation	21–23, 26, 34
A	s^{-2}	0.1	[26, 27]	Amplification constant; $A = v_{\text{RF}} \beta_{\text{sub}} n_{cG}$	25, 26
$t_R, t_{RG},$ etc.	s			Short delays in various activation steps	1, 4, 5, 19
t_{eff}	s	0.02	[26, 27]	Effective delay contributed by all short steps	20, 24, 29 21–23
C. Inactivation parameters					
τ_R	s	0.4	[120] non-dominant	Time constant for inactivation of R^* activity	29, 30
τ_E	s	1.5	[120] dominant	Time constant for inactivation of G^*-E^* complex	29, 30
$1/\beta_0$	s	1		Time constant for decay of cGMP (Ca clamped)	
f_{C_a}	—	0.1–0.15	[46]	Fraction of cGMP-activated current carried by Ca^{2+}	31
K_{ex}	nM	1600	[70]	$[\text{Ca}^{2+}]$, giving half-maximal exchange current	32
$J_{\text{ex, sat}}$	pA	–20	[70]	Saturated exchange current at high $[\text{Ca}^{2+}]$	32
K_{cyc}	nM	100–230	[81, 121, 122]	$[\text{Ca}^{2+}]$, giving half-maximal cyclase activity	33
n_{cyc}	—	2	[81, 121, 122]	Hill coefficient for cyclase activation by $[\text{Ca}^{2+}]$	33
α_{\min}	$\mu\text{M s}^{-1}$	~0	[81, 121, 122]	Min. value of α at high $[\text{Ca}^{2+}]$	33
α_{\max}	$\mu\text{M s}^{-1}$	~40	[81, 121, 122]	Max. value of α at low $[\text{Ca}^{2+}]$	33

^a Notes: 1. The variables listed in part A of the Table can in general take several forms. For example, the concentration of cGMP (represented by the variable cG) can be given in the forms: $cG(t)$, as a function of time; cG_0 , at some resting steady level; cG_{dark} , in darkness; and $\Delta cG(t)$, as the incremental change from the resting level cG_0 . (One exception is Φ , which has the single meaning of the number of photoisomerizations delivered to the outer segment at time zero.).

2. A dash “—” in the units column signifies a dimensionless quantity.

$$v_{\text{enc}}(t) = \frac{4\pi(D_R + D_G)C_G}{\ln[4(D_R + D_G)t/\rho^2] - 2\gamma} \quad (2)$$

where D_R and D_G are the lateral diffusion coefficients for R^* and G–GDP respectively, while $\rho \approx 5 \text{ nm}$ is the encounter radius for contact between the two mole-

cules, and $\gamma \approx 0.57722$ is Euler's constant. In amphibian rods at room temperature, we may take $D_R = 0.7 \mu\text{m}^2 \text{s}^{-1}$, and $D_G = 1.2 \mu\text{m}^2 \text{s}^{-1}$ [26,27].

Equation (2) automatically takes account of the local depletion of G-GDP that occurs near the R*, and accordingly it predicts that the encounter rate v_{enc} should not be constant, but should instead decline with time according to the logarithmic term in the denominator. Evaluation of the denominator during the interval from 5–500 ms after formation of the R* shows that the decline is quite modest, though, and that for amphibian rods a good approximation may be provided by the rate determined at 50 ms, i.e.,

$$v_{\text{enc}} \approx 1.3(D_R + D_G)C_G \quad (3)$$

The value of v_{enc} estimated from (3) for an amphibian rod at room temperature is 6000 s^{-1} , and for a mammalian rod at body temperature (at an appropriately early time) $16,000 \text{ s}^{-1}$ [26,27].

These calculated rates of encounter represent the diffusion-limit to the possible rate of reaction, since reaction can only occur upon encounter; hence, if every encounter were successful, then the reaction rate v_{RG} would equal the encounter rate v_{enc} . However, in the likely scenario that R* fails to trigger activation at every encounter with a G-GDP, then first the reaction rate will be lower than this diffusion limit, and second it will exhibit even less time-dependence (since the pool of inactive G-GDPs will suffer less local depletion in the neighborhood of the R*). Both these theoretical predictions are borne out by numerical simulations [110]. In sum, then, it is expected that a single fully-activated R* will generate G*s at a nearly constant rate, which we shall denote by the symbol v_{RG} . Therefore, provided we can ignore inactivation of R* and of G*, we predict the number of activated G*s in a rod stimulated at $t=0$ by a flash producing Φ photoisomerizations should be well approximated by a 'ramp' function of time

$$G^*(t) = \Phi v_{RG}(t - t_{RG}), \quad t > t_{RG} \quad (4)$$

Here $t_{RG} = t_R + t_G$, where t_R is as defined above, and t_G is a delay no greater than the time between successful encounters between R* and G-GDP.

4.3. E* production

As G* (=G α -GTP) is acylated, it is likely that after separation from R* and G $\beta\gamma$ the G* continues to move at the surface of the disc membrane. Since the PDE effector protein is firmly anchored to the membrane, interaction between G* and the PDE γ -subunit requires the molecules to encounter each another by lateral diffusion. Quantitative analysis of this step is complicated by the fact that the G*s are produced not at a fixed location, but at whatever location the R* has moved to at the particular instant in question. Nevertheless a simplified analytical treatment was developed [26], and its accuracy was subsequently investigated quantitatively using numerical simulation [110].

The bottom line of the latter investigation was that over a wide range of plausible values of the parameters that affect v_{RG} (such as the diffusion coefficients, and the

probability of successful encounter), the generation of E^* ($= PDE^*$) was again predicted to follow a ramping function of time

$$E^*(t) = \Phi v_{RE}(t - t_{RGE}), \quad t > t_{RGE} \quad (5)$$

Here v_{RE} is the effective rate with which a single R^* triggers activation of E^* s, and t_{RGE} is given by $t_{RGE} = t_R + t_G + t_E$, where t_E is a brief delay that arises between buildup of G^* and buildup of E^* [110]. Thus, t_{RGE} is a cumulative delay that combines the 'micro' delays introduced by the three steps.

The form of the kinetic predictions embodied in Eqs. (1), (4) and (5) are illustrated in Figs. 5A and 5B.

Since, in the absence of inactivation reactions, $G^*(t)$ and $E^*(t)$ are predicted to follow an identical time-course (a ramp with time), it is convenient to define the 'coupling efficiency' of the step from G^* to E^* as the ratio of their slopes of activation. Thus we denote the coupling efficiency c_{GE} as

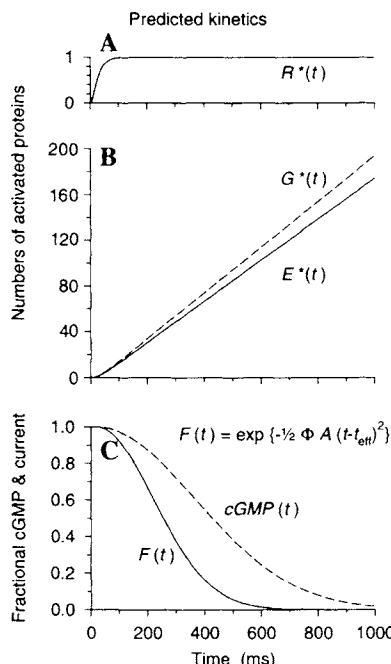


Fig. 5. Predicted kinetics of activation, for the disc membrane proteins, cGMP, and electrical response. Inactivation reactions have been ignored at this stage. (A) Following photoisomerization, a single R^* is activated with a time constant t_R ; see Eq. (1). (B) According to Eqs. (4) and (5), the quantities $G^*(t)$ and $E^*(t)$ of activated G-protein and PDE increase linearly with time after R^* activation; the slope is estimated to be around 150 s⁻¹ per R^* , see Section 5.9. (C) Activation of E^* causes the cGMP concentration to decline, according to Eq. (20). Consequently cGMP-gated channels close, and the fractional circulating current $F(t)$ declines according to Eq. (25). Responses in C are shown for a flash delivering $\Phi = 250$ photoisomerizations, with $A = 0.1 \text{ s}^{-2}$.

$$c_{GE} = v_{RE}/v_{RG} \quad (6)$$

Even at the highest possible rate of E^* formation, when G^* is produced at the diffusion limit and causes activation of E^* at the diffusion limit, the numerical simulations show that the coupling efficiency c_{GE} should be at least 0.65, for the protein densities measured in the rod (Table 3); and at lower rates the coupling is predicted to approach unity [110].

These numerical simulations have shown that the ramping behavior of E^* predicted by (5) is very robust, i.e., it holds over a wide range of possible values of the lateral diffusion coefficients and probabilities of reaction of the underlying molecules [110]. It can hardly be over-emphasized how greatly the subsequent analysis of the electrical response is simplified by this ramping behavior – the linear rise leads to tractable solutions.

Potential complication. A potential complication with the applicability of Eq. (5) arises from the existence of two hydrolytic subunits per PDE molecule. In the analysis above, it was assumed that the two subunits act entirely independently, and the symbol $E^*(t)$ was used to denote the concentration of activated subunits. Accordingly, in the analysis of cGMP hydrolysis that follows, each E^* subunit will be assigned a hydrolytic rate of half the k_{cat} measured for the doubly-activated PDE holomer in *in vitro* assays. If instead cooperativity occurs, so that the singly-activated E^* ($\equiv G^*-PDE^*$) exhibits less than half the activity of the doubly-activated E^{**} ($\equiv G^*-PDE^{**}-G^*$) then the situation is more complicated. However, unpublished simulations show that the time course of activation of E^{**} also closely follows a ramp with time, so that the kinetic form of the light response would be unaltered [128]. Cooperativity of this kind might have a significant advantage for transduction, by lowering the level of dark activation of PDE; thus any residual concentration of G^* would be very weakly effective, and E^{**} would only be activated at locations of R^* activity where the concentration of G^* was greatly elevated.

For a stochastic simulation of the molecular interactions of the disc-associated reactions, see Ref. [128].

5. Quantitative analysis of activation: cGMP and the electrical response

Four processes govern the concentration of cGMP at any location in the outer segment: the local rates of synthesis and of hydrolysis of cGMP (by guanylyl cyclase and phosphodiesterase, respectively), the buffering of cGMP at its binding sites, and the diffusion of cGMP under concentration gradients.

5.1. Buffering of cGMP in the cytoplasm

The term ‘buffering power’ describes the relationship between the total and the free concentrations of a substance. Thus, the buffering power B_X for substance X in a compartment is defined as the ratio of the increment dX_{tot} in the total concentration of X accompanying a small increment dX in the free concentration X of the sub-

stance. We adopt the convention that all concentrations represent the free level, unless explicitly denoted by the subscript 'tot'. Hence for cGMP in the outer segment cytoplasm, the buffering power is defined as $B_{cG} = dcG_{tot}/dcG$.

This definition of buffering power is a steady-state (or equilibrium) concept, and the magnitude of B is determined by the concentration and affinity of binding sites, rather than by any kinetic parameters. For the case of a single rapidly equilibrating buffer present at concentration Q , and with dissociation constant K , the buffering power for X can be calculated as

$$B_X = 1 + QK/(X + K)^2 \approx 1 + Q/K \quad (7)$$

where the approximation applies when $X \ll K$, i.e., when most of the buffer is free. This expression will break down if the binding/unbinding reactions are slow, or if the binding is cooperative (i.e., with a non-unity Hill coefficient). For a cooperative (but again rapidly equilibrating buffer) with Hill coefficient n , the buffering power can be shown to be

$$B_X = 1 + QK^n/(X^n + K^n)^2 \approx 1 + nQX^{n-1}/K^n \quad (8)$$

which reduces to expression (7), for $n = 1$.

At least two distinct proteins in the outer segment have binding sites for cGMP: the CNGCs and the PDE. Each CNGC contains four cGMP binding sites, one on each subunit (whether α or β). Kinetic measurements have shown that the opening and closing of the CNGCs in response to changes in cGMP occurs on a millisecond time scale [49,129]; thus, the binding can be considered rapidly reversible on the time scale of the light response. Assuming that the density of the CNGCs in the plasma membrane is $500 \mu\text{m}^{-2}$ (Table 3), and that the dimensions of the rod are as given in Table 1, then the concentration of the channels referenced to the cytoplasm would range from $0.7 \mu\text{M}$ (salamander rod) to $3.5 \mu\text{M}$ (mammalian rod). For a free cGMP concentration of $2\text{--}4 \mu\text{M}$, and with $n_{cG} \geq 2$, Eq. (8) indicates that strictly cooperative binding would lead to negligible buffering, i.e., $B_{cG} \approx 1$. If one could treat two of the binding sites on the CNGCs as independent and non-cooperative, then the buffering power could rise as high as $B_{cG} \approx 1.4$ for the smallest rods. In summary, it seems unlikely that the CNGCs contribute appreciably to cGMP buffering.

The PDE contains not only the hydrolytic sites for cGMP, but additionally two non-catalytic sites (one each on the α - and β -subunits) that tightly bind cGMP. In contrast to the sites on the channels, these non-catalytic binding sites on the PDE equilibrate exceedingly slowly, over a time course of many minutes, so that for most purposes they can be considered as permanent stores of cGMP [130]. Since the quantity of PDE holomer in the outer segment is around $30 \mu\text{M}$ (Table 3), these sites bind approximately $60 \mu\text{M}$ cGMP and account for more than 90% of the total cGMP that can be recovered biochemically from rod outer segments.

Our previous analysis of other studies suggested that the lower affinity non-catalytic binding site on the PDE might contribute a buffering power of $B_{cG} \approx 2$, on the assumption that this site could equilibrate rapidly, and that Eq. (7) could be applied

using the measured binding constant of 830 nM [26,131]. Other binding measurements have suggested that B_{cG} could be as high as 3–4 in the dark [132].

5.2. Diffusion of cGMP in the cytoplasm

The diffusion of cGMP in the cytoplasm is of fundamental significance to rod phototransduction, for it is by diffusion that the concentration change caused by hydrolysis of cGMP at the disc membrane is communicated to the plasma membrane. It has been established that, of the total number of cGMP-gated channels that are open in the dark, about 3–5% are closed by a single photoisomerization [34,38]. As the activation of PDE is almost certainly confined to the disc containing the R* (Fig. 4), these results indicate that hydrolytic activity at a single disc leads to the closure of plasma membrane ion channels over at least 3–5% of the 60 μm length of a toad rod outer segment; i.e., over more than 1 μm in each direction (± 30 discs). Recent experiments have measured the spread to take place over a distance of at least 3 μm in each direction (± 100 discs) [133]. The only plausible explanation for this spread of excitation is the diffusion of cGMP longitudinally within the outer segment cytoplasm [26,134].

Application of diffusion theory to the geometry of the amphibian rod outer segment shows that radial equilibration of cGMP should occur extremely rapidly [134]. Thus a change in cGMP concentration imposed anywhere on a disc membrane should lead, within just a few ms, to a concentration change that is essentially uniform throughout that interdiscal space. Hence, on the time scale of the photoresponse it is entirely acceptable to neglect radial gradients of cGMP, so that only longitudinal gradients are of significance for signaling [134].

Although the diffusion of cGMP in the outer segment cytoplasm is essential for communication between the disc and plasma membranes, and for the longitudinal spread of excitation at the lowest flash intensities, quantitative analysis shows that for most of the range of flash intensities of interest, even this longitudinal diffusion can safely be overlooked. Thus, at moderately bright flash intensities, the distance between neighboring photon hits is so short that longitudinal gradients of cGMP can in practice be ignored, and the outer segment assumed to behave as a well-stirred or ‘lumped’ compartment. Adoption of this assumption greatly simplifies analysis of the electrical response. Its validity and generality will be examined briefly in Section 5.10, where it will be shown that the key determinant is the magnitude of the effective longitudinal diffusion coefficient of cGMP.

5.3. Differential equation for hydrolysis of cGMP by PDE

In the lumped case, the rate of hydrolysis of cGMP over the whole outer segment, due to E*, can be expressed in terms of the Michaelis–Menten relation, which governs the rate of reaction between an enzyme (PDE) and its substrate (cGMP). If $E^*(t)$ denotes the number of activated PDE catalytic subunits throughout the outer segment at time t , and $cG(t)$ denotes the free cytoplasmic concentration of cGMP, then

$$N_{\text{Av}} V_{\text{cyto}} B_{\text{cG}} \frac{dcG}{dt} = -E^*(t) \frac{1}{2} k_{\text{cat}} \frac{cG}{cG + K_m} \quad (9)$$

where N_{Av} is Avogadro's number, V_{cyto} is the cytoplasmic volume, k_{cat} is the turnover rate (in s^{-1}) of the doubly-activated PDE** holomer (with $\frac{1}{2}k_{\text{cat}}$ being the average turnover rate per activated PDE subunit, E^*), and K_m is the Michaelis constant of the reaction. Equation (9) gives the rate of removal of cGMP, in molecules s^{-1} , calculated over the whole outer segment. On the left-hand side, the buffering power B_{cG} converts free concentration to total concentration, the cytoplasmic volume V_{cyto} converts molar to moles, and N_{Av} converts moles to molecules.

In a normal outer segment, the free concentration of cGMP is always much smaller than K_m : the highest value of cG is that in the dark, estimated as 2–4 μM [82,131]. From analysis of many investigations undertaken in the 1970s and 1980s the value previously extracted for K_m was ca. 100 μM (Table V of [27], [78]). However, the most recent experiments indicate that the K_m is 10 μM [127]. On either estimate, $K_m \gg cG$, so that Eq. (9) simplifies to

$$\begin{aligned} \frac{dcG}{dt} &= -E^*(t) \frac{\frac{1}{2}k_{\text{cat}}/K_m}{N_{\text{Av}} V_{\text{cyto}} B_{\text{cG}}} cG \\ &= -E^*(t) \beta_{\text{sub}} cG \\ &= -\Delta\beta(t) cG \end{aligned} \quad (10)$$

where the second and third lines serve to introduce two new parameters, β_{sub} and $\Delta\beta(t)$. The first of these, β_{sub} , denotes the hydrolytic rate constant for cGMP (averaged over the whole outer segment) elicited per activated catalytic subunit of PDE (E^*). From Eq. (10), this may be written as

$$\beta_{\text{sub}} = \frac{\frac{1}{2}k_{\text{cat}}/K_m}{N_{\text{Av}} V_{\text{cyto}} B_{\text{cG}}}. \quad (11)$$

As discussed below, this parameter turns out to be very useful in explaining the contribution that PDE-mediated hydrolysis of cGMP makes to the overall amplification of the cascade. The second parameter, $\Delta\beta(t)$, denotes the total increase in hydrolytic rate constant elicited by the $E^*(t)$ subunits of activated PDE generated by the light stimulus,

$$\Delta\beta(t) = E^*(t) \beta_{\text{sub}} \quad (12)$$

and will be used shortly.

5.4. Combined synthesis and hydrolysis of cGMP

When account is taken of both synthesis and hydrolysis of cGMP, in a well-stirred outer segment, then the differential equation for free cGMP concentration may be written as

$$\frac{dcG}{dt} = \alpha(t) - \beta(t)cG \quad (13)$$

where $\alpha(t)$ denotes the rate of synthesis by guanylyl cyclase (in $\mu\text{M s}^{-1}$) and $\beta(t)$ denotes the rate constant of hydrolysis (in s^{-1}). During the light response these parameters will in general both be time-varying functions; we nevertheless employ the conventional term rate ‘constant’ for $\beta(t)$.

Under steady-state conditions (either in darkness, or during steady illumination) both sides of Eq. (13) are zero, so that

$$\alpha_0 = \beta_0 cG_0 \quad (14)$$

where the subscript ‘0’ indicates the initial steady-state condition; in the special case where this state is darkness we shall employ the subscript ‘dark’. It is convenient to consider increments from the steady level, by defining

$$\alpha(t) = \alpha_0 + \Delta\alpha(t), \quad \beta(t) = \beta_0 + \Delta\beta(t) \quad (15)$$

Substitution of these definitions into Eq. (13) yields

$$\begin{aligned} \frac{dcG}{dt} &= \alpha_0 + \Delta\alpha(t) - (\beta_0 + \Delta\beta(t))cG \\ &= \Delta\alpha(t) - \Delta\beta(t)cG + \beta_0(cG_0 - cG) \end{aligned} \quad (16)$$

where the second line follows from the equality in (14).

We now make two approximations that restrict analysis to early times or small responses. Any increment $\Delta\alpha(t)$ in cGMP synthesis during the light response will result from the decline of $[\text{Ca}^{2+}]_i$ that occurs as a consequence of the closure of cGMP-gated channels and the continued extrusion of Ca^{2+} by the exchanger. Such changes will take time to develop, so that at sufficiently early times in the light response we can make the approximation that $\Delta\alpha(t) \approx 0$. Since we are limited to early times, where $cG \approx cG_0$, the final term $\beta_0(cG_0 - cG)$ will also approximate to zero. Thus the first and third terms in the second line of Eq. (16) disappear and, within the validity of this approximation, the differential equation simplifies to

$$\frac{dcG}{dt} \approx -\Delta\beta(t)cG \quad (17)$$

Thus, when synthesis occurs at a fixed rate, the differential equation approximates to the exact form in Eq. (10), which applies in the absence of synthesis.

5.5. Solution for the light-induced change in cGMP concentration

Equation (17) has the general solution

$$\frac{cG(t)}{cG_0} = \exp \left[- \int_0^t \Delta\beta(t') dt' \right] \quad (18)$$

We now require an expression for $\Delta\beta(t)$, which, in the case of a brief flash delivering Φ photoisomerizations to the outer segment at time zero, we obtain from Eqs. (5) and (12), as

$$\Delta\beta(t) = \Phi v_{RE} \beta_{sub}(t - t_{RGE}) \quad \text{for } t > t_{RGE} \quad (19)$$

Substitution of (19) into (18) yields the solution

$$\frac{cG(t)}{cG_0} = \exp\left[-\frac{1}{2}\Phi v_{RE} \beta_{sub}(t - t_{RGE})^2\right] \quad \text{for } t > t_{RGE} \quad (20)$$

which indicates that the cGMP concentration should decline according to a ‘delayed Gaussian’ function of time following a brief flash (Fig. 5c). The range of validity of the approximations underlying Eqs. (17) and (19) will be investigated after the electrical response has been derived.

5.6. Solution for the electrical response to a flash of light

The change in intracellular concentration of cGMP can be translated into the cell’s electrical response through knowledge of the gating relation for the outer segment channels. From experiments on excised patches of outer segment membrane (Section 3.5; see also Ref. [46]), the fraction of open channels can be expressed by the cooperativity expression (or Hill equation) as

$$\frac{J_{cG}}{J_{cG,\max}} = \frac{cG^{n_{cG}}}{cG^{n_{cG}} + K_{cG}^{n_{cG}}} \quad (21)$$

Here J_{cG} is the current through the cGMP-gated channels in a region of membrane (at a fixed membrane voltage), and $J_{cG,\max}$ is its maximum value at high concentrations of cGMP. The exponent n_{cG} is termed the Hill coefficient, and K_{cG} is the concentration of cGMP that produces a half-maximal current. In excised patches of rod membrane n_{cG} has been found to be 2–3, while K_{cG} is typically about 20 μM .

Equation (21) is also expected to govern the cGMP-activated currents of whole rod outer segments, although testing the relation in intact cells is complicated by the problem of delivering cGMP uniformly to the outer segment, and by the impracticality of space-clamping the rod membrane potential when all the cGMP-gated channels are open [135]. The most compelling results supporting the validity of Eq. (21) for whole outer segments have been obtained with the truncated rod outer segment preparation [121,136]; it bears mention that in the latter investigations n_{cG} was found to be ~ 2 .

Recently it has been found that in intact photoreceptors K_{cG} may shift as a result of the calcium-dependent binding of calmodulin, thus contributing to light adaptation (see Section 8). This finding may also account for the fact that in different studies the values reported for n_{cG} range from about 1.8 to 3; thus, it is possible that spatial variations in K_{cG} within the outer segment might make the cooperativity of the ensemble of channels appear lower than the actual cooperativity of the individual channel [137].

The application of Eq. (21) to the intact photoreceptor is simplified by two factors. First, the concentration of cGMP is always much less than the half-activation concentration (i.e. $cG < cG_{\text{dark}} \ll K_{cG}$), so that Eq. (21) simplifies to a power relation

$$\frac{J(t)}{J_0} = \left[\frac{cG(t)}{cG_0} \right]^{n_{cG}} \quad (22)$$

where, for simplicity, we have dropped the subscript 'cG' from $J(t)$. Second (at least in rods), the current through the outer segment channels is essentially independent of transmembrane voltage over the normal operating range (see Section 3.5). Thus, it is valid to substitute the relationship for $cG(t)$ from (20) into (22) to obtain

$$F(t) = \frac{J(t)}{J_0} = \exp \left[-\frac{1}{2} \Phi v_{\text{RE}} \beta_{\text{sub}} n_{cG} (t - t_{\text{eff}})^2 \right] \quad \text{for } t > t_{\text{eff}} \quad (23)$$

The term $F(t)$ has been introduced to denote the circulating current during the flash response, expressed as a fraction of the original resting steady-state level; thus $F(t)$ always begins at $F(0) = 1$.

In Eq. (23) a new delay term, t_{eff} , has been introduced, because intervening between the decline in cGMP concentration predicted by (20) and the decline in circulating current are at least three additional delay processes: (i) the time t_r for radial equilibration of cGMP concentration in the outer segment, (ii) the time t_B for equilibration of cGMP with 'fast' buffer sites in the cytoplasm, and (iii) the time t_C for gating of the channels in response to an applied change in cGMP concentration. As discussed in Section 5.2, diffusion theory predicts that t_r should be of the order of a few ms for an amphibian rod, and much shorter for a mammalian rod [134]. We have no information on the size of t_B but expect it to be very small, while t_C has been measured as 2–3 ms at room temperature [129]. On the time scale of the light response, these delays are very brief, and can simply be accumulated with the other delays discussed in Section 4. Thus, the effective delay t_{eff} in (23) may be written as the sum

$$t_{\text{eff}} = t_R + t_G + t_E + t_r + t_B + t_C \quad (24)$$

From analysis of voltage-clamped responses from salamander rods, the total delay time t_{eff} has been estimated as about 15 ms. In mammalian rods at body temperature it is no more than 2 ms [26,138,139].

Two points should now be mentioned about Eq. (23). First, this expression accounts only for current flowing through the cGMP-gated channels, and excludes current carried by the calcium exchanger (Section 7.3), as well as capacitive current (treated below). Second, in our previous work [26,27] we used the symbol F to denote J/J_{dark} (i.e., relative to the dark state), but here we are using F in a more general sense to denote current relative to the steady resting condition in any arbitrary background intensity. For the special case where the background is zero, we shall use the symbol $F_{\text{dark}}(t)$.

The form of Eq. (23) is plotted in Fig. 5C. Interestingly, the electrical response has exactly the same delayed Gaussian shape as the cGMP concentration. Thus the

effect of the channel gating cooperativity is simply to increase the steepness of the response, without fundamentally changing its nature.

If the photoreceptor is not voltage-clamped, then capacitive charging of the cell membrane contributes an additional low-pass filtering step to the photocurrent, with a time constant τ_m given by the product of the cell's membrane capacitance and its leakage resistance. The size of this membrane time constant can either be estimated from the kinetics of the responses to extremely intense flashes, or can be measured directly from experiments on isolated cells in the whole-cell patch clamp configuration (e.g., [49]). Typical values (Table 1) are roughly: 10–20 ms for amphibian rods; 40–70 ms for salamander and fish cones; 1 ms for mammalian rods *in vivo*; and 2–4 ms for mammalian cones *in vivo* [48,49,52,57,64,125,139,140].

For the slow responses elicited by flashes of low or moderate intensity, τ_m can be treated as a fixed delay which can be cumulated with t_{eff} along with any additional delays contributed by electronic or digital filtering used by the investigator. (In papers in which we have applied Eq. (23), we have used the symbol t'_{eff} to represent t_{eff} plus these additional delays [26,27,138,141].) For intense flashes, one would ideally wish to obtain a full analytical solution taking account of the individual 'chemical' delays set out in Eq. (24), but this is impractical and those delays are simply incorporated into t_{eff} . On the other hand, as the membrane time constant and the equipment delays are readily measurable, their effects can be explicitly incorporated into any analysis. Thus, the filtering effect of the membrane time constant can be calculated either by numerical convolution of Eq. (23) with an exponential decay [140], or by substitution into an analytical solution [139]. And the delay in the electronics can be compensated for by a shift on the time axis (as in Fig. 3).

5.7. Significance of the equations: Amplification and response kinetics

Equation (23) has great utility, both theoretically, in explaining the nature of the amplification of the phototransduction cascade and the basis for the shape of the rising phase kinetics, and also practically, in providing a simple means of fitting experimentally measured responses and extracting from them quantitative information about the cascade.

Amplification. Equation (23) embodies the manner in which the individual stages of the transduction cascade illustrated in Fig. 4A contribute to the overall amplification (or gain) of the response. Thus, we can rewrite Eq. (23) in the simpler form

$$F(t) = \exp\left[-\frac{1}{2}\Phi A(t - t_{\text{eff}})^2\right], \quad t > t_{\text{eff}} \quad (25)$$

(which we shall use from here on), where we define

$$A = v_{RG} c_{GE} \beta_{\text{sub}} n_{cG}, \quad (26)$$

as the 'amplification constant' of phototransduction (in s^{-2} per photoisomerization); the rate v_{RE} has been replaced by $v_{RG} c_{GE}$, using Eq. (6).

This definition of amplification is referenced to an input of a single photoisomerization per outer segment, and the four factors on the right-hand side of

Eq. (26) allocate the overall gain to four discrete stages. The first stage of the cascade is defined as having unity gain: an isomerization activates a single R^* molecule. The second stage, the enzymatic activation of G^* by R^* , generates a component of amplification characterized by the catalytic rate v_{RG} (in s^{-1}). The third stage, linking G^* to E^* activation, contributes an amplification somewhat less than unity, characterized by the coupling efficiency c_{GE} . The fourth stage, the PDE-catalyzed hydrolysis of cGMP, contributes the second major component of amplification, characterized by β_{sub} (in s^{-1}), the rate constant of decline in free cGMP concentration elicited by a single E^* subunit per volume of the outer segment cytoplasm (Eq. (11)). Finally the fifth stage, the cooperative gating of the channels by cGMP, contributes a component of amplification characterized by the Hill coefficient n_{cG} .

According to Eq. (11), the factor β_{sub} is inversely proportional to V_{cyto} , revealing the important role that the volume of the outer segment plays in amplification. Thus, the 25-fold smaller outer segment volume of mammalian rods accounts for much of the factor of 100-fold by which their amplification constant ($A = 5-10 s^{-2}$) exceeds that of amphibian rods ($A = 0.05-0.1 s^{-2}$) [27]. Because of the term $A t^2$ in Eq. (25), the time taken to reach a given fractional suppression of circulating current is predicted to vary inversely as \sqrt{A} . Hence, for a given number of photoisomerizations, the response of a mammalian rod should achieve a given fractional suppression of the cGMP-activated current about $\sqrt{100} = 10$ times faster than the response of an amphibian rod.

To further explore the implications of Eq. (25), we consider the relative merits of packaging a given quantity of rhodopsin (and its associated transduction machinery) into a single large outer segment, versus packaging it into 25 smaller outer segments. Because the total number of rhodopsin molecules is the same in the two cases, we can assume that a given intensity of incident light will elicit the same total number of photoisomerizations in the two cases. Accordingly the *average* response per rod will be the same in the two cases – but the qualification ‘average’ is crucial. If just a single photon were absorbed, the situation in the two scenarios would be very different. Absorption of the single photon in the large outer segment would generate a response that we can take as a reference. But absorption of a single photon in the group of 25 smaller rods would generate no response in 24 of them, together with a response in one rod that rose in $\frac{1}{5}$ of the time of the reference response in the large rod (or, at a fixed early time, to 25 times the level in the large rod). Hence Eq. (25) shows the important advantage that accrues in the ‘photon counting’ regime of scotopic light intensities through the use of small outer segments, such as possessed by some fish and birds, and by mammals. As the reactions occur in a smaller cytoplasmic volume, the response at a fixed time is much larger (and the time taken to reach a given level is much shorter). Provided that the retinal circuitry can handle the signals from the greater number of rods, this increased amplification is likely to provide a significant advantage in increased time resolution in the photon counting regime.

Contributions to response kinetics. The theoretical development captures the way in which the sequential steps in phototransduction contribute to the waveform of the

activation phase. As summarized in Fig. 5, three of the cascade stages act as 'integrating' mechanisms: (i) the absorption of a photon is integrated to a *step* of activity, through the change in conformation of R to its active state R*; (ii) the catalytic activity of R* leads to a second stage of integration, generating a ramp of activation of G* and E*; (iii) the catalytic hydrolysis of cGMP by E*'s contributes a third stage of integration, converting the E* ramp into a Gaussian time-course of cGMP concentration, which at early times approximates an inverted parabola. Thus, an impulse of activity at the input is shaped, via three stages of integration, into a parabolic decline in cGMP concentration, and in electrical current.

5.8. Comparison between experiment and theory

The practical significance of Eq. (25) lies in its general applicability to the responses of a great variety of photoreceptors, including not only single-cell measurements but also the massed extracellular potential of the electroretinogram (ERG). Thus, it provides a general tool for non-invasive and comparative assessment of the amplification of photoreceptor responses in many species, including humans.

Perhaps the main reason for the ready applicability of Eq. (25) to experimental results arises from the fact that only a single parameter, A , is required to fit (and to explain) the entire family of responses over a wide range of stimulus intensities. What this means is that all the parameters of the molecular description – the protein concentrations and diffusion coefficients, the enzyme activities, the physical dimensions of the cell, the buffering power, and the channel gating properties – collapse down into just a single parameter, A . The way in which these parameters coalesce may be appreciated by substitution of β_{sub} from Eq. (11) into Eq. (26), to obtain

$$A = v_{RE} \left(\frac{\frac{1}{2}k_{\text{cat}}/K_m}{N_A V_{\text{cyto}} B_{cG}} \right) n_{cG} \quad (27)$$

Figure 6 compares the predictions of Eq. (25) with experimental results from a salamander rod and a mammalian rod using the suction pipette recording technique, while Fig. 7 illustrates the comparison for the a -wave of the ERG for both rod-driven and cone-driven responses from human and mouse retina.

For the dark-adapted salamander rod in Fig. 6A, the predictions of Eq. (25) provide a good description of the rising phase of the response, over the entire range of intensities, from about 10 to 2000 photoisomerizations per flash, for the first 500 ms or so. At later times, however, the theoretical predictions diverge from the experimental traces, as the onset of inactivation reactions renders the simple model invalid. In this experiment, the calcium buffer BAPTA had been incorporated into the cytoplasm in order to retard the decline in $[Ca^{2+}]_i$ that normally accompanies the light response [65]. In the same cell under control conditions (prior to incorporation of BAPTA) the responses began diverging from theory at even earlier times (see Fig. 7A of [26]), showing that the earliest signs of inactivation under normal conditions are calcium mediated. Similar fits with changes in $[Ca^{2+}]_i$ pre-

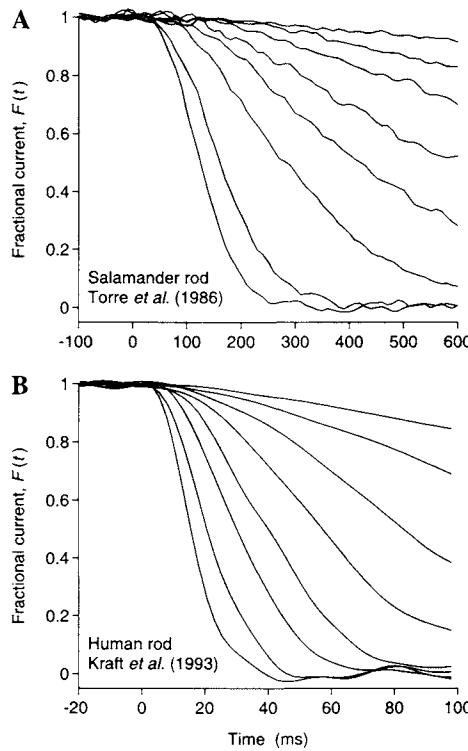


Fig. 6. Comparison of the predictions of Eq. (25) with experimentally recorded suction pipette photocurrents, for a salamander rod and a human rod. In both panels, Eq. (25) has been plotted using the calculated number of photoisomerizations, Φ , and a single value of the amplification constant and effective delay. (A) Recordings from the salamander rod illustrated in Fig. 3A, following incorporation of the calcium buffer, BAPTA; data from Fig. 2B of Ref. [65]. Dark current, -29 pA; amplification constant, $A = 0.065 \text{ s}^{-2}$; delay time, $t_{\text{eff}} = 20$ ms. (B) Recordings from a human rod, for flashes delivering from 34 to 3800 isomerizations; data from Fig. 4 of Ref. [53], kindly supplied by Dr. J.L. Schnapf. Dark current, -13.5 pA; amplification constant, $A = 2 \text{ s}^{-2}$; delay time, $t_{\text{eff}} = 2.2$ ms. In both panels the origin of time has been set to the middle of the light flash, after allowance for the delay introduced by electronic filtering.

vented have been illustrated in Figs. 10 and 11 of Ref. [120] and in Fig. 4 of Ref. [142].

Figure 6B illustrates suction pipette recordings from a human rod (from Fig. 4 of Ref. [53]). Apart from the much faster time scale (due to the higher amplification constant, A), the form of the responses is remarkably similar to that of the amphibian rod, and again the rising phase of the whole family of responses is well described by Eq. (25), out to at least 50 ms.

Figure 7 shows recordings of the a -wave of the electroretinogram (ERG) from an anesthetized mouse, under conditions that isolate rods (Fig. 7A), and from a human subject for conditions that isolate rods (Fig. 7B) or cones (Fig. 7C). There is

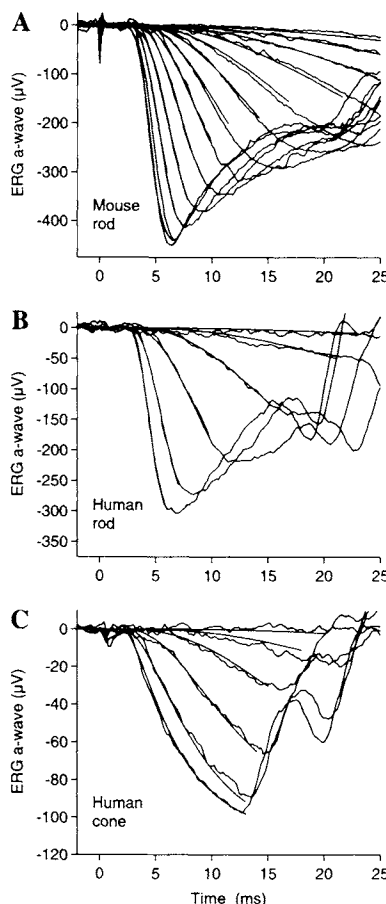


Fig. 7. Comparison of the predictions of Eq. (25) with experimentally recorded ERG *a*-waves. Prior to intrusion by the *b*-wave, the *a*-wave provides a measure of the circulating current in the photoreceptors. In each panel, Eq. (25) has been plotted using the number of isomerizations, Φ , together with constant values for the amplification constant, membrane time constant, and effective delay. (A) Mouse rod *a*-waves; data from Figs. 2 and 3 of Ref. [141]. Amplification constant, $A = 5.6 \text{ s}^{-2}$; membrane time constant ignored; delay time, $t_{\text{eff}} = 3.6 \text{ ms}$; maximal response, $a_{\text{max}} = -450 \mu\text{V}$. (B) Human rod *a*-waves; data from Fig. 5 of [139]. Amplification constant, $A = 4.5 \text{ s}^{-2}$; membrane time constant, $\tau_m = 1.1 \text{ ms}$; delay time, $t_{\text{eff}} = 2.3 \text{ ms}$; maximal response, $a_{\text{max}} = -350 \mu\text{V}$. (C) Human cone *a*-waves; data from Fig. 6 of Ref. [139]. Amplification constant, $A = 6.7 \text{ s}^{-2}$ (assuming that the conversion factor from photopic Td s to photoisomerizations per red-sensitive cone is $K_{\text{red}} = 200$ isomerizations per cone per Td s; see Ref. [139]); membrane time constant, $\tau_m = 4.4 \text{ ms}$; delay time, $t_{\text{eff}} = 1.5 \text{ ms}$; maximal response, $a_{\text{max}} = -55 \mu\text{V}$ in both the red- and green-sensitive cones. Eq. (25) is plotted solid for the early times over which fitting was performed, and is shown as gray thereafter.

now overwhelming evidence that the *a*-wave arises from suppression of the photoreceptors' circulating current [138,139,143,144], and in each panel the earliest phase of the response is well described by the theory. But in the case of ERG recordings, the discrepancy between theory and experimental traces at later times is caused by intrusion of the *b*-wave (and other post-receptor signals) rather than by the occurrence of inactivation reactions (for a discussion of the origin of these other components of the ERG, see Refs. [145,146]).

5.9. Rate of activation of G-protein and PDE

We now consider the *magnitude* of the rates of protein activation per photoisomerization, for the G-protein (v_{RG}) and the PDE (v_{RE}), determined from different experimental approaches. We stress, however, that any uncertainty in the magnitude of these parameters has no effect on the *shape* of the electrical response; it simply affects the *gain* of transduction.

Equation (27) expresses the amplification constant, A , in terms of six physical parameters of the rod (and Avogadro's number). Although the value of A can be determined accurately, either from the photocurrent responses of single cells or from the massed receptor field potentials of the rod or cone *a*-waves, in conjunction with accurate light measurements, there is much greater difficulty in estimating some of the individual parameters that underlie it.

For an amphibian rod, where $A \approx 0.1 \text{ s}^{-2}$, we can be confident that $n_{cG} = 2\text{--}3$ and $V_{cyto} \approx 1 \text{ pl}$, and we also have reasonable grounds for estimating B_{cG} to be near 2. With these parameters, Eq. (27) yields $v_{RE} (k_{cat}/K_m) \approx 10^{11} \text{ s}^{-2} \text{ M}^{-1}$ (see also Eq. (27) of Ref. [27]). Since aqueous diffusion places an upper limit on the value that can be achieved for the ratio k_{cat}/K_m of an enzyme, of around $5 \times 10^8 \text{ s}^{-1} \text{ M}^{-1}$ [147], this calculation implies that the rate of PDE* activation per photoisomerization must be around $v_{RE} \approx 200 \text{ s}^{-1}$. This estimate lies far below the diffusion-limit for the rate of activation of the G-protein, determined in Section 4.2 as $v_{enc} \approx 6000 \text{ s}^{-1}$, and also well below the estimates for v_{RG} of $1100\text{--}3300 \text{ s}^{-1}$ obtained from light-scattering experiments at room temperature (reviewed in Ref. [27]).

Until recently, the accepted values in the biochemical literature for the kinetic parameters of amphibian rod PDE, at room temperature, were $k_{cat} \approx 4400 \text{ s}^{-1}$ and $K_m \approx 100 \mu\text{M}$ [78], giving a ratio of $k_{cat}/K_m \approx 4 \times 10^7 \text{ s}^{-1} \text{ M}^{-1}$. To achieve the observed amplification of $A \approx 0.1 \text{ s}^{-2}$, in conjunction with the other parameters, one would require $v_{RE} \approx 2000 \text{ s}^{-1}$.

However, despite careful efforts (reviewed in Ref. [27]), no direct biochemical assay has ever measured a rate of G-protein or PDE activation (v_{RG} or v_{RE}) exceeding about 200 s^{-1} . Very recent work [127] provides a resolution of the conflict between the relatively low estimates of v_{RG} and v_{RE} from biochemical assays and the apparently higher values required by the analysis of the previous paragraph. The new work reports that the K_m of the amphibian rod PDE is around $10 \mu\text{M}$, nearly 10-fold lower than previous estimates. The likely explanation for the discrepancy between this newer estimate and earlier estimates arises from the fact that all previous investigations have employed full activation of the PDE (using bright light or

trypsin activation), and under these conditions the local concentration of cGMP near the catalytic sites is forced to be much lower than in the bulk solution. Only when a small proportion of the PDE is activated, so that competition for substrate is minimized, will the true K_m be observable. The importance of this 10-fold lower estimate of K_m is that the estimate of the rate of PDE* activation per R* based on Eq. (27) drops by about 10-fold, so that for an amphibian rod at room temperature the required value would be $v_{RE} \approx 100\text{--}200\text{ s}^{-1}$, in excellent agreement with direct biochemical measurements. This lower estimate of v_{RE} (and thus, of v_{RG}) resolves the apparent conflict between the physiological-based analysis and biochemical measurements, yet it does not alter the kinetic conclusions of our analysis of amplification. The new lower value for the rate of activation raises questions about the large gap between v_{RG} and its theoretical limit, given by the encounter rate v_{enc} : i.e. which molecular interaction contributes the rate-limit to the activation of G* by R*, and why is the rate of activation so much lower than the calculated rate of encounter?

5.10. Validity of the solutions, and limitations

The two main approximations made in deriving the simplified analytical solution of Eq. (25) were that all inactivation reactions could be ignored, and that the outer segment could be regarded as an isotropic compartment. We now investigate the validity of these approximations, and discuss the restrictions that need to be observed in applying the solution.

Neglect of inactivation. At least five recovery processes have been neglected in the simplified analytical solution: (i) termination of R* activity; (ii) termination of G*-E* activity; (iii) resting hydrolysis of cGMP (β_0 in Eq. (16)); (iv) the Ca^{2+} -dependent activation of GC via GCAPs ($\Delta\alpha$ in Eq. (16)); and (v) the Ca^{2+} -dependent modulation of R* shut-off via recoverin. In Section 7 we shall show that the first three of these processes each contribute an ‘effective time constant of inactivation’ to the recovery to the flash response. Numerical solution of the differential equation shows that the critical issue in neglecting inactivation is the magnitude of the shortest of these effective time constants. For example, if the shortest inactivation time constant is ca. 500 ms for a dark-adapted amphibian rod, then the analytical approximation will only be valid for times up to about 300–400 ms. For a dark-adapted mammalian rod, the time window of validity is likely to be 10-fold shorter, ending at around 40 ms. Fortunately, this does not present a significant limitation in fitting the *a*-wave of the mammalian ERG, where the photoreceptor response can only be recorded for 5–25 ms before being obliterated by the *b*-wave and other post-receptor signals (Fig. 7).

However, a serious problem arises in applying the simplified equations to single-cell responses obtained under light-adapted conditions. As we show subsequently in Section 7, even quite modest background intensities can increase the PDE rate constant of cGMP hydrolysis from its dark-adapted level of $\beta_{dark} \approx 1\text{ s}^{-1}$ (in a salamander rod) by 10-fold, to a steady level of $\beta_0 \approx 10\text{ s}^{-1}$, corresponding to an effective inactivation time constant of just 100 ms. Under these conditions the

predictions of Eq. (25) cannot be relied upon beyond the first 50–100 ms after the flash, by which time a recordable response has barely developed. In order to quantify light-adapted responses, Section 7.5 will present a more comprehensive analytical treatment that has been developed recently [142].

Neglect of longitudinal diffusion in the outer segment. Analytical treatment of the case with longitudinal diffusion in the outer segment showed that, for a single photoisomerization, the predicted response begins rising at early times along exactly the same trajectory as given by Eq. (25) with $\Phi = 1$ (Appendix B of Ref. [26]). Thus, at sufficiently early times, the neglect of diffusion in the simplified approach causes no error. More recently, by extending the numerical simulation of the ordinary differential equations for activation and inactivation to encompass the partial differential equations for longitudinal diffusion in the outer segment, we find that the lumped simplification provides a remarkably good approximation to the full case (unpublished observations; see [128]).

Other restrictions. The simplified analysis will fail at extremely high flash intensities for several reasons. First, the ‘delayed ramp’ approximation for G^* and E^* activation will be inappropriate, and it will be necessary to take explicit account of the nature of the several short delay stages discussed in the context of Eq. (24) (see Refs. [26,49,140]). Second, account has not been taken of the limited quantities of G^* and E^* available for activation, or of the occurrence of multiple R^* s on a small area of disc membrane, so that rate saturation will not be correctly predicted. Third, we have not included the contribution of the electrogenic calcium exchanger, and therefore the slow tail of decay of exchange current that is seen in saturating responses will be missing. Finally, one must be aware of the filtering effect of the cell’s membrane time constant, especially with high-intensity flashes, and if necessary use analytical or numerical convolution to take account of it [139,140]. But for intensities from less than 100 to more than 10,000 photoisomerizations the simple theory provides a reasonable approximation, valid out to at least several hundred ms in a dark-adapted amphibian rod, and for responses over an even greater range of intensities at times of up to 30–40 ms in mammalian rods.

6. Termination and modulation: The participating proteins and calcium

The second section of Table 3 summarizes the properties of the protein constituents of the rod outer segment that regulate the G-protein cascade. Three of the proteins serve to terminate or down-regulate the activity of the cascade’s two primary enzymatic amplifiers, R^* and E^* . Thus rhodopsin kinase (RK) and arrestin (Arr) in combination lead to the termination of R^* ’s catalytic activity, while RGS9 accelerates the termination of G^*-E^* activity by stimulating the intrinsic GTPase function of $G\alpha$. A fundamental feature of phototransduction is its regulation by intracellular calcium concentration, $[Ca^{2+}]_i$, and it is therefore significant that all of the modulatory proteins in Table 3, with the exception of arrestin and RGS9, are known to be calcium-dependent.

6.1. R* shut-off: Rhodopsin kinase (RK), arrestin (Arr), and recoverin (Rec)

The reactions underlying inactivation of R* are illustrated in Fig. 4B. The participating proteins are rhodopsin kinase (RK), arrestin (Arr) and recoverin (Rec).

Rhodopsin kinase. RK is a prototypical member of the family of G-protein-coupled receptor kinases (GRKs), and was in fact the first member of this family to be discovered and characterized; hence RK is also known as GRK1 [148,149]. RK and other GRKs down-regulate the catalytic activity of their corresponding GPCR by phosphorylation of serine and/or threonine residues exposed to the cytoplasm [149]. A large body of biochemical and physiological evidence indicates that phosphorylation by RK of one or more of the serine residues near the C-terminus of rhodopsin is the initial step in inactivation of R* (reviewed in Refs. [150,151]).

The earliest evidence came from biochemical studies *in vitro* [152], while additional evidence *in situ* came from electrophysiological experiments using isolated gecko rod outer segments: dialysis of rods with sangivamycin, an inhibitor of RK, greatly slowed the recovery phase of the photoresponse [153]. More recently, three studies using mice rods have provided significant constraints on the molecular mechanism by which RK operates *in vivo*. First, in mice exposed to a single flash isomerizing approximately 15% of the rhodopsin, only Ser-338 was reported to be appreciably phosphorylated; steady illumination also yielded phosphorylation at Ser-334 [154]. Second, for mice in which about 10% of the expressed rhodopsin was of a form truncated near its C-terminus, single-cell recordings showed greatly slowed recovery kinetics (despite normal activation kinetics) for approximately the same proportion (10%) of responses in a train of dim-flash ('single-photon') trials [39]. Third, in the rods of mice with RK 'knocked out', the response kinetics of all dim-flash trials were similar to those of the slowed responses in the C-terminal truncation mutation [155]. Fig. 8 compares the dim-flash responses from rods of mice lacking RK (RK -/-) with similar responses obtained from rods of normal mice, and mice lacking arrestin (discussed further below). Scaled to match in the early activation phase, the responses of the RK -/- phenotype clearly show the requirement for RK for normal shut-off kinetics. Taken together, the studies cited in this paragraph indicate that the initial event in the termination of R* activity in normal rods is either the binding of RK to R*, or else the phosphorylation of serine residues that it induces.

Arrestin. Arr is a 48 kDa protein, discovered in rods in the late 1970s [156], that was shown to reduce the catalytic activity of R* after phosphorylation [152]. It was found to be identical to a previously characterized protein – the so-called 'S-antigen', implicated in some forms of uveitis. Arrestin is a prototypical member of a family of GPCR binding-proteins, which bind to the corresponding GPCR after it has been phosphorylated, thereby 'capping' it, and preventing access of the G-protein to its binding site [86,87,157,158].

While much biochemical evidence has supported the role of arrestin in down-regulating the rod cascade *in vitro*, compelling evidence for its role *in situ* is relatively recent. First, isolated gecko rods dialyzed with heparin (an inhibitor of

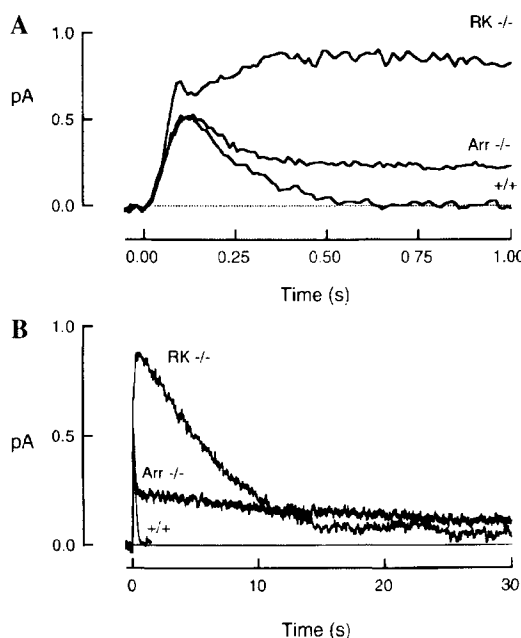


Fig. 8. Averaged photocurrents of normal ($+/+$) and transgenic mouse rods to very dim flashes, on fast (A) and slow (B) time scales. RK $-/-$ mice have null mutations in the rhodopsin kinase gene, and therefore fail to express RK; Arr $-/-$ mice have null mutations in the arrestin gene and therefore fail to express Arr. Responses have been scaled vertically to the respective single-photon response amplitudes for the three populations of cells, as follows. Wild-type ($+/+$), amplitude scaled to 0.53 pA at the peak; Arr $-/-$, scaled to the same peak as WT; RK $-/-$, scaled to 0.91 pA at the peak. Figure kindly supplied by Drs M.E. Burns and D.A. Baylor; data from [40] and [155].

arrestin binding to phosphorylated R*) show prolonged responses, particularly to bright flashes [153]. Second, responses of mouse rods with arrestin knocked out show prolonged recoveries, both for bright flashes and at the single-photon level [40]. Fig. 8 illustrates the effect of knocking out arrestin on the dim-flash response (traces labeled Arr $-/-$). While the response follows the normal pattern until its peak, shortly thereafter the trace for the Arr $-/-$ mice peels away from the normal recovery, revealing a long, slow tail having a time constant of many seconds, thus demonstrating an essential need for arrestin in normal inactivation, even following dim flashes. The electrophysiological results discussed in this paragraph are consistent with the role postulated for arrestin in the earlier biochemical investigations: namely, that arrestin binding serves to 'cap' phosphorylated R*, thereby blocking access of G-protein to the active site and thus very substantially shutting-off the ability of photoisomerized rhodopsin to activate G*.

Recoverin. Rec is a member of a family of calcium-binding proteins, the neuron-specific calcium-binding protein (NCBP) family [93]. The first member of the family to be described and characterized was calmodulin (CM). Photoreceptor-specific

members of the family include CM, Rec, GCAP1 and GCAP2. The typical size of an NCBP protein is 23 kDa (\approx 200 amino acids), and the proteins have potentially four Ca^{2+} binding sites, with EF-hand structure. The number of functional Ca^{2+} -binding sites of NCBPs varies, however. Recoverin has only two functional binding sites, with dissociation constants of 0.11 and 6.9 μM [159]. Calcium binding in the NCBP family is typically cooperative, and for normal, myristoylated bovine recoverin the cooperativity (Hill) coefficient is 1.75 and the K_1 is ca. 17 μM [159]. Rec-2Ca binds to rod disc membranes with a dissociation constant (expressed in terms of rhodopsin concentration) of ca. 200 μM ; this binding requires myristylation of the protein [88,159–162].

Kawamura [163] discovered that recoverin (which he named S-modulin in frog rods) inhibits RK-mediated phosphorylation of R* in a calcium-dependent manner, and these observations have been confirmed and extended [85,164]. The precise mechanism of recoverin's action has not yet been established, but the evidence is consistent with the hypothesis diagrammed in Fig. 4B, namely, that Rec-2Ca binds to RK in a manner that prevents the latter from binding to and phosphorylating R*. An important factor relating to recoverin, that has generally been overlooked, is that it probably constitutes the dominant calcium buffer in the rod outer segment. The recoverin concentration in amphibian rods has been estimated as around 30 μM [85,163].

For further review, see Refs. [89,93,149,151].

6.2. G*-E* shut-off: RGS9, G β 5 and phosducin

One of the most elusive problems in research on the photoreceptor G-protein cascade has been the role of hydrolysis of the terminal phosphate of G* (=G α -GTP) in response termination. Early biochemical investigations established incontrovertibly that GDP/GTP exchange acted as the activation switch [165,166], but the role of terminal phosphate hydrolysis in inactivation remained highly controversial for many years. In the 1980s a number of investigations reported time constants for hydrolysis of the terminal phosphate of G α -GTP *in vitro* of many tens of seconds (reviewed in Ref. [131]). The problem was that these values were up to 100-fold slower than the 'dominant time constant' of recovery of the flash response. The dominant time constant is the slowest time constant apparent in the recovery of rod responses *in situ*; it is about 2 s in amphibian rods, and about 0.2 s in mammalian rods [120,141,167,168].

By the mid-1990s the consensus view was that at least two 'GTPase-accelerating proteins' (GAPs) must be present in the living outer segment, but ineffective *in vitro*. One was established to be the γ subunit of the PDE, i.e., the target binding site of G α -GTP [169–172]. Recently, a second disc-associated GAP factor has been discovered, now named Regulator of G-protein Signaling, 9 (RGS9) [91], and a third cofactor, type 5 G-protein β subunit (G β 5), has also been implicated [92].

Although many details remain to be elucidated, the results published to date are consistent with the biochemical scheme presented in Fig. 4C. During the activation phase, G* binds to the PDE γ subunit, to form the activated PDE, denoted as

G^*-E^* . The critical feature in termination of activity is that RGS9–G β 5 binds to (G α -GTP)–PDE γ to form (at least transiently) a quaternary complex: RGS9–G β 5–(G α -GTP)–PDE γ . Formation of this complex may allow access of water to the GTP-binding site, which (unlike the representation in the simplified schematic in Fig. 4) is located in the interior of the G α subunit. It is probably most realistic to view this interaction as tripartite, because the RGS9–G β 5 complex is so tightly bound that it can effectively be regarded as a single entity [92].

The requirement for concerted action of three distinct entities is almost certainly related to the need to time the shut-off of G^*-E^* . The slow GTPase rate intrinsic to G^* allows high efficiency of cascade activation, by ensuring that excitation does not normally decay until the G^* has bound to the PDE effector enzyme. However, once the PDE has had an opportunity to function, then it is critical that the activity of the cascade is terminated rapidly, so that the photoreceptor can recover quickly and be ready to respond to further illumination. The employment of a third protein complex (the RGS9–G β 5) to detect and quench the active state of G^*-E^* seems ideally suited to achieving the desired timing [173].

Phosducin. Phosducin (PD) is a 28 kDa soluble ‘phospho-protein’ that binds tightly to G $\beta\gamma$ when G α is not attached [174–178]. Although no function has yet been established for PD in phototransduction in living rods, it bears mention for several reasons. First, it is present in mammalian rod outer segments at a concentration at least as high as the G-protein. Second, its capacity to bind to G $\beta\gamma$ is regulated by a cycle of phosphorylation–dephosphorylation: G $\beta\gamma$ only binds to phosducin when PD is unphosphorylated [95]. Third, the phosphorylation is regulated by protein kinase A (PKA), which is in turn regulated by CM [179]. Fourth, PD is a member of a family of phosducin-like phospho-proteins ('Phlops') which appear to play modulatory roles in other G-protein cascades (e.g., [180,181]).

Phosducin could function during light adaptation to lower the amplification constant of mammalian rods (Section 5.7) by effectively removing holo-G-protein from the available pool. While there is at present no experimental evidence to support this hypothesis, it remains possible that such a mechanism could be used by the rod primarily when it is in saturation, and therefore not signaling. Lowering the gain of the cascade while the rod is in the saturated, non-signaling state would conserve metabolic energy that would otherwise be spent in vain.

6.3. Regulation of cGMP synthesis:

Guanylyl cyclase (GC) and its activating proteins (GCAPs)

Guanylyl cyclase. In order to maintain a cGMP concentration of the order of 1 μ M in the face of hydrolysis by PDE, either in the dark or in the presence of steady light, it is necessary for synthesis of cGMP to occur. This is mediated by guanylyl cyclase (GC), an enzyme that synthesizes cGMP from GTP. Two general classes of guanylyl cyclase exist – soluble and membrane-bound ('particulate') – and the rod GC is of the latter class. The rod guanylyl cyclase appears to function as a dimer, formed by a pair of identical 110–114 kDa proteins, and it is present in the disc membrane at a concentration (surface density) of around 0.2–0.5% that of rho-

dopsin – i.e., from around 1 GC:500 R (Table 3) to 1 GC:200 R (K.-W. Koch, personal communication).

At least two distinct particulate guanylyl cyclases (termed GC1 and GC2) have been found in photoreceptors, but their functional differences and distinctive roles (if any) in rods and cones are not yet clear. Both have been identified in a number of species, where they have been given various names. GC1 has been localized to the outer segments of both rods and cones [182–184], and its properties measured *in vitro* appear consistent with the GC activity deduced from electrophysiological experiments on intact and truncated rods (reviewed in Ref. [81]). GC2 has been localized to the outer segments of rods [185], and appears to have properties broadly similar to, though distinct from, those of GC1. Recent work in which GC-E, the rodent homologue of GC1, has been knocked out in mice, shows that rods lacking GC1 can nonetheless generate normal circulating currents, suggesting the possibility that GC2 either accounts for basal cyclase activity, or can substitute for GC1 [186]. Interestingly, cones degenerate in the GC-E knockout mice at 4–5 weeks, suggesting that GC-E is necessary for cone function [186]. This latter result is consistent with previous evidence that homologues of GC1 are strongly expressed in the cone outer segments of some species [184].

A fundamentally important feature of photoreceptor GCs is their regulation by intracellular Ca^{2+} concentration. Although it has been shown that other particulate GCs, with weak homology to the rod GC, are regulated by extracellular signals such as ANF [187], the only established regulation of rod outer segment guanylyl cyclase activity *in situ* is by either of two calcium-binding 23 kDa ‘guanylyl cyclase activating proteins’ (GCAP1 and GCAP2) [188–190]. Thus, it is GCAPs that confer functional Ca^{2+} -sensitivity on guanylyl cyclase.

Guanylyl cyclase activating proteins. GCAPs are members of a large family of calcium-binding proteins, which includes CM and Rec. The mode of GCAP’s action in stimulating guanylyl cyclase is illustrated schematically in Fig. 4A. In the dark, when $[\text{Ca}^{2+}]_i$ is relatively high (Table 2), a high proportion of GCAP molecules have Ca^{2+} ions bound to them, and in this form they remain soluble in the cytoplasm and do not interact with the guanylyl cyclase. But when the Ca^{2+} concentration declines during the light response, Ca^{2+} ions unbind and the calcium-free form of GCAP is able to bind to a cytoplasmic site on the GC, thereby switching on its enzymatic activity. The quantitative details of this activation will be presented in Section 7.5.

Physiological and biochemical investigations had established the logical need for, and the existence of, a calcium-dependent regulator of the rod guanylyl cyclase a decade before the first such protein, GCAP1, was positively identified [188,190]. A second and distinct GC regulator, GCAP2, was soon discovered [191,192]. Although both types of GCAP have been shown to regulate the guanylyl cyclase activity of rod outer segments, it has been established through work with recombinant GC mutants that they act at distinct cytoplasmic epitopes, with GCAP1 acting near the N-terminal and GCAP2 acting near the C-terminal [193,194]. Both GCAPs activate GC1, but the saturated activity evoked by GCAP2 is higher than that evoked by GCAP1 [193,194]. Investigations underway in several laboratories, using mutant mice with different combinations of GCs and GCAPs knocked out, should soon

help to resolve the roles of these four proteins in mammalian rod phototransduction.

In cones, too, guanylyl cyclase is of course present and regulated by calcium [56,195]. In contrast with other enzymes of the transduction cascade, which are expressed as distinct isoforms in rods and cones, it seems that GCl is expressed in both classes of cell [182,183,196], along with GCAP1 [197].

6.4. Ca^{2+} efflux: The $\text{Na}^+/\text{Ca}^{2+}, \text{K}^+$ exchanger (NCKX)

Virtually all tissues seem to express one or more forms of $\text{Na}^+/\text{Ca}^{2+}$ exchanger (NCX); in particular, the NCX1 gene has been reported to be expressed ubiquitously in mammalian tissues, along with several isoforms and splice-variants [198–202]. $\text{Na}^+/\text{Ca}^{2+}$ exchangers use the energy stored in the transmembrane Na^+ concentration gradient to extrude Ca^{2+} against its electrochemical gradient, which exceeds 1000-fold in most cells. The standard stoichiometry of operation for the $\text{Na}^+/\text{Ca}^{2+}$ exchanger is 1 Ca^{2+} extruded in exchange for 3 Na^+ ions entering. The NCX molecule is thought to comprise 11 transmembrane segments, and contains a large hydrophilic domain between the fifth and sixth segments that appears likely to serve in ion translocation [200–202].

The exchanger in the rod (and probably cone) outer segment is of a distinct variety from the NCX exchanger, because it has an obligatory requirement for internal K^+ ; to highlight this distinctive requirement, we adopt the label 'NCKX'. The normal stoichiometry of the rod exchanger was established to be 1 Ca^{2+} and 1 K^+ extruded, in exchange for 4 Na^+ ions entering [203]. The functional utility of the distinctive stoichiometry was proposed to be its ability to reduce the cytoplasmic calcium concentration to a lower level than was possible with the conventional exchanger [203]. In the absence of any other Ca^{2+} influx or efflux pathways (e.g., when the cGMP-gated channels are completely closed), the NCKX on its own could theoretically set a final steady-state level of internal free calcium concentration, $[\text{Ca}^{2+}]_i$, given by the relation

$$[\text{Ca}^{2+}]_i = [\text{Ca}^{2+}]_o \frac{[\text{Na}^+]_i^4 [\text{K}^+]_o}{[\text{Na}^+]_o^4 [\text{K}^+]_i} \exp(V_m F / RT) \quad (28)$$

(analogous to the Nernst potential relation). The fourth-power dependence of $[\text{Ca}^{2+}]_i$ on the inward Na^+ concentration gradient, and the assistance provided by the outward K^+ gradient, in principle enable the rod to achieve $[\text{Ca}^{2+}]_i$ concentrations less than 1 nM in the light, as much as 500-fold lower than would be possible if the standard NCX stoichiometry applied [203]. Although it is extremely doubtful that this theoretical limit could be approached under any physiological conditions, the calculation nonetheless shows the potential utility of the NCKX mechanism. A low $[\text{Ca}^{2+}]_i$ in the light is needed to ensure that guanylyl cyclase is maximally activated, and might also serve to maximally engage other calcium-dependent inactivation processes, as discussed below.

The genes for bovine and human photoreceptor NCKX1 have been cloned [204,205], and while hydropathy plots are consistent with the 11-transmembrane

segment model of the NCX family, the sequence homology between the two gene families is quite small except in the transmembrane segment region. The first functional expression of the bovine NCKX in a heterologous system could not demonstrate the K^+ sensitivity that is the hallmark of the exchanger [206], but this sensitivity has been found in a more recent heterologous expression of dolphin NCKX [207].

For further review, see Refs. [41–43,200,202,208,209].

6.5. Regulation of the cyclic GMP gated channel by CM

Calmodulin (CM), a ubiquitous calcium binding protein with four functional EF-hand motifs, is present in frog and bovine rods at a concentration of 5–10 μM [94,210,211]. Calmodulin binds four Ca^{2+} ions in a highly cooperative manner, with a K_1 of about 2.4 μM [212]. The calcium-associated form, Ca–CM, binds to the cGMP-gated channels of rods, and this binding increases the affinity of CM for Ca^{2+} by 10-fold or more [94], with the result that most of the channels have Ca–CM bound in the dark-adapted state. There are two sites for CM binding on the rod channel, on the N- and C-terminal cytoplasmic tails of the β subunit [213,214]. The binding of Ca–CM to the channels increases the K_{cG} of the channels for cGMP by about 1.5-fold, without altering the Hill coefficient or the maximal current [94,215,216].

From these properties of CM and its interaction with the cGMP-gated channels, it can be predicted that the dissociation of CM from the channels at lowered $[Ca^{2+}]_i$ will, by increasing their affinity for cGMP, serve to restore some of the circulating current that would otherwise be suppressed during exposure to steady light. In rods, though, this restoration effect is predicted to be relatively small [94,136,217]. For cone channels, a related but much more powerful mechanism exists, that utilizes a calcium-binding protein distinct from CM [218].

7. Recovery phase of the response: Predicted form of flash families

7.1. Equations for the inactivation of R^* and of G^*-E^*

Inactivation of R^ .* As discussed in Section 6.1, the catalytic activity of R^* is decreased by RK-mediated phosphorylation and by the subsequent binding of arrestin. The phosphorylation of a single R^* is inherently a stochastic event: that is, the attachment of a single phosphate is a discrete (rather than a gradual) event, and furthermore it will occur not at a precisely repeatable time after each photoisomerization, but at a time exhibiting some randomness (to a degree that will depend on the precise nature of the mechanisms involved). From a simple model analogous to that in Section 4.2 (Eqs. (2) and (3)), the mean time to first encounter between an R^* and an RK would be of the order of 10 ms in an amphibian rod, and 3–4 ms in a dark-adapted mammalian rod (assuming the density to be 1 RK per 500 rhodopsin molecules; Table 3). However, at least 70% (and perhaps more than 90%) of the RK is expected to be complexed with Rec-2Ca in the dark-adapted rod, and any en-

counter between R^* and Rec-2Ca-RK is unlikely to be successful, since the latter does not phosphorylate R^* (Section 6.1). Allowing for the amount of RK complexed with Rec-2Ca, the time to initial encounter between R^* and a free RK in a dark-adapted rod may exceed 100 ms in amphibian rods and tens of milliseconds for mammalian rods. Since it is unlikely that every encounter between an R^* and an RK will lead to binding and phosphorylation, it follows that the time to a 'productive' encounter could be several hundred milliseconds in amphibian rods, and several tens of milliseconds in mammalian rods.

Likewise, the binding of arrestin to R^*-P would be a stochastic event, though the expected time for initial encounter would be much shorter, due to the much higher concentration of Arr. It follows that once an R^*-P is produced, its capping by arrestin is likely to occur relatively rapidly.

Although it is critical to take account of the stochastic nature of R^* shut-off when analyzing single-photon events, the responses to flashes delivering many photons (say 10 or more) can be treated by the much simpler 'mean' behavior. In particular, if one assumes that the stochastic termination of R^* activity occurs with a rate constant that is independent of time, then the average time-course of $R^*(t)$ following a brief flash will be a simple exponential decay, characterized by an effective time constant τ_R (see Fig. 9A). This assumption clearly represents an oversimplification of the actual molecular mechanism (as discussed in Section 8), it nevertheless constitutes a productive starting point for analysis [142].

Inactivation of G^-E^* .* As discussed in Section 6.2, it is now apparent that under physiological conditions inactivation of G^* does not occur significantly until the G^* is bound to PDE γ (in the active E^* complex), and in addition a second GAP factor, the RGS9-G β 5 complex, also binds. Although the inactivation of each individual $G^*-E^*-RGS9-G\beta5$ ternary complex will again be stochastic in nature, the time-course of $E^*(t)$ can be treated by mass action principles because there will typically be at least hundreds of activated E^* complexes present during most of the response to a single R^* . In other words, if a population of E^* 's were created instantaneously at $t = 0$, then as time proceeded the average number still active would decay exponentially with a time constant τ_E .

Combining the mass action inactivation reactions for R^* and G^*-E^* , the equation for $E^*(t)$ derived previously in Eq. (5) in the absence of inactivation can be replaced by

$$E^*(t) = \Phi v_{RE} U_{RE}(t - t_{RGE}) \quad (29)$$

where the function $U_{RE}(t)$ represents the convolution of a ramp with two first-order time constants τ_R and τ_E , and is defined by

$$U_{RE}(t) = \frac{\exp(-t/\tau_R) - \exp(-t/\tau_E)}{\tau_R - \tau_E} \tau_R \tau_E, \quad \text{for } t > 0 \quad (30)$$

Equation (29) is plotted in Fig. 9B. Note that as $t \rightarrow 0$, when the exponential terms admit first-order expansion, $U_{RE}(t) \rightarrow t$ (i.e., a unit ramp), so that at very early times Eq. (29) is identical to Eq. (5).

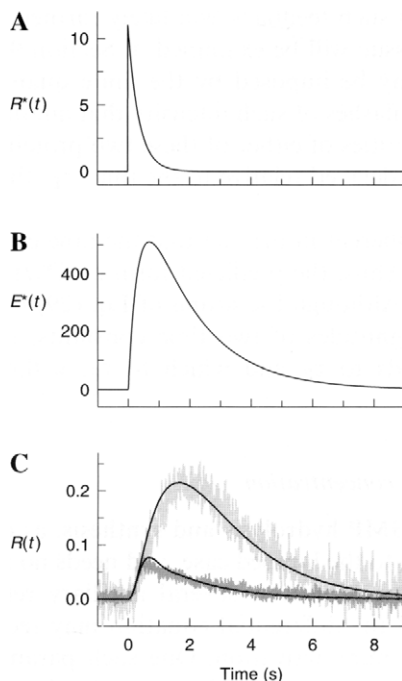


Fig. 9. Predicted kinetics of recovery for R^* , E^* and the electrical response. Compare these traces with the pure activation model in Fig. 5. (A) Following photoisomerization, the average number of R^* 's is predicted to decline exponentially, with time constant τ_R . (B) The number of activated PDEs, $E^*(t)$, as predicted by Eq. (29). The initial rising phase has exactly the same slope, Φv_{RE} , as in the case of pure activation. The shape of the function is derived from the convolution of the R^* activity in A with the impulse response for E^* activity, which has a time constant of τ_E . (C) Electrical response, in the cases where calcium is either clamped (upper trace) or free to change (lower trace), as predicted by numerical integration of Eqs. (16) and (31), with E^* time course as in panel B (Eq. (30)), and with Eqs. (22), (32) and (33). The noisy traces are normalized responses of a salamander rod to stimuli estimated to deliver 11 photoisomerizations per flash, in calcium clamping solution (larger response) and in Ringer's solution (smaller response); data from Fig. 13 of Ref. [142]. For the theoretical traces in this figure, the parameters of activation were: $\Phi = 11$ photoisomerizations; $v_{RE} = 150 \text{ s}^{-1}$; $A = 0.16 \text{ s}^{-2}$ (implying $\beta_{\text{sub}} \sim 4 \times 10^{-4} \text{ s}^{-1}$). The primary parameters of inactivation were: $\tau_R = 0.35 \text{ s}$; $\tau_E = 1.7 \text{ s}$; $1/\beta_{\text{dark}} = 0.9 \text{ s}$; the additional parameters specifying calcium feedback are given in Ref. [142].

Limitations. As mentioned above, the assumption of first-order termination of R^* activity ignores any dynamic modulation of the R^* shut-off reaction. This issue will be examined in Sections 8.3.3 and 9.3, where we consider the possibility of Ca^{2+} feedback onto R^* lifetime via recoverin and RK. The assumption of first-order termination also ignores any stochastic features of R^* inactivation, which will clearly be important for the description of the single-photon response. The stochastic termination of R^* activity may in part be governed by the calcium-recoverin

feedback mechanism, and such feedback will likely further result in deviation from exponential decay. This issue will be examined in Section 9.

Another limitation may be imposed by the finite quantity of RGS9-G β 5 and PDE (Table 3). Thus, for flashes of such intensity that amounts of G* are generated in excess of the total quantities of either of these two proteins, the inactivation time of the 'excess' G* may be delayed relative to the time, τ_E , that applies at lower flash intensities.

A third limitation is inherent in the fact that the time constants in Eqs. (29) and (30) are interchangeable. Thus, the predicted form of $E^*(t)$ remains unaltered if τ_R and τ_E are interchanged. Although the fitting of Eq. (29) to the results (see Figs. 9 and 10) provides the magnitudes of two time constants, it is not possible to determine which corresponds to τ_R and which to τ_E , without additional evidence [142].

7.2. Equations for cGMP concentration

The relation governing cGMP hydrolysis and synthesis, as expressed in Eq. (13) or (16), is completely general to the lumped case, and needs no modification in order to describe response recovery. However, several ancillary relations and parameters implicit in the solution of the differential equation may require modification from those used in the case of pure activation. One such parameter is the incremental cyclase activity, $\Delta\alpha(t)$, which was previously assumed to be negligible, but which will now require explicit formulation (Section 7.4), because of the dynamic change in $[Ca^{2+}]_i$ that accompanies the light response.

7.3. Equations for calcium fluxes and concentration

On the assumption that the only calcium fluxes into or out of the cytoplasm are carried by the cGMP-gated channels and the NCKX exchanger, and that the outer segment behaves as a well-stirred compartment, the differential equation governing the free calcium concentration can be expressed as

$$\frac{dCa}{dt} = -\frac{\frac{1}{2}f_{Ca}J_{cG}(t) - J_{ex}(t)}{\mathcal{F}V_{cyto}B_{Ca}} \quad (31)$$

where Ca symbolizes $[Ca^{2+}]_i$, J_{ex} is the electrogenic exchange current, f_{Ca} is the fraction of the current, J_{cG} , through the cGMP-gated channels that is carried by Ca^{2+} , B_{Ca} is the buffering power of the cytoplasm for calcium, and \mathcal{F} is Faraday's constant (the charge carried by a mole of monovalent cations) [50,70,121,136]. Note that the minus sign multiplying the equation arises from the convention that current flowing outward across the membrane is positive; thus J_{cG} and J_{ex} are normally both negative. The factor multiplying $f_{Ca}J_{cG}$ is $\frac{1}{2}$ because each Ca^{2+} ion carries two charges, while the factor multiplying J_{ex} is unity because the extrusion of each Ca^{2+} ion is accompanied by the net movement inward of a single positive charge, i.e., $4Na^+ - (Ca^{2+} + K^+)$.

An expression for J_{cG} was derived in Section 5.6, while J_{ex} has been found to follow the Michaelis saturation relation [70]

$$\frac{J_{ex}(t)}{J_{ex,sat}} = \frac{Ca(t)}{Ca(t) + K_{ex}} \quad (32)$$

where $J_{ex,sat}$ is the maximal exchange current, and K_{ex} is the half-saturating Ca^{2+} concentration of the exchanger. For salamander rods K_{ex} has been estimated as 1.6 μM , and $J_{ex,sat}$ as about 20 pA [70].

7.4. Equations for calcium-dependent activation of guanylyl cyclase

The relationship between free calcium concentration and the activity of GC can be expressed as

$$\alpha(t) = \alpha_{min} + \frac{\alpha_{max} - \alpha_{min}}{1 + (Ca(t)/K_{cyc})^{n_{cyc}}} \quad (33)$$

Here α_{min} is the residual component of cyclase activity at very high calcium concentrations, and $(\alpha_{max} - \alpha_{min})$ is the calcium-sensitive component of cyclase activity, while K_{cyc} is the calcium concentration for half-maximal activation, and n_{cyc} is the cooperativity coefficient. This equation has been shown to provide a good account of rod GC activity in a number of *in vitro* measurements, using $\alpha_{min} = 0$. Eleven studies of mammalian rod GC near body temperature reported values of K_{cyc} ranging from 30 to 280 nM (154 ± 95 nM, mean \pm s.d.), and six of the studies provided estimates of n_{cyc} ranging from 1.7 to 3.9 (2.0 ± 0.3 , mean \pm s.d., after exclusion of a single outlier at 3.9) (reviewed in Ref. [81]).

A limitation of most *in vitro* studies of GC activity is that the absolute rates are not readily quantifiable in units applicable to physiology; e.g., in $\mu\text{M s}^{-1}$ with respect to the cytoplasm of a single rod. However two investigations of amphibian rods deserve special mention, because they overcame these limitations. Experiments with truncated and dialyzed toad rods gave estimates of $\alpha_{max} \approx 20-30 \mu\text{M s}^{-1}$, $\alpha_{min} \approx 0$, $K_{cyc} = 100$ nM, and $n_{cyc} = 2$ [121], while experiments with fractured bull-frog rods gave estimates of $\alpha_{max} \approx 10 \mu\text{M s}^{-1}$, $\alpha_{min} = 1.9 \mu\text{M s}^{-1}$, $K_{cyc} = 250$ nM, and $n_{cyc} = 1.8$ [122]. Other studies using intact vertebrate rods are reviewed in Table II of Ref. [81].

7.5. Solution for the flash response in the presence of inactivation reactions

The solution for the flash response in the presence of inactivation reactions can be obtained by solving the differential equation for cGMP metabolism, Eq. (16), with the ‘output’ given by the CNG channel relation, Eq. (22), with the time-course of E^* specified by Eqs. (29) and (30) and the PDE hydrolytic activity given by Eq. (12), and with ‘calcium feedback’ specified by Eqs. (31)–(33). Solutions have recently been obtained, both analytically and numerically, in the interesting (but also complicated) case where the internal calcium concentration is free to change, as well as in the more straightforward case where the calcium concentration is clamped [142].

The predicted time-course for R^* , E^* , and the electrical response, are presented graphically in Fig. 9.

Protein activation and recovery. Fig. 9A plots the exponential decline in R^* activity predicted for the population of molecules, while Fig. 9B plots the time-course of E^* activity, described by the function $U_{RE}(t)$ in Eq. (30). In the language of systems theory, this equation is the convolution of two exponentially decaying functions: the R^* activity (with time constant τ_R) and the E^* activity (with lifetime τ_E).

It is interesting to compare the predictions for R^* and E^* in Figs. 9A and 9B with the corresponding predictions in Fig. 5, where inactivation was ignored. In the absence of inactivation, each photon generates a step increase in R^* , and this increase is maintained indefinitely; in the presence of R^* inactivation, the mean number of active molecules, $R^*(t)$, declines exponentially with time constant τ_R . In both Figs. 5A and 9B the activity of E^* is predicted to begin rising linearly (i.e., as a ramp with time). The effects of inactivation are only seen at later times, and $E^*(t)$ is found to recover with a final time constant given by the slower of τ_R and τ_E .

cGMP and the electrical response. The time-course of PDE hydrolytic activity, defined by the PDE time course in Fig. 9B, then acts as the ‘driving function’ for the hydrolysis of cGMP, and the resulting cGMP concentration determines the electrical response. In the simpler of the two cases that we wish to consider, the cytoplasmic calcium concentration is clamped, so that no change in the cyclase activity is permitted; i.e., $\Delta\alpha(t) = 0$. In this case the predicted time-course of cGMP concentration is obtained as the convolution of the incremental PDE activity, $\Delta\beta(t)$, with the impulse response of a ‘first-order filter’ with time constant $1/\beta_0$. The resulting expression for $\Delta cG(t)$ therefore corresponds to a cascade of three first-order reactions, with time constants of τ_R , τ_E and $1/\beta_0$. This solution can be expressed as the weighted sum of three exponential terms with these time constants (Eq. (19) of Ref. [142]).

In the normal (unclamped) case, where the cytoplasmic calcium concentration is free to change, the equations for calcium metabolism, (31)–(33), must also be included, in order to predict the response. The analysis in this case is more complicated, and the small signal response (obtained by deriving linear approximations for the equations) is intrinsically second order [35,63,142,220]. The solution for $\Delta cG(t)$ is given by Nikonov et al. (Eq. (20) of Ref. [142]; see also Eq. (19) of Ref. [63]).

The kinetics of the electrical response predicted in the two cases (calcium clamped and calcium free to change) are shown in Fig. 9C as the smooth traces (where they are also compared with experimental responses obtained under the respective conditions; noisy traces). Importantly, the early rising phase of the predicted response is the same in the two cases, and furthermore is the same as in the absence of inactivation. Thus, as in Fig. 5C, the electrical response at early times is again predicted to follow the delayed Gaussian time-course, $R(t) \approx \frac{1}{2}\Phi At^2$ (where the short delay t_{eff} has been ignored).

In both cases, the driving function of PDE activity, $\Delta\beta(t)$, is the same, as illustrated by the trace in Fig. 9B. In the calcium-clamped case, the cGMP concentration is simply the convolution of this trace with an exponential decay of time constant

$1/\beta_0$. In the unclamped case, $\Delta\beta(t)$ is instead convolved with a second-order function, representing the impulse response of the feedback loop: cGMP → current → Ca^{2+} → cyclase → cGMP (see Eq. (A6.8) of Ref. [142]). Thus, the differences between the two predicted curves in Fig. 9C correspond to activation of the guanylyl cyclase feedback loop. The intrinsically second-order character of the equations describing the feedback loop has been noted by other investigators [35,63,220].

In both cases, the steady-state cGMP-hydrolysis rate constant β_0 has an important role in shaping the dim-flash responses. In the calcium-clamp condition its reciprocal, $1/\beta_0$, is one of the three time constants in the cascaded reactions, and it therefore affects both the speed and amplitude of the response. In the normal Ringer's condition the role of β_0 is less obvious, because of the complexity of the relations governing the feedback to the cyclase, i.e., Eqs. (31)–(33). Nevertheless, it can be shown that β_0 retains an important role in determining the shape and amplitude of the dim-flash response, particularly in the presence of steady illumination, which causes β_0 to increase above its dark-adapted value β_{dark} (see Section 8). At very late times, the final form of recovery of the electrical response is determined by the slowest of the three time constants τ_R , τ_E and a third time constant, which can be shown to be smaller than $1/\beta_0$ (Eq. (6.8) of Ref. [142]).

Brighter flashes: non-linearity. For brighter flashes the predicted responses cannot be obtained analytically, because of the existence of non-linearities in the set of equations, and instead numerical integration is required. In Fig. 10 the responses of a salamander rod at a range of sub-saturating flash intensities are compared with the predictions of numerical integration [142].

7.6. Validity of the solutions, and limitations

Perhaps the most important caveat in the theoretical prediction of the flash response is the approximation of the decay of R^* activity as a simple exponential with time constant τ_R . This issue will be considered further in Section 8.

Another concern is that the Michaelis relation in Eq. (32) might oversimplify the behavior of the exchange current, which exhibits at least two components of decay following a saturating flash [73,74,221]. This does not in fact appear to be a shortcoming. Rather it seems likely that the occurrence of distinct components in the decay of exchange current results from the release of Ca^{2+} from binding sites with different affinities, and that this in no way conflicts with Eq. (32). A distinct but related concern stems from the voltage-dependence of the exchange current [70]. Although the hyperpolarization of the rod can be neglected in computing the decline in cGMP-gated current (Eq. (22)), because of the shallowness of the current-voltage relation for the cGMP-gated channels, the corresponding approximation may not be appropriate when considering the behavior of the NCKX. However, neglect of the exchanger's voltage-dependence will cause least error in the case of dim flashes, which elicit minimal hyperpolarization.

Another concern, mentioned in the presentation of Eqs. (29) and (30), is the allocation of the two time constants to τ_R and τ_E . This issue will be examined in Section 8.3.3, after we review additional evidence relating to light adaptation.

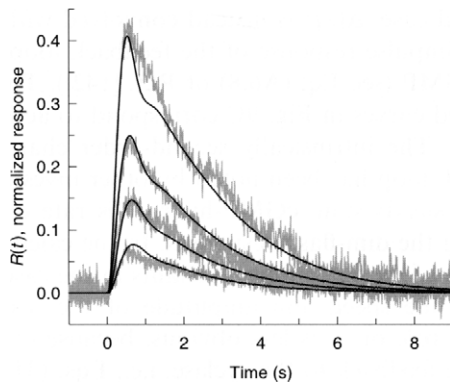


Fig. 10. Dim-flash responses for salamander rod: 4 intensities. Flash responses of a salamander rod at four dim intensities, compared with theoretical predictions. The responses were obtained in Ringer's solution from the same rod as those in Fig. 9, and are replotted from Fig. 12 of Ref. [142]. For the theoretical traces in this figure the number of photoisomerizations was $\Phi = 11, 23, 45$ and 94 , respectively. The parameters were as in Fig. 9.

A more general set of concerns for validity arises because of the considerable number of additional parameters that must be assigned values in order to predict the response (see Tables III and IV in Ref. [142]), including for example, the total cGMP-activated current. The need for independent estimates of numerous parameters in order to apply the theory of recovery contrasts with the simplicity of the theory of activation, which depends largely on a single parameter, the amplification constant, A (Eqs. (25) and (26)). One parameter required for the analysis applied to the responses in Figs. 9 and 10, whose value has been questioned, is B_{Ca} , the buffering capacity for calcium. It bears emphasis that B_{Ca} is expected to depend on $[Ca^{2+}]_i$ and that the treatment of Nikonov et al. [142], used here, deals only with the dark-adapted rod, in which B_{Ca} will be determined by the dark level of $[Ca^{2+}]_i$. Extension of the analysis to light-adapted responses requires explicit consideration of the dependence of B_{Ca} on $[Ca^{2+}]_i$. As we suggested earlier, recoverin may well be the dominant high-affinity calcium buffer in the rod, and so a natural extension of the preceding theoretical approach is to incorporate recoverin's calcium-dependence in modeling the buffering. For a discussion of this issue, see Ref. [222].

8. Light adaptation: A composite of activation, termination and modulation

The average surface illumination of the earth varies over 11 orders of magnitude during a cycle of day and night [223]. To function effectively over the diurnal cycle the visual system needs the capacity to adjust automatically to the ambient illumination. Under most circumstances this adjustment, known as 'light adaptation', occurs very rapidly. However, the rapid automatic adjustment breaks down under one condition – the return to total darkness after exposure to an extremely intense

'bleaching' light – and this special case is usually known as 'dark adaptation' or 'bleaching adaptation'.

Part of the adaptational adjustment of the retina is effected by switching between rod and cone circuitry, with rod pathways governing the lowest 3–4 decades of sensitivity, and cone pathways the remainder. This division of labor corresponds to the profound functional differences between rods and cones, which can be expressed by two statements: (1) rods reliably signal the capture of single photons (Section 9); and (2) cones never saturate in response to steady illumination [224–226]. In evolutionary terms, it seems that vertebrates first evolved a cone system that was able to function from sunlight down to moonlight conditions, and that subsequently, when rods evolved with their ability to detect single photons, an additional pathway was 'tacked on' to the retina, enabling the organism to function at far lower intensities [227].

The ability of cones to escape saturation endows them with a prodigious operating range – a feature that has been sacrificed in rods, possibly as a consequence of the molecular mechanisms needed to achieve single-photon detection. Although rods are found to saturate at moderate intensities, they do nevertheless retain the ability to adapt over a range of low background intensities [134,228–231]. As we shall explain, this adaptation serves to extend the range of intensities over which they are able to operate. Because much more is at present known about the molecular mechanisms of light adaptation in rods, this section will focus primarily on those cells, though the principles also apply to cones.

For other recent reviews of light adaptation, see Refs. [74,119,209,232,233].

8.1. General characteristics of light adaptation:

Response desensitization and acceleration, and calcium dependence

Photoreceptor light adaptation is characterized by a reduction in sensitivity and an acceleration of response kinetics [56,229,230,234–236]. The flash sensitivity, S_F (defined as the peak amplitude of the dim-flash response divided by the number of photoisomerizations) obeys Weber's Law, declining approximately inversely with steady intensity over the cell's 'operating range' of background intensities; in salamander rods, the Weber range occupies roughly 2–3 decades of background intensity (Fig. 11B). Associated with the decline in sensitivity is a speeding-up of the response recovery, illustrated in the case of dim-flash responses in Fig. 12.

A wealth of evidence indicates that cytoplasmic calcium concentration plays a central role in photoreceptor light adaptation. When $[Ca^{2+}]_i$ is maintained near its resting (dark) level, rods and cones fail to show normal adaptational behavior, and instead function over only a very restricted range of intensities [56,231,237,239–241]. Figs. 11A and 11B plot the steady-state circulating current and flash sensitivity of salamander rods from several studies, with $[Ca^{2+}]_i$ either free to change (open symbols) or clamped (filled symbols). These results illustrate the severe range restriction imposed by blocking the normal decline in $[Ca^{2+}]_i$, and conversely they show that the operating range is extended more than 100-fold when $[Ca^{2+}]_i$ is free to change.

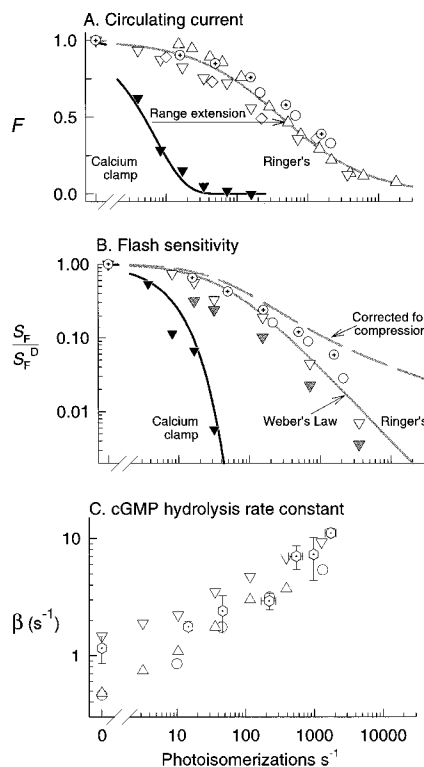


Fig. 11. Normalized circulating currents (A), flash sensitivities (B) and steady-state cGMP hydrolysis rate constants (C) of salamander rods as a function of the intensity of steady illumination (note that all panels share a common abscissa). Open symbols represent data obtained in Ringer's solution; the filled triangles represent data obtained in a solution that held $[Ca^{2+}]_i$ at its resting (dark) level, while the gray-filled symbols in panel B illustrate data obtained in solutions that held $[Ca^{2+}]_i$ at the lowered levels set during a prior exposure (in Ringer's solution) to a steady background of the given intensity. The data were taken from the following studies. In panels A, B: \diamond from Fig. 2 of Ref. [118]; \blacktriangledown and ∇ , Fig. 2 of Ref. [237]; open up triangles, Fig. 9 of Ref. [136]; \circ , \odot , from Ref. [119]. In panel C: \circ from Fig. 2 of Ref. [118], \triangle , ∇ from Figs. 5 and 7 of Ref. [238]; and \odot [119]. For the octagons, the vertical error bars are SDs of measurements from at least three different rods; the horizontal error bars are SDs of the intensities over which measurements were pooled. The smooth curves through the data are empirical and serve to illustrate the main trends of the data. In panel A, the curve through the calcium-clamped data has the formula $F = \exp(-I/I_0)$, with $I_0 = 7$ photoisomerizations s^{-1} , and the curve drawn through the Ringer's data in panel A has the form $F = I'/(I' + I'_0)$, with $I'_0 = 425$, $n = 0.7$. In panel B, the curve near the filled triangles has the same equation as that through the corresponding data in panel A, while the curve near Ringer's data is given by Weber's Law, $S_F/S_F^D = I/(I + I_0)$, with $I_0 = 40$ photoisomerizations s^{-1} ; the 'corrected' curve was obtained by dividing Weber's Law by the smooth curve through the Ringer's data in panel A.

8.2. Role of calcium

One idea that has pervaded the literature on light adaptation is that the reduction in calcium concentration *causes* the decline in flash sensitivity, but this simplistic idea does not survive rigorous examination. Figure 11A illustrates that when changes in $[Ca^{2+}]_i$ are prevented, the rod is driven into saturation at intensities of about 50 photoisomerizations s^{-1} , and Fig. 11B shows that when this occurs the cell's sensitivity is drastically attenuated. Thus, in the absence of changes in calcium concentration, the cell's sensitivity is reduced enormously. In contrast, when the cell's calcium concentration is free to change, saturation does not occur at such low intensities and the cell instead desensitizes in a gradual manner with increasing light intensity. From this perspective it is more reasonable to take the view that the normal decline in $[Ca^{2+}]_i$ *rescues* the cell from saturation, and prevents its sensitivity from being annihilated at low backgrounds, thereby extending the operating range (to nearly 10,000 photoisomerizations s^{-1} in Fig. 11). In other words, the decline in $[Ca^{2+}]_i$ does not actually *cause* the desensitization – rather, it tends to do exactly the opposite.

This viewpoint also makes it clear that mechanisms that extend the cell's range of operating intensities need not necessarily reduce its sensitivity, although conversely mechanisms that directly reduce the sensitivity are almost certain to extend the operating range. With this distinction between extension of operating range and reduction of gain in mind, it is useful to analyze the individual mechanisms underlying light adaptation. Accordingly, Table 5 gathers together current hypotheses about the molecular mechanisms underlying light adaptation, and considers the explicit effect of each mechanism on (i) the operating range, and (ii) the sensitivity, of phototransduction [119,222]. In addition it specifies (iii) whether the mechanism is directly activated by the decline in $[Ca^{2+}]_i$.

8.3. Analysis of individual mechanisms underlying light adaptation

We shall now consider the nine potential mechanisms of light adaptation listed in Table 5, in the order of the proteins underlying the effects. We begin with one that does not involve any particular protein.

8.3.1. Response compression (row 1 of Table 5)

As a consequence of the partial closure of cGMP-activated channels during steady illumination, the circulating current available for modulation by an incremental flash is reduced. In order to 'correct' for this reduction, so as to uncover the state of the transduction mechanism, it turns out that one simply needs to normalize the circulating current $J(t)$ with respect to its value J_0 in the steady state prior to the flash [65].

The basis for this statement may be seen most readily in the case of calcium clamping. Section 5.5 showed that the *fractional* change in cGMP concentration should be independent of the initial cGMP level. Thus, Eq. (18) showed that for a given driving function $\Delta\beta(t)$ the normalized solution $cG(t)/cG_0$ will be independent of cG_0 , or of any other aspect of the adaptational state. Hence, in the absence of any

adaptational process other than output compression, the normalized current response, $r(t) = 1 - F(t)$, at early times after a flash of constant intensity should be independent of background intensity (Eq. (23)).

In Fig. 11B the correction has been applied to the curve (rather than to the raw data points). Accordingly the broken curve reveals the component of sensitivity reduction that must be accounted for through biochemical mechanisms distinct from compression. In the next subsection we instead apply the normalization to the raw responses.

8.3.2. Reduction in the intrinsic gain of R^* (row 2 of Table 5)

It has been hypothesized that a component of the light-induced decrease in flash sensitivity might result from a lowering of the 'gain' with which R^* produces G^* s [243]; i.e. from a reduction in v_{RG} in Eq. (4). The characteristic feature of such a reduction in R^* gain (as distinct from a reduction in R^* lifetime) is that it will be manifest at the very earliest times in the light response. Compelling evidence against an effect of this kind has recently been reported in salamander rods, for light adaptation that produces up to two-thirds suppression of the circulating current [119,222]. Thus, when response families are normalized to the steady circulating current (as described in the previous paragraphs), the activation phase of the response to a given flash is found to be independent of background intensity. Fig. 12 illustrates this invariance in the case of dim flashes: it shows that the early phase of the normalized dim flash response is independent of background. From this analysis it has recently been concluded that none of the factors that contribute to the amplification constant in Eq. (26) are decreased by light adaptation, and specifically that the R^* 'gain' is unaltered [119]; this conclusion contrasts with the interpretations of other recent work [73,74,209,243,244].

Figure 12 additionally reveals two further important results. First, it shows that the simple 'activation only' model of Eq. (25) provides a good description of the kinetics of the onset phase of the dim-flash responses, for background intensities that suppress up to two-thirds of the dark current. Second, it reveals one manifestation of the conclusion to be presented in the next paragraph: that the lifetime of one or more of the steps in phototransduction is reduced in the presence of an adapting light.

8.3.3. Reduction in the lifetime of R^* (row 3 of Table 5)

A substantial body of physiological evidence supports the conclusion that the lifetime of one or more of the disc-associated intermediates in amphibian rod phototransduction is shortened by light adaptation, and that this shortening is calcium-dependent [65,73,168,241,245,246]. In addition, there is evidence that the period of calcium-sensitivity is quite short, so that the effect disappears with a time constant of ca. 0.5 s [245,246]. The prime candidate for the intermediate whose lifetime is shortened by the decline in $[Ca^{2+}]$ is R^* itself [36,65,120,245,246].

There are three lines of evidence supporting this identification. First, biochemical experiments have shown that the activity of RK, the enzyme that initiates the inactivation of R^* , is modulated by the calcium-binding protein Rec, as indicated

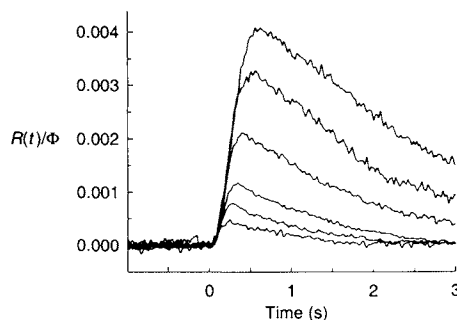


Fig. 12. Normalized dim-flash responses of a salamander rod in the presence of different backgrounds. The topmost trace was obtained in the dark, and successive traces in the presence of steady illumination producing 16, 50, 157, 500 and 1570 photoisomerizations s^{-1} . Each trace is the average of 3–5 individual responses, and was obtained from the raw response $r(t)$ by first dividing by the maximum response (i.e. the circulating current magnitude), to obtain $R(t) = r(t)/r_{\max}$; this was then divided by the number of photoisomerizations produced by the flash, Φ , to obtain normalized response per photoisomerization. The corresponding circulating currents and raw sensitivities (i.e. not normalized by the circulating current) were plotted in Fig. 11 as \odot . The smooth curve through the rising phase of the responses was computed with the pure activation model of Eq. (25), with amplification constant $A = 0.06 s^{-2}$, and delay $t_{\text{eff}} = 55$ ms. The good fit of this curve to the initial portion of all the responses is consistent with the idea that the gain of the activation reactions is not changed by light adaptation. Data from Ref. [119].

schematically in Fig. 4B; see Section 6.1. Thus, there exists a mechanism by which the R^* lifetime could be shortened in a calcium-dependent manner. Second, there is clear biochemical evidence that the inactivation of the G^*-E^* complex is *not* calcium-sensitive [248] (Section 6.2). Third, the ‘dominant’ or rate-limiting step in the inactivation of the disc-associated reactions *in situ* has also been shown to be insensitive to light adaptation and to changes in calcium [120,142,167]. The latter observations support the identification of the dominant time constant of inactivation with shut-off of the G^*-E^* complex, and consequently they indicate that the R^* lifetime is ‘non-dominant’ (i.e., short). This conclusion fits neatly, both with the idea that R^* lifetime is modulated by calcium concentration, and with experimental results, because alteration of the non-dominant lifetime will not affect the kinetics of recovery (as measured in ‘Pepperberg plots’ [167]), but will instead primarily appear to alter the sensitivity of the response, measured at the peak. Similarly, it will not affect the early rising phase of the response, provided that this is measured at sufficiently early times. (For a different view of the dominant inactivation time constant of amphibian rods, see Refs. [35,167], where the case is argued that R^* activity in amphibian rods decays with a time constant of ca. 2 s.)

The hypothesized connection between R^* lifetime and recoverin level can be formulated through the equation $\tau_R \propto 1/RK_{\text{free}}$, where RK_{free} is the concentration of RK without Rec bound to it. This molecular description, when coupled with the reaction scheme for recoverin’s interaction with calcium and RK [85,249], has been shown [222] to provide a good account of the observed acceleration of the bright-

Table 5
Mechanisms of photoreceptor light adaptation

Mechanism/hypothesis (as background increases)	Protein mediating the effect	Predicted effect on operating range	Predicted effect on 'cascade' sensitivity	Predicted effect on 'electrical' sensitivity	Ca ²⁺ involvement	Identity of regulatory Ca ²⁺ -binding protein	Comment	Refs.
1 Response compression (fewer channels open)	—	Reduces	No effect	Decreases	No	—	Saturation causes drastic decline in S _f	[59,234, 237,242]
2 Decrease in R* catalytic gain	R*	Extends	Decreases	Increases			Can be rejected; see text	[243,244]
3 Decrease in R* lifetime (τ_R)	RK	Extends	Decreases	Increases	Yes	Recoverin	Accelerates recovery	[36,54,65, 136,168, 241,245, 246]
4 Increase in steady-state cGMP hydrolysis rate constant (β_0)	PDE	Reduces	No effect	Decreases	No	—	Principal Ca ²⁺ - independent factor	[118,142]
5 Steady increase in cGMP synthesis rate (α_0)	GC	Extends	No effect	Increases	Yes	GCAP1,2	Restores circulating current	[81,93,118, 121,136, 217,231]
6 Transient increase in cGMP synthesis rate ($\Delta\alpha(t)$)	GC	Slightly increases	No effect	Slightly decreases	Yes	GCAP1,2	Accelerates recovery	[142]
7 Decrease in K_{eq} of channels	Channel	Extends	No effect	Increases	Yes	Calmodulin	Restores circulating current	[94,213-216, 218,247]
8 Increase in Ca ²⁺ buffering (B_{Ca}) of cytoplasm	Recoverin	Slightly decreases	No effect	Slightly increases	Yes	Recoverin	Results from decrease in Rec-2Ca	[119,222]
9 Pigment bleaching	Cone photo- pigment	Extends	Decreases	May increase or decrease	No	—	Incapacitates rods, yet underlies much cone light adaptation	[226]

Note: The column 'cascade sensitivity' refers to the sensitivity of the biochemical cascade, as PDE activity per incident photon. The column 'electrical sensitivity' refers to the overall sensitivity of the photoreceptor, in units of electrical response per incident photon, which is plotted as S_f in Fig. 11.

flash response that is elicited by a preceding step of light (the so-called ‘step/flash’ protocol [241]). This molecular model also explains the absence of the step/flash effect in mice lacking Rec [54].

8.3.4. Increase in β_0 , the steady cGMP hydrolytic rate constant (row 4 of Table 5)
Until recently it had not been appreciated that the steady-state level of phosphodiesterase activity might play a major role in the desensitization and acceleration of the response that accompanies background illumination. In the presence of steady background illumination generating E^* activated catalytic subunits of PDE, the enzymatic activity of the PDE is defined by the hydrolytic rate constant $\beta_0 = E^* \beta_{\text{sub}} + \beta_{\text{dark}}$, the steady-state equivalent of Eq. (12). As we discussed in Section 7.5, the reciprocal of β_0 acts as one of the three time constants contributing to recovery of the dim-flash response [142]. In the case of clamped calcium, it is straightforward to show that an increase in β_0 should shorten the time-to-peak and decrease the flash sensitivity S_F . Although the analysis is more complicated when $[Ca^{2+}]_i$ is free to change, the same prediction is found to hold [142]. Furthermore, calculations and simulations employing measured values of the transduction parameters show that the increase in β_0 with steady illumination is the single most important factor in decreasing the flash sensitivity [222]. It is worth emphasizing that this effect of elevated β_0 is not caused by the decline in $[Ca^{2+}]_i$, i.e., is not a calcium-mediated mechanism.

Bath-tub analogy. This situation can be appreciated in qualitative terms by considering an analogy, which is a qualitative description of the behavior of Eq. (16), the general rate equation governing free cGMP in the outer segment. Imagine a bath-tub, with water running in from a tap (the cyclase) at a fixed rate, and with water draining out through the plug-hole (the PDE) at a rate proportional to the depth of water (the cGMP concentration). When a steady-state is reached, the depth of water will equal the rate of influx (α_0) divided by the rate constant of efflux (β_0); i.e., $cG_0 = \alpha_0 / \beta_0$. Now imagine that a second plug-hole is briefly opened and then closed, causing a transient increment in the rate of efflux ($\Delta\beta(t)$). This will elicit a transient drop in water level ($\Delta cG(t)$) and eventual recovery to the original steady level.

Next, as an analogy with the application of a steady background illumination, imagine that the size of the plug-hole is enlarged (increased β_0), and in addition that the tap is turned on harder so as to increase the steady influx of water (increased α_0). If the two parameters were increased in the same ratio, then the steady-state depth of water would be unchanged. Finally, imagine that the same incremental stimulus is given as previously – the transient opening of a second plug-hole. This stimulus will now cause a smaller drop in water level than previously, together with a faster recovery; in fact the initial rate of drop in water level will be the same as previously, but recovery will occur more rapidly. In general terms, the effect of enlarging the plug-hole will be to accelerate the rate at which the water level re-equilibrates whenever it is perturbed, whereas the effect of opening up the tap will simply be to scale-up the depth of the water. Hence, if one expresses the depth of water relative to its original resting level (i.e., $cG(t)/cG_0$) the result will be independent of how rapidly (α_0) the water is flowing in from the tap (provided that this rate is constant). And

one can show from analysis of Eq. (16) that the kinetic shape of the response corresponds to the convolution of the driving function ($\Delta\beta(t)$) with the exponential time constant of equilibration ($1/\beta_0$).

A final point worth drawing from the bathtub analogy concerns the condition when the bathtub is empty. Then, the effect of having different sized plug-holes completely disappears. This condition parallels that when a bright flash is given and the rod response is driven into saturation: this happens when β/α_{\max} is very large, so that $cG(t)$ is driven too low to hold any channels open. The steady cGMP hydrolysis rate constant β_0 only has an effect on the rod's response kinetics when a finite level of cGMP is present.

8.3.5. Guanylyl cyclase: Steady-state increase in activity (row 5 of Table 5)

Perhaps the most thoroughly investigated molecular mechanism of photoreceptor light adaptation is the activation of guanylyl cyclase that is brought about by the decline in $[Ca^{2+}]_i$ accompanying the steady-state light response (Section 7.4). From Eqs. (14) and (22) one can readily derive the steady-state relationship

$$\frac{J_0}{J_{\text{dark}}} = \left[\frac{\alpha_0/\beta_0}{\alpha_{\text{dark}}/\beta_{\text{dark}}} \right]^{n_{\text{cG}}} = \left[\frac{\alpha_0/\alpha_{\text{dark}}}{\beta_0/\beta_{\text{dark}}} \right]^{n_{\text{cG}}} \quad (34)$$

which would apply exactly in the absence of any effect of calcium on the cGMP-gated channels. From this relationship two conclusions follow. First, in the absence of GC activation, an x -fold increase in PDE activity β_0 would cause the circulating current to decrease by $x^{n_{\text{cG}}}$; thus a quadrupling of β_0 would decrease the current to just 1/64 of its previous level, for $n_{\text{cG}} = 3$. Secondly, in the face of such an x -fold increase in PDE activity, the original circulating current could be completely restored through an x -fold increase in GC activity, α_0 . Many studies have shown that, when Ca^{2+} drops, GC can be activated to at least 10-times its basal level by GCAPs (Section 7.4). In salamander rods the level of PDE activity that drives the cell into saturation corresponds roughly to a 20-fold increase over the dark level ($\beta_0 \approx 20 \text{ s}^{-1}$ [222]; see Fig. 11C). Together these findings are consistent with the view that a substantial component of range extension in salamander rods is mediated by the activation of GC, but that this mechanism of extension is exhausted beyond a ca. 10-fold activation, as discussed previously [121,217]. Finally, as indicated in Table 5, it is important to note that by rescuing the transduction mechanism from saturation, the elevation of steady cyclase activity has the effect of *increasing* the photoreceptor's sensitivity from the level that would apply in the absence of this mechanism.

8.3.6. Guanylyl cyclase: Transient increment in activity (row 6 of Table 5)

During the normal flash response, $[Ca^{2+}]_i$ declines transiently, and causes a transient increase $\Delta\alpha(t)$ in GC activity. Paradoxically, this transient activation of cyclase has an effect on sensitivity opposite to that of the steady activation, described in the previous paragraph. Thus, the transient flash-induced increment in cyclase activity accelerates the recovery of the flash response and thereby *reduces* the sensitivity

measured at the peak (cf. Fig. 9C). On the other hand, this transient mechanism has relatively little effect on the *shape* of the sensitivity vs background relation, because the desensitizing effect (relative to the calcium-clamped condition) is about the same magnitude, independent of background intensity. This may be seen in Fig. 11C, where the decline of sensitivity under calcium-clamped conditions (symbols) closely parallels the normal decline [237].

8.3.7. Calmodulin effect on channels (row 7 of Table 5)

A second well understood mechanism of range-extension is the calmodulin-dependent shift in the K_{cG} of the cyclic nucleotide gated channels (Section 6.5); however, the contribution of this mechanism to the overall range extension in rods is far less than the contribution of the activation of GC [217]. Indeed, for primate rods, the range extension has been modeled in terms of GC activation alone [231]. For amphibian rods, where the range extension by decline in $[Ca^{2+}]_i$ is greater, the behavior has been modeled with a combination of GC activation, a CM-dependent shift in the K_{cG} of the channels, and a third mechanism, identified as a reduction in the average number of phosphodiesterase catalytic subunits (E^*) activated per photo-excited rhodopsin (R^*) at higher background intensities [136,217]. A candidate molecular mechanism for this third effect is the regulation of rhodopsin kinase by Rec, as discussed previously.

In cones, it appears that the modulation of the K_{cG} of the channels is much larger than in rods [218], and this no doubt contributes to the much larger operating range of cones [56,226]. Therefore it is possible that cones may have retained more prominently a feature of the progenitor cell of photoreceptors and olfactory neurons, since olfactory receptor cells also display a very large calmodulin-dependent modulation of the K_{\downarrow} of their cyclic nucleotide-gated channels [117].

8.3.8. Increased calcium buffering (row 8 of Table 5)

Calcium buffering acts to slow the transient decrease in $[Ca^{2+}]_i$ that accompanies the light response, and in doing so it retards the transient increase in GC activation discussed in Section 8.3.6, and thereby delays recovery and increases the peak response amplitude (and thus the flash sensitivity). As noted earlier (Section 6.1) it appears likely that the primary calcium buffer in rods is recoverin, with a concentration in excess of 30 μM . Analysis of the binding of Ca^{2+} to recoverin shows that, as $[Ca^{2+}]_i$ declines with increasing steady illumination, the free concentration of recoverin (Rec_{free}) will increase, and that over an intermediate range of calcium concentrations the calcium buffering power will also increase. An interesting feature of buffering by Rec is that, because of its cooperative binding of calcium, it is effective over a narrower range of calcium concentrations than a buffer with a single, non-cooperative binding site (compare Eqs. (7), (8)). We calculate that the incremental buffering power for calcium reaches its maximum when $[Ca^{2+}]_i$ drops to 100 nM, and that this peak is at least 3-fold higher than the buffering power in darkness [222]. This increase in buffering power will increase the rod's flash sensitivity relative to that which would be calculated if the buffering were independent of $[Ca^{2+}]_i$.

8.3.9. *Pigment bleaching in cones (row 9 of Table 5)*

Rod photoreceptors are substantially desensitized by bleached pigment, even (in the case of cells isolated from the retinal pigment epithelium) after long periods in darkness; reviewed in Refs. [250,251]. In contrast, cone photoreceptors can function almost normally with substantial fractions of their pigment in the bleached state – i.e., in the absence 11-*cis* retinal bound to their opsin (see Fig. 1B of Ref. [226]).

By avoiding saturation up to the bleaching range of intensities, cones are guaranteed to achieve Weber Law behavior at all higher levels (even though these levels may rarely be encountered). In the steady-state, the amount of pigment remaining unbleached at very high intensities is inversely proportional to the incident intensity, provided that the regeneration rate is unchanged [252]. Furthermore, the rate of photon capture is directly proportional to the amount remaining unbleached. Accordingly, the number of photoisomerizations elicited by a flash of fixed intensity superimposed on the background will be inversely proportional to background intensity, so that in the ‘large bleach’ regime the cone’s flash sensitivity will obey Weber’s Law purely through reduced quantal catch.

8.4. Summary

Some useful general conclusions can be drawn from our analysis of light adaptation, by reviewing Table 5. Increasing steady illumination is known or hypothesized (column 1) to affect the activity of proteins throughout the transduction cascade (column 2). To fully understand the mechanisms, one must consider their effects on both the overall operating range of the cell (column 3), and on its biochemical sensitivity (column 4) and on its electrical sensitivity (column 5). In many cases, the actions are caused by the decline in $[Ca^{2+}]_i$ (column 6) that accompanies steady illumination, and are mediated by specific calcium-binding proteins (column 7). However, Table 5 shows that no general rule applies to the mechanisms underlying adaptation. Indeed, perhaps the most important conclusion from the analysis is that there is no universal relationship between the effect of an adaptational mechanism on operating range and its effect on flash sensitivity. Another important conclusion is that the two dominant mechanisms in desensitization of the rod, response compression (row 1) and elevated cGMP hydrolysis rate constant (row 4), are not caused by the decline in $[Ca^{2+}]_i$ [222].

9. Single-photon responses: Implications of observed variability

We now turn to one of the most perplexing problems in the history of rod physiology: that of understanding the molecular mechanisms governing the single-photon response. This problem is no mere curiosity, since, as discussed at the beginning of Section 8, the ability of rods to generate reliable responses to single photons is a defining characteristic. We have saved this problem for last, because its analysis and discussion necessarily require prior analysis of the mechanisms of response activation and inactivation. Moreover, a notable feature of a long series (or ensemble) of single-photon responses is their similarity in shape and, as we shall discuss,

the mechanisms underlying this reproducibility are likely to include those we have examined in the context of light adaptation.

9.1. Reproducibility: Ensemble behavior

A number of investigations have reported that rod responses to single-photon are highly reproducible in amplitude and shape. The reproducibility of the amplitude has been characterized by the coefficient of variation ($cv = s.d. / \text{mean}$) of the response amplitude; in five separate studies of two species the cv of the amplitude (measured at the time-to-peak of the mean response) has been reported to be about 0.2 [34–36,38,253]. In four of these studies it was reported that the shapes of the individual responses were very similar to the shape of the mean response.

These results have been difficult to reconcile with the presumption that the inactivation of R^* is likely to be triggered by a single molecular event (phosphorylation of a single residue), since this would suggest that shut-off should be inherently stochastic. The apparent contradiction has led to the suggestion that a series of undiscovered intra-molecular processes must occur, to 'smooth' the decline of activity of an individual R^* [35]. However, a recent paper has presented compelling evidence that the variability in kinetics is considerably greater than previously reported, in a way that appears compatible with stochastic shut-off of R^* triggered by a single molecular event [36].

A sample set of single-photon responses from a toad rod is illustrated in Fig. 13A; the traces show 50 consecutive responses to very dim flashes (delivering on average less than 1 photoisomerization per trial). At the bottom of the panel a group of 'failures' is clearly separated from a group of presumed 'singleton' events that (as a group) have peak amplitudes of a little under 2 pA: these events are in turn separated from four larger events that are presumed to represent multiple photon hits. The amplitude histogram measured at the time-to-peak of the mean response (1.9 s) is plotted in Fig. 13B, for the complete set of 350 trials delivered to the cell. This histogram closely resembles the form reported in all such studies, with a failures peak clearly evident at 0 pA, and with a broader peak (near 1.8 pA in this cell) that presumably represents singletons.

One of the main lines of evidence supporting the notion that the shape of the single-photon response is stereotypical has come from comparison of the shape of the variance, $\sigma^2(t)$, with the shape of the squared mean, $\mu^2(t)$, of the ensemble of responses [34,35,38,253]. This comparison is made in Fig. 13C. Up to well beyond the peak (until about 3 s), the shape of $\sigma^2(t)$ is indistinguishable from the shape of a suitably scaled version of $\mu^2(t)$.

However, it turns out that this finding does not provide evidence that the single-photon responses all have the same underlying shape. Although analysis of the Poisson distribution (of photon hits) indicates that if the shapes of the single-photon responses were all identical, then the ensemble variance would have the same time course as the squared ensemble mean, the converse cannot be concluded; namely, that a match between the ensemble variance and the mean squared response implies identity of shape of the individual responses. Instead, for very dim flashes, it can be

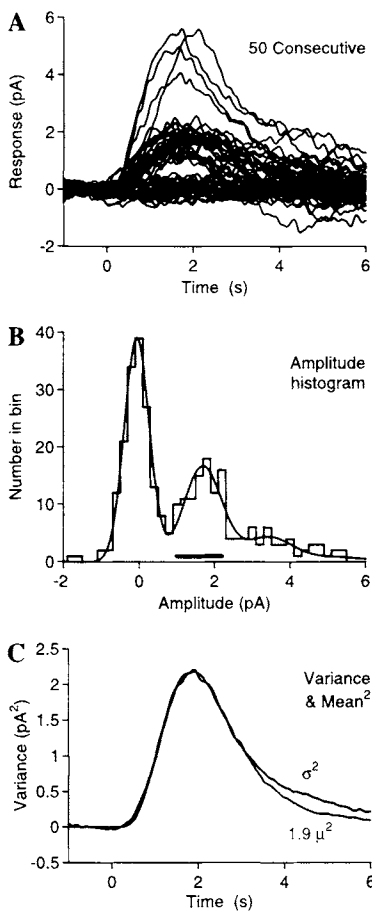


Fig. 13. Suction electrode recordings from a toad rod stimulated with a series of 350 very dim flashes, in the 'single photon' range. In each trial a brief flash was presented at time zero, delivering $0.08 \text{ photons } \mu\text{m}^{-2}$, estimated to cause about 0.6 photoisomerizations on average. (A) Sample of 50 consecutive responses from the 350 trials. Note that the responses separate fairly clearly into: failures, singletons, and multiple-photon responses. (B) Amplitude histogram for the complete set of 350 responses, determined at the time-to-peak of the average response, $t_{\text{peak}} = 1.9 \text{ s}$. The curve is the 'sum of Gaussians' expression from Eq. (10) of Ref. [34], with: $\Phi = 0.65$; mean single-photon response amplitude, $a = 1.75 \text{ pA}$; standard deviation of the failures, $\sigma_0 = 0.33 \text{ pA}$; additional standard deviation of the singletons, $\sigma_1 = 0.38 \text{ pA}$. Horizontal bar shows the range of amplitudes taken as conventional singletons. (C) Ensemble variance, $\sigma^2(t)$, for the complete set of 350 responses, compared with a scaled version of the square of the mean response, $\mu^2(t)$. Modified from Fig. 1 of Ref. [36].

shown that the ensemble variance will be dominated by the fact that the responses divide into 'failures' on the one hand and 'singletons' or 'multiples' on the other. The resulting component of the ensemble variance, which will have the time course of the mean squared response, is likely to swamp the component of variance contributed by variations between individual singleton responses.

9.2. Variability of the individual singletons

Rather than attempting to apply an ensemble test, there would be much to be gained by examining the individual responses. Although visual inspection of Fig. 13A might lead one to think that individual singleton events are broadly similar in shape, the problem is that individual variations are obscured by the process of superimposing the traces. In their recent study, Whitlock and Lamb [36] suspected that fluctuations in the amplitude of the individual responses might have been camouflaging fluctuations in kinetics in Fig. 13A. To try to avoid fluctuations in the underlying amplification, they selected (from the complete set of 85 singletons recorded in this experiment) the 40 responses that initially rose along a time-course most closely resembling the rise of the mean response. These 40 selected traces are superimposed in Fig. 14A, where they have been color-coded into five groups according to their amplitude at a later time (4 s); this color-coding has been introduced as an aid to visualization of inter-trace variability at later times. Although the individual singleton traces rise broadly along a common curve (because they have been selected to do so), they exhibit widely different behavior at later times. Thus, some traces reach peak much later than others, and in doing so they attain larger amplitudes and take considerably longer to achieve final recovery. Because of the significant level of recording noise in the individual traces, the authors averaged the colored groups of responses, to generate the traces in Fig. 14B; this panel confirms the general properties that can be seen in the raw traces in Fig. 14A.

In order to test the possibility that the recorded traces might have arisen from stochastic shut-off of R^* , the authors developed a simplified model of the response kinetics that would be expected if R^* activity were 'all-or-nothing' rather than graded. (To do this they used the model developed in the Section 7, with $\tau_R = \infty$, and they calculated the response to a step 'on' minus the response to a delayed step 'off'.) By least-squares fitting of this model to the raw traces, they extracted the R^* lifetimes that provided the best fit for each individual singleton response, and the distribution of these extracted lifetimes is plotted in Fig. 14C. The lifetimes extracted in this way ranged from less than 0.8 s to more than 2.5 s for the illustrated cell, with a mean of 1.7 s and a coefficient of variation of 0.4 – much larger than the coefficient of variation for the kinetics of 0.2 reported previously [35].

9.3. Implications of the observed variability

The first conclusion of this analysis was that, despite the close similarity in form of the ensemble variance and squared mean responses, the individual singleton responses exhibit marked variations in kinetics. Furthermore, the time-course of the individual responses appears in no way inconsistent with the occurrence of an all-or-nothing lifetime for R^* . Nevertheless the degree of variability in kinetics (with $cv \approx 0.4$) was smaller than expected on the simplest models of stochastic R^* lifetime [35,254].

In an attempt to account for the extracted distribution of presumed R^* lifetimes, and to account for the results of other experiments with calcium buffering, Whitlock and Lamb [36] proposed a molecular model incorporating three main features: (1)

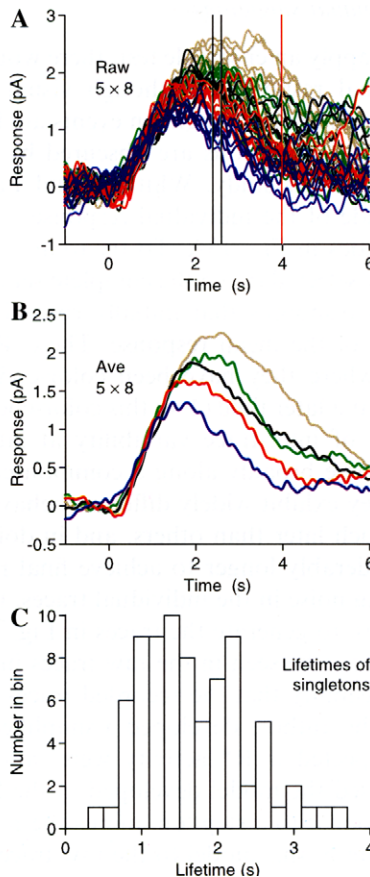


Fig. 14. Variability of the recovery kinetics of singleton responses. (A) Forty selected singleton responses. From the 350 trials in Fig. 13, the forty responses that most closely matched the early rising phase of the mean singleton response have been selected. In this particular selection, responses exhibiting spontaneous thermal isomerizations have automatically been eliminated, by the selection of only those traces that were well described by a theoretical model of the recovery phase; see Ref. [36] for details. Purely as a visual aid, the selected raw responses have been color-coded into 5 groups of 8, according to their amplitude over the indicated time window (2.5 ± 0.1 s). (B) Averages of the 5 groups of colored raw responses from A. (C) Distribution of extracted lifetimes, t_{lifetime} , of the singletons, when a stochastic model of R^* shut-off was applied to the individual singleton responses, over the time interval up to 4 s indicated by the vertical red line in A. Note that the extracted lifetimes range from less than 1 s to more than 2.5 s. Modified from Fig. 2 of Ref. [36].

all-or-nothing activity of R^* ; (2) feedback modulation of R^* lifetime, via Ca^{2+} , through the binding of Rec-2Ca to RK; and (3) the longitudinal diffusion of cGMP and Ca^{2+} in the outer segment. The second feature is critical, because it serves to change the rate of encounters of R^* with RK in a calcium-dependent manner (as

described in Section 8). Initially, when $[Ca^{2+}]_i$ is high, most RRs are bound to Rec, so that very few RRs are capable of interacting with R^* . As the response proceeds, and $[Ca^{2+}]_i$ declines, Rec dissociates and more and more RRs become available to interact; thus the rate constant of R^* shut-off increases steadily as the response proceeds, in a manner that is cooperatively dependent on $[Ca^{2+}]_i$. The third feature, which has not been incorporated into any previous models of rod photoresponses, also appears important, because calculations and measurements suggest that the decline in $[Ca^{2+}]_i$ may be highly localized spatially [133,134]. As a result the magnitude of the change in $[Ca^{2+}]_i$ at the disc where the single R^* was activated could be many-fold greater than the average change over the whole outer segment. It was estimated that, in response to a single photoisomerization, $[Ca^{2+}]_i$ at the site of photon absorption could drop to one-third of its resting value within 2 s; a change as great as this might well be sufficient to trigger a massive rise in the rate of R^* shut-off.

While the proposed molecular scheme is not yet proven (and is likely to undergo refinement), it points towards a resolution of one of the most perplexing issues in the history of rod phototransduction – how the shut-off of a single R^* molecule could be stochastic, yet could lead to kinetic variability ($cv \approx 0.4$) far lower than expected on models with fixed parameters.

References

1. Scott, K., Becker, A., Sun, Y., Hardy, R. and Zuker, C. (1995) *Neuron* **15**, 919–927.
2. Gold, G.H. (1999) *Ann. Rev. Physiol.* **61**, 857–871.
3. Mombaerts, P. (1999) *Ann. Rev. Neurosci.* **22**, 487–509.
4. Zufall, F. and Leinders-Zufall, T. (1998) *Ann. N. Y. Acad. Sci.* **855**, 199–204.
5. Krieger, J. and Breer, H. (1999) *Science* **286**, 720–723.
6. Huff, R.M. (1996) *Cell. Signal.* **8**, 453–459.
7. Lohse, M.J. (1996) *Zeit. Kardiol.* **85** Suppl 7, 1–3.
8. Strosberg, A.D. (1997) *Ann. Rev. Pharmacol.* **37**, 421–450.
9. Doupnik, C.A., Davidson, N., Lester, H.A. and Kofuji, P. (1997) *Proc. Natl Acad. Sci. USA* **94**, 10461–10466.
10. Catterall, W.A. (1997) *Adv. Second Mess. Phosphoprot. Res.* **31**, 159–181.
11. Ikeda, S.R. and Dunlap, K. (1999) *Adv. Second Mess. Phosphoprot. Res.* **33**, 131–151.
12. GCRDb G Protein Receptor Database. http://www.gcrdb.uthscsa.edu/GCR_Fam.html.
13. SwiftEMBL. <http://swift.embl-heidelberg.de/7tm>.
14. Buck, L. and Axel, R. (1991) *Cell* **65**, 175–187.
15. Skoufos, E., Marenco, L., Healy, M.D., Singer, M.S., Nadkarni, P.M., Miller, P.L. and Shepherd, G.S. The Olfactory Receptor Database. <http://ycmi.med.yale.edu/senselab/ORDB/>.
16. Bourne, H., Sanders, D. and McCormick, F. (1991) *Nature* **349**, 117–126.
17. Sondek, J., Lambright, D., Noel, J., Hamm, H.E. and Sigler, P. (1994) *Nature* **372**, 276–279.
18. Lambright, D., Noel, J., Hamm, H.E. and Sigler, P. (1994) *Nature* **369**, 621–628.
19. Coleman, D., Berghuis, A., Lee, E., Linder, M., Gilman, A. and Sprang, S. (1994) *Science* **265**, 1405–1412.
20. Mixon, M., Lee, E., Coleman, D., Berghuis, A., Gilman, A. and Sprang, S. (1995) *Science* **270**, 954–960.
21. Wall, M., Coleman, D., Lee, E., Iniguez-Lluhi, J., Posner, B., Gilman, A. and Sprang, S. (1995) *Cell* **83**, 1047–1058.
22. Sondek, J., Bohm, A., Lambright, D., Hamm, H.E. and Sigler, P. (1996) *Nature* **379**, 369–374.

23. Sprang, S. (1997) *Annu. Rev. Biochem.* **66**, 639–678.
24. Hamm, H.E. (1998) *J. Biol. Chem.* **273**, 669–672.
25. Liri, T., Farfel, Z. and Bourne, H. (1998) *Nature* **394**, 35–38.
26. Lamb, T.D. and Pugh, E.N. Jr (1992) *J. Physiol.* **449**, 719–758.
27. Pugh, E.N. Jr and Lamb, T.D. (1993) *Biochim. Biophys. Acta* **1141**, 111–149.
28. Snyder, A.W. and Menzel, R. (1975) *Photoreceptor Optics*. Springer, Berlin.
29. Enoch, J.M. and Tobey, F.L. (1981) *Vertebrate Photoreceptor Optics*. Springer, Berlin.
30. Stiles, W.S. and Crawford, B.H. (1933) *Proc. Roy. Soc. B* **113**, 496–530.
31. Stiles, W.S. (1939) *Proc. Roy. Soc. B* **127**, 64–105.
32. Harosi, F.I. and Mallerba, F.E. (1975) *Vision Res.* **15**, 379–388.
33. Lieberman, P.A. (1972) in: *Photochemistry of Vision*, Vol. VII, ed H.J.A. Dartnall. pp. 481–528. Springer, New York.
34. Baylor, D.A., Lamb, T.D. and Yau, K.-W. (1979) *J. Physiol.* **288**, 613–634.
35. Rieke, F. and Baylor, D.A. (1998) *Biophys. J.* **75**, 1836–1857.
36. Whitlock, G.G. and Lamb, T.D. (1999) *Neuron* **23**, 337–351.
37. Aho, A.C., Donner, K., Helenius, S., Larsen, L.O. and Reuter, T. (1993) *J. Comp. Physiol. A* **172**, 671–682.
38. Baylor, D.A., Nunn, B.J. and Schnapf, J.L. (1984) *J. Physiol.* **357**, 575–607.
39. Chen, J., Makino, C.L., Peachey, N.S., Baylor, D.A. and Simon, M.I. (1995) *Science* **267**, 374–377.
40. Xu, J., Dodd, R.L., Makino, C.L., Simon, M.I., Baylor, D.A. and Chen, J. (1997) *Nature* **389**, 505–509.
41. Lagnado, L. and McNaughton, P.A. (1990) *J. Memb. Biol.* **113**, 177–191.
42. Schnetkamp, P.P. (1995) *Cell Calcium* **18**, 322–330.
43. Schnetkamp, P.P. (1989) *Prog. Biophys. Molec. Biol.* **54**, 1–29.
44. Molday, R.S. and Molday, L.L. (1993) *Methods Neurosci.* **15**, 131–150.
45. Finn, J.T., Grunwald, M.E. and Yau, K.-W. (1996) *Ann. Rev. Physiol.* **58**, 395–426.
46. Molday, R.S. and Kaupp, U.B. (2000) in: *Handbook of Biological Physics*, Vol. 3, eds D.G. Stavenga, W.J. DeGrip and E.N. Pugh Jr. pp. 143–181, Elsevier, Amsterdam.
47. Nakatani, K. and Yau, K.-W. (1988) *J. Physiol.* **395**, 695–729.
48. Baylor, D.A. and Nunn, B.J. (1986) *J. Physiol.* **371**, 115–145.
49. Cobbs, W.H. and Pugh, E.N. Jr (1987) *J. Physiol.* **394**, 529–572.
50. Miller, J.L. and Korenbrot, J.I. (1994) *J. Gen. Physiol.* **104**, 909–940.
51. Baylor, D.A., Lamb, T.D. and Yau, K.-W. (1979) *J. Physiol.* **288**, 589–611.
52. Schneeweis, D.M. and Schnapf, J.L. (1995) *Science* **268**, 1053–1056.
53. Kraft, T.W., Schneeweis, D.M. and Schnapf, J.L. (1993) *J. Physiol.* **464**, 747–765.
54. Dodd, R.L. (1998) The role of arrestin and recoverin in signal transduction by retinal rod photoreceptors. Ph.D. thesis. Stanford University.
55. Hestrin, S. and Korenbrot, J.I. (1990) *J. Neurosci.* **10**, 1967–1973.
56. Matthews, H.R., Fain, G.L., Murphy, R.L.W. and Lamb, T.D. (1990) *J. Physiol.* **420**, 447–469.
57. Perry, R.J. and McNaughton, P.A. (1991) *J. Physiol.* **433**, 561–587.
58. Baylor, D.A. and Hodgkin, A.L. (1973) *J. Physiol.* **234**, 163–198.
59. Baylor, D.A., Hodgkin, A.L. and Lamb, T.D. (1974) *J. Physiol.* **242**, 685–727.
60. Baylor, D.A. and Fettiplace, R. (1975) *J. Physiol.* **248**, 433–464.
61. von Greef, R. (1902) *A Guide to Microscopic Examination of the Eye*. Blackiston, Philadelphia.
62. Miller, W.H. and Snyder, A.W. (1973) *Vision Res.* **13**, 2185–2194.
63. Schnapf, J.L., Nunn, B.J., Meister, M. and Baylor, D.A. (1990) *J. Physiol.* **427**, 681–713.
64. Schneeweis, D.M. and Schnapf, J.L. (1999) *J. Neurosci.* **19**, 1203–1216.
65. Torre, V., Matthews, H.R. and Lamb, T.D. (1986) *Proc. Natl Acad. Sci. USA* **83**, 7109–7113.
66. Hodgkin, A.L. (1971) *Proc. Roy. Soc. A* **326**, v–xx.
67. Ratto, G.M., Payne, R., Owen, W.G. and Tsien, R.Y. (1988) *J. Neurosci.* **8**, 3240–3246.
68. McCarthy, S.T., Younger, J.P. and Owen, W.G. (1994) *Biophys. J.* **67**, 2076–2089.
69. Korenbrot, J.I. and Miller, D.L. (1989) *Vision Res.* **29**, 939–948.
70. Lagnado, L., Cervetto, L. and McNaughton, P.A. (1992) *J. Physiol.* **455**, 111–142.

71. Sampath, A.P., Matthews, H.R., Cornwall, M.C. and Fain, G.L. (1998) *J. Gen. Physiol.* **111**, 53–64.
72. Sampath, A.P., Matthews, H.R., Cornwall, M.C., Bandarchi, J. and Fain, G.L. (1999) *J. Gen. Physiol.* **113**, 267–277.
73. Gray-Keller, M.P. and Detwiler, P.B. (1994) *Neuron* **13**, 849–861.
74. Detwiler, P.B. and Gray-Keller, M.P. (1996) *Curr. Opin. Neurobiol.* **6**, 440–444.
75. Unger, V.M., Hargrave, P.A., Baldwin, J.M. and Schertler, G.F. (1997) *Nature* **389**, 203–206.
76. DeGrip, W.J. and Rothschild, K.J. (2000) in: *Handbook of Biological Physics*, Vol. 3, eds D.G. Stavenga, W.J. DeGrip and E.N. Pugh Jr. pp. 1–54. Elsevier, Amsterdam.
77. Mathies, R.A. and Lugtenburg, J. (2000) in: *Handbook of Biological Physics*, Vol. 3, eds D.G. Stavenga, W.J. DeGrip and E.N. Pugh Jr. pp. 55–90. Elsevier, Amsterdam.
78. Dumke, C., Arshavsky, V.Y., Calvert, P., Bownds, M. and Pugh, E.N. Jr. (1994) *J. Gen. Physiol.* **103**, 1071–1098.
79. Artemyev, N.O., Surendran, R., Lee, J.C. and Hamm, H.E. (1996) *J. Biol. Chem.* **271**, 25382–25388.
80. Shyjan, A.W., de Sauvage, F.J., Gillett, N.A., Goeddel, D.V. and Lowe, D.G. (1992) *Neuron* **9**, 727–737.
81. Pugh, E.N. Jr., Duda, T., Sitaramayya, A. and Sharma, R.K. (1997) *Biosci. Rep.* **17**, 429–473.
82. Yau, K.-W. and Baylor, D.A. (1989) *Ann. Rev. Neurosci.* **12**, 289–327.
83. Rispoli, G., Navangione, A. and Vellani, V. (1996) *Ann. N.Y. Acad. Sci.* **779**, 346–355.
84. Schwarzer, A., Kim, T.S.Y., Hagen, V., Molday, R.S. and Bauer, P.J. (1997) *Biochem.* **36**, 13667–13676.
85. Klenchin, V.A., Calvert, P.D. and Bownds, M.D. (1995) *J. Biol. Chem.* **270**, 16147–16152.
86. Granzin, J., Wilden, U., Choe, H.W., Labahn, J., Krafft, B. and Buldt, G. (1998) *Nature* **391**, 918–921.
87. Hirsch, J.A., Schubert, C., Gurevich, V.V. and Sigler, P.B. (1999) *Cell* **97**, 257–269.
88. Ames, J.B., Ishima, R., Tanaka, T., Gordon, J.I., Stryer, L. and Ikura, M. (1997) *Nature* **389**, 198–202.
89. Kawamura, S. (1994) *Neurosci. Res.* **20**, 293–298.
90. Kawamura, S., Kuwata, O., Yamada, M., Matsuda, S., Hisatomi, O. and Tokunaga, F. (1996) *J. Biol. Chem.* **271**, 21359–21364.
91. He, W., Cowan, C.W. and Wensel, T.G. (1998) *Neuron* **20**, 95–102.
92. Makino, E.R., Handy, J.W., Li, T. and Arshavsky, V.Y. (1999) *Proc. Natl Acad. Sci. USA* **96**, 1947–1952.
93. Polans, A., Baehr, W. and Palczewski, K. (1996) *Trends Neurosci.* **19**, 547–554.
94. Bauer, P.J. (1996) *J. Physiol.* **494**, 675–685.
95. Wilkins, J.F., Bitensky, M.W. and Willardson, B.M. (1996) *J. Biol. Chem.* **271**, 19232–19237.
96. Yokoyama, R. and Yokoyama, S. (2000) in: *Handbook of Biological Physics*, Vol. 3, eds D.G. Stavenga, W.J. DeGrip and E.N. Pugh Jr. pp. 257–296. Elsevier, Amsterdam.
97. Birge, R.R. (1990) *Biochim. Biophys. Acta* **1016**, 293–327.
98. Nathans, J. (1999) *Neuron* **24**, 299–312.
99. Ohguro, H., Fukada, Y., Takao, T., Shimonishi, Y., Yoshizawa, T. and Akino, T. (1991) *EMBO J.* **10**, 3669–3674.
100. Kokame, K., Fukada, Y., Yoshizawa, T., Takao, T. and Shimonishi, Y. (1992) *Nature* **359**, 749–752.
101. Bigay, J., Faurobert, E., Franco, M. and Chabre, M. (1994) *Biochem.* **33**, 14081–14090.
102. Fukada, Y., Matsuda, T., Kokame, K., Takao, T., Shimonishi, Y., Akino, T. and Yoshizawa, T. (1994) *J. Biol. Chem.* **269**, 5163–5170.
103. Hofmann, K.-P. (2000) in: *Handbook of Biological Physics*, Vol. 3, eds D.G. Stavenga, W.J. DeGrip and E.N. Pugh Jr. pp. 91–142. Elsevier, Amsterdam.
104. Hofmann, K.-P. (1986) *Photobiochem. Photobiophys.* **13**, 309–327.
105. Bornancin, F., Pfister, C. and Chabre, M. (1989) *Euro. J. Biochem.* **184**, 687–698.
106. Kahlert, M. and Hofmann, K.-P. (1991) *Biophys. J.* **59**, 375–386.
107. Stroop, S.D. and Beavo, J.A. (1992) *Adv. Second Mess. Phosphoprot. Res.* **25**, 55–71.
108. Catty, P. and Deterre, P. (1991) *Euro. J. Biochem.* **199**, 263–269.

109. Catty, P., Pfister, C., Bruckert, F. and Deterre, P. (1992) *J. Biol. Chem.* **267**, 19489–19493.
110. Lamb, T.D. (1994) *Biophys. J.* **67**, 1439–1454.
111. Beavo, J.A. (1995) *Physiol. Rev.* **75**, 725–748.
112. Fuortes, M.G.F. and Hodgkin, A.L. (1964) *J. Physiol.* **172**, 239–263.
113. Hagins, W.A. (1972) *Ann. Rev. Biophys. Bioeng.* **1**, 131–158.
114. Miller, W.H. (1981) *Current Topics in Membranes and Transport* **15**. Academic, New York.
115. Fesenko, E.E., Kolesnikov, S.S. and Lyubarsky, A.L. (1985) *Nature* **313**, 310–313.
116. Kaupp, U.B. (1995) *Curr. Opin. Neurobiol.* **5**, 434–442.
117. Yau, K.-W. and Chen, T.Y. (1995) in: *Ligand- and Voltage-Gated Ion Channels*, ed R.A. North. CRC Press, Boca Raton, FL, pp. 307–335.
118. Hodgkin, A.L. and Nunn, B.J. (1988) *J. Physiol.* **403**, 439–471.
119. Pugh, E.N. Jr, Nikonorov, S. and Lamb, T.D. (1999) *Curr. Opin. Neurobiol.* **9**, 410–418.
120. Lyubarsky, A.L., Nikonorov, S. and Pugh, E.N. Jr (1996) *J. Gen. Physiol.* **107**, 19–34.
121. Koutalos, Y., Nakatani, K., Tamura, T. and Yau, K.-W. (1995) *J. Gen. Physiol.* **106**, 863–890.
122. Calvert, P.D., Ho, T.W., LeFebvre, Y.M. and Arshavsky, V.Y. (1998) *J. Gen. Physiol.* **111**, 39–51.
123. Hofmann, K.-P. and Heck, M. (1996) *Biomemb.* **2A**, 141–198.
124. Baumann, C. (1978) *J. Physiol.* **279**, 71–80.
125. Penn, R. and Hagins, W.A. (1972) *Biophys. J.* **12**, 1073–1094.
126. Naqvi, K.R. (1974) *Chem. Phys. Lett.* **28**, 280–284.
127. Leskov, I.B., Klenchin, V.A., Handy, J.W., Whitlock, E.E., Govardovskii, V.I., Bownds, M.D., Lamb, T.D., Pugh, E.N. Jr and Arshavsky, V.Y. (2000) *Neuron* **27**, 1–20.
128. Lamb, T.D. “Walk”: A program for numerical simulation of activation in the G-protein cascade. <http://www.physiol.cam.ac.uk/staff/Lamb/Walk>.
129. Karpen, J.W., Zimmerman, A.L., Stryer, L. and Baylor, D.A. (1988) *Proc. Natl Acad. Sci. USA* **85**, 1287–1291.
130. Gillespie, P.G. and Beavo, J.A. (1989) *Proc. Natl Acad. Sci. USA* **86**, 4311–4315.
131. Pugh, E.N. Jr and Lamb, T.D. (1990) *Vision Res.* **30**, 1923–1948.
132. Cote, R.H. and Brunnock, M.A. (1993) *J. Biol. Chem.* **268**, 17190–17198.
133. Gray-Keller, M., Denk, W., Shraiman, B. and Detwiler, P.B. (1999) *J. Physiol.* **519**, 679–692.
134. Lamb, T.D., McNaughton, P.A. and Yau, K.-W. (1981) *J. Physiol.* **319**, 463–496.
135. Cameron, D.A. and Pugh, E.N. Jr (1990) *J. Physiol.* **430**, 419–439.
136. Koutalos, Y., Nakatani, K. and Yau, K.-W. (1995) *J. Gen. Physiol.* **106**, 891–921.
137. Ruiz, M.L., Brown, R.L., He, Y., Haley, T.L. and Karpen, J.W. (1999) *Biochem.* **38**, 10642–10648.
138. Breton, M.E., Schueller, A.W., Lamb, T.D. and Pugh, E.N. Jr (1994) *Invest. Ophthalmol. Vis. Sci.* **35**, 295–309.
139. Smith, N.P. and Lamb, T.D. (1997) *Vision Res.* **37**, 2943–2952.
140. Cideciyan, A.V. and Jacobson, S.G. (1996) *Vision Res.* **36**, 2609–2621.
141. Lyubarsky, A.L. and Pugh, E.N. Jr (1996) *J. Neurosci.* **16**, 563–571.
142. Nikonorov, S., Engheta, N. and Pugh, E.N. Jr (1998) *J. Gen. Physiol.* **111**, 7–37.
143. Hood, D.C. and Birch, D.G. (1990) *Vis. Neurosci.* **31**, 2070–2081.
144. Hood, D.C. and Birch, D.G. (1993) *Vision Res.* **33**, 1605–1618.
145. Pugh, E.N. Jr, Falsini, B. and Lyubarsky, A.L. (1998) in: *Photostasis and Related Phenomena*, eds T.P. Williams and A.B. Thistle, pp. 93–128. Plenum Press, New York.
146. Robson, J.G. and Frishman, L.J. (1998) *Doc. Ophthalmol.* **95**, 187–215.
147. Fersht, A. (1977) *Enzyme Structure and Mechanism*. W.H. Freeman, San Francisco.
148. Palczewski, K. and Benovic, J.L. (1991) *Trends Biochem. Sci.* **16**, 387–391.
149. Palczewski, K. (1997) *Euro. J. Biochem.* **248**, 261–269.
150. Zhao, X., Palczewski, K. and Ohguro, H. (1995) *Biophys. Chem.* **56**, 183–188.
151. Hurley, J.B., Spencer, M. and Niemi, G.A. (1998) *Vision Res.* **38**, 1341–1352.
152. Wilden, U., Hall, S.W. and Kuhn, H. (1986) *Proc. Natl Acad. Sci. USA* **83**, 1174–1178.
153. Palczewski, K., Rispoli, G. and Detwiler, P.B. (1992) *Neuron* **8**, 117–126.
154. Ohguro, H., Van Hooser, J.P., Milam, A.H. and Palczewski, K. (1995) *J. Biol. Chem.* **270**, 14259–14262.

155. Chen, C.-K., Burns, M.E., Spencer, M., Niemi, G.A., Chen, J., Hurley, J.B., Baylor, D.A. and Simon, M.I. (1999) Proc. Natl Acad. Sci. USA **96**, 3718–3722.
156. Kühn, H. (1978) Biochem. **17**, 4389–4395.
157. Palczewski, K. (1994) Protein Sci. **3**, 1355–1361.
158. Gurevich, V.V. (1998) J. Biol. Chem. **273**, 15501–15506.
159. Ames, J.B., Porumb, T., Tanaka, T., Ikura, M. and Stryer, L. (1995) J. Biol. Chem. **270**, 4526–4533.
160. Zozulya, S. and Stryer, L. (1992) Proc. Natl Acad. Sci. USA **89**, 11569–11573.
161. Ames, J.B., Tanaka, T., Stryer, L. and Ikura, M. (1996) Curr. Opin. Struct. Biol. **6**, 432–438.
162. Ames, J.B., Tanaka, T., Stryer, L. and Ikura, M. (1994) Biochem. **33**, 10743–10753.
163. Kawamura, S. (1993) Nature **362**, 855–857.
164. Chen, C.-K., Inglese, J., Lefkowitz, R.J. and Hurley, J.B. (1995) J. Biol. Chem. **270**, 1–7.
165. Fung, B.K., Hurley, J.B. and Stryer, L. (1981) Proc. Natl Acad. Sci. USA **78**, 152–156.
166. Fung, B.K. and Stryer, L. (1980) Proc. Natl Acad. Sci. USA **77**, 2500–2504.
167. Pepperberg, D.R., Jin, J. and Jones, G.J. (1994) Vis. Neurosci. **11**, 53–62.
168. Murnick, J.G. and Lamb, T.D. (1996) J. Physiol. **495**, 1–13.
169. Arshavsky, V.Y. and Bownds, M.D. (1992) Nature **357**, 416–417.
170. Arshavsky, V.Y., Dumke, C.L. and Bownds, M.D. (1992) J. Biol. Chem. **267**, 24501–24507.
171. Angleson, J.K. and Wensel, T.G. (1994) J. Biol. Chem. **269**, 16290–16296.
172. Angleson, J.K. and Wensel, T.G. (1993) Neuron **11**, 939–949.
173. Arshavsky, V.Y. and Pugh, E.N. Jr (1998) Neuron **20**, 11–14.
174. Lee, R.H., Brown, B.M. and Lolley, R.N. (1984) Biochem. **23**, 1972–1977.
175. Lee, R.H., Fowler, A., McGinnis, J.F., Lolley, R.N. and Craft, C.M. (1990) J. Biol. Chem. **265**, 15867–15873.
176. Lee, R.H., Lieberman, B.S. and Lolley, R.N. (1987) Biochem. **26**, 3983–3990.
177. Lee, R.H., Ting, T.D., Lieberman, B.S., Tobias, D.E., Lolley, R.N. and Ho, Y.K. (1992) J. Biol. Chem. **267**, 25104–25112.
178. Yoshida, T., Willardson, B.M., Wilkins, J.F., Jensen, G.J., Thornton, B.D. and Bitensky, M.W. (1994) J. Biol. Chem. **269**, 24050–24057.
179. Willardson, B.M., Wilkins, J.F., Yoshida, T. and Bitensky, M.W. (1996) Proc. Natl Acad. Sci. USA **93**, 1475–1479.
180. Muller, S., Straub, A., Schroder, S., Bauer, P.H. and Lohse, M.J. (1996) J. Biol. Chem. **271**, 11781–11786.
181. Lohse, M.J., Bluml, K., Danner, S. and Krasel, C. (1996) Biochem. Soc. Trans. **24**, 975–980.
182. Liu, X., Seno, K., Nishizawa, Y., Hayashi, F., Yamazaki, A., Matsumoto, H., Wakabayashi, T. and Usukura, J. (1994) Exp. Eye Res. **59**, 761–768.
183. Hisatomi, O., Honkawa, H., Imanishi, Y., Satoh, T. and Tokunaga, F. (1999) Biochem. Biophys. Res. Comm. **255**, 216–220.
184. Cooper, N., Liu, L., Yoshida, A., Pozdnyakov, N., Margulis, A. and Sitaramayya, A. (1996) J. Mol. Neurosci. **6**, 211–222.
185. Lowe, D.G., Dizhoor, A.M., Liu, K., Gu, Q., Spencer, M., Laura, R., Lu, L. and Hurley, J.B. (1995) Proc. Natl Acad. Sci. USA **92**, 5535–5539.
186. Yang, R.-B., Robinson, S.W., Xiong, W.H., Yau, K.-W., Birch, D.G. and Garbers, D.L. (1999) J. Neurosci. **19**, 5889–5897.
187. Paul, A.K., Marala, R.B., Jaiswal, R.K. and Sharma, R.K. (1987) Science **235**, 1224–1226.
188. Gorczyca, W.A., Gray-Keller, M.P., Detwiler, P.B. and Palczewski, K. (1994) Proc. Natl Acad. Sci. USA **91**, 4014–4018.
189. Gorczyca, W.A., Polans, A.S., Surgucheva, I.G., Subbaraya, I., Baehr, W. and Palczewski, K. (1995) J. Biol. Chem. **270**, 22029–22036.
190. Palczewski, K., Subbaraya, I., Gorczyca, W.A., Helekar, B.S., Ruiz, C.C., Ohguro, H., Huang, J., Zhao, X., Crabb, J.W. and Johnson, R.S. (1994) Neuron **13**, 395–404.
191. Dizhoor, A.M., Lowe, D.G., Olshevskaya, E.V., Laura, R.P. and Hurley, J.B. (1994) Neuron **12**, 1345–1352.

192. Dizhoor, A.M., Olshevskaya, E.V., Henzel, W.J., Wong, S.C., Stults, J.T., Ankoudinova, I. and Hurley, J.B. (1995) *J. Biol. Chem.* **270**, 25200–25206.
193. Duda, T., Goracznak, R.M., Pozdnyakov, N., Sitaramayya, A. and Sharma, R.K. (1998) *Biochem. Biophys. Res. Comm.* **242**, 118–122.
194. Krishnan, A., Goracznak, R.M., Duda, T. and Sharma, R.K. (1998) *Molec. Cell. Biochem.* **178**, 251–259.
195. Matthews, H.R., Fain, G.L. and Cornwall, M.C. (1996) *J. Physiol.* **490**, 293–303.
196. Otto-Bruc, A., Buczykko, J., Surgucheva, I., Subbaraya, I., Rudnicka-Nawrot, M., Crabb, J.W., Arendt, A., Hargrave, P.A., Baehr, W. and Palczewski, K. (1997) *Biochem.* **36**, 4295–4302.
197. Howes, K., Bronson, J.D., Dang, Y.L., Li, N., Zhang, K., Ruiz, C., Helekar, B., Lee, M., Subbaraya, I., Kolb, H., Chen, J. and Baehr, W. (1998) *Invest. Ophthalmol. Vis. Sci.* **39**, 867–875.
198. Yu, L. and Colvin, R.A. (1997) *Molec. Brain Res.* **50**, 285–292.
199. Kim, I., Koh, G.Y. and Lee, C.O. (1998) *Comp. Biochem. Physiol. B* **119**, 157–161.
200. Reeves, J.P. (1998) *J. Bioenerg. Biomemb.* **30**, 151–160.
201. Cook, O., Low, W. and Rahamimoff, H. (1998) *Biochim. Biophys. Acta* **1371**, 40–52.
202. Blaustein, M.P. and Lederer, W.J. (1999) *Physiol. Rev.* **79**, 763–854.
203. Cervetto, L., Lagnado, L., Perry, R.J., Robinson, D.W. and McNaughton, P.A. (1989) *Nature* **337**, 740–743.
204. Reilander, H., Achilles, A., Friedel, U., Maul, G., Lottspeich, F. and Cook, N.J. (1992) *EMBO J.* **11**, 1689–1695.
205. Tucker, J.E., Winkfein, R.J., Cooper, C.B. and Schnetkamp, P.P. (1998) *Invest. Ophthalmol. Vis. Sci.* **39**, 435–440.
206. Navanglone, A., Rispoli, G., Gabellini, N. and Carafoli, E. (1997) *Biophys. J.* **73**, 45–51.
207. Cooper, C.B., Winkfein, R.J., Szerencsei, R.T. and Schnetkamp, P.P. (1999) *Biochem.* **38**, 6276–6283.
208. Perry, R.J. and McNaughton, P.A. (1991) *Curr. Opin. Neurobiol.* **1**, 98–104.
209. Rispoli, G. (1998) *J. Photochem. Photobiol. B* **44**, 1–20.
210. Kohnken, R.E., Chafouleas, J.G., Eadie, D.M., Means, A.R. and McConnell, D.G. (1981) *J. Biol. Chem.* **256**, 12517–12522.
211. Nagao, S., Yamazaki, A. and Bitensky, M.W. (1987) *Biochem.* **26**, 1659–1665.
212. Huppertz, B., Weyand, I. and Bauer, P.J. (1990) *J. Biol. Chem.* **265**, 9470–9475.
213. Grunwald, M.E., Yu, W.P., Yu, H.H. and Yau, K.-W. (1998) *J. Biol. Chem.* **273**, 9148–9157.
214. Weitz, D., Zoche, M., Müller, F., Beyermann, M., Körschen, H.G., Kaupp, U.B. and Koch, K.W. (1998) *EMBO J.* **17**, 2273–2284.
215. Hsu, Y.T. and Molday, R.S. (1994) *J. Biol. Chem.* **269**, 29765–29770.
216. Hsu, Y.T. and Molday, R.S. (1993) *Nature* **361**, 76–79.
217. Koutalos, Y. and Yau, K.-W. (1996) *Trends Neurosci.* **19**, 73–81.
218. Rebrik, T.I. and Korenbrot, J.I. (1998) *J. Gen. Physiol.* **112**, 537–548.
219. Hilgemann, D.W., Nicoll, D.A. and Philipson, K.D. (1991) *Nature* **352**, 715–718.
220. Hodgkin, A.L. (1988) in: *Proceedings of the Retina Research Foundation*, ed D.M.K. Lam. Portfollio Publishing Co., pp. 6–30, The Woodlands, Texas.
221. McCarthy, S.T., Younger, J.P. and Owen, W.G. (1996) *J. Neurophysiol.* **76**, 1991–2004.
222. Nikonorov, S., Lamb, T.D. and Pugh, E.N. Jr (2000) *J. Gen. Physiol.*, in press.
223. Rodieck, R.W. (1998) *The First Steps in Seeing*. Sinauer, Sunderland.
224. Shevell, S.K. (1977) *Vision Res.* **17**, 427–434.
225. Finkelstein, M.A. and Hood, D.C. (1981) *Vision Res.* **21**, 319–328.
226. Burkhardt, D.A. (1994) *J. Neurosci.* **14**, 1091–1105.
227. Wässle, H. (1999) in: *Color Vision: From Genes to Perception*, eds K.R. Gegenfurtner and L.T. Sharpe. CUP, New York.
228. Matthews, H.R. (1991) *J. Physiol.* **436**, 93–105.
229. Tamura, T., Nakatani, K. and Yau, K.-W. (1989) *Science* **245**, 755–758.
230. Nakatani, K., Tamura, T. and Yau, K.-W. (1991) *J. Gen. Physiol.* **97**, 413–435.
231. Tamura, T., Nakatani, K. and Yau, K.-W. (1991) *J. Gen. Physiol.* **98**, 95–130.

232. Bownds, M.D. and Arshavsky, V.Y. (1995) *Behav. Brain Sci.* **18**, 415–424.
233. Perlman, I. and Normann, R.A. (1998) *Progr. Ret. Eye Res.* **17**, 523–563.
234. Baylor, D.A. and Hodgkin, A.L. (1974) *J. Physiol.* **242**, 729–758.
235. Fain, G.L. (1976) *J. Physiol.* **261**, 71–101.
236. Baylor, D.A., Matthews, G.G. and Yau, K.-W. (1980) *J. Physiol.* **309**, 591–621.
237. Matthews, H.R., Murphy, R.L.W., Fain, G.L. and Lamb, T.D. (1988) *Nature* **334**, 67–69.
238. Cornwall, M.C. and Fain, G.L. (1994) *J. Physiol.* **480**, 261–279.
239. Nakatani, K. and Yau, K.-W. (1988) *Nature* **334**, 69–71.
240. Nakatani, K. and Yau, K.-W. (1989) *J. Physiol.* **409**, 525–548.
241. Fain, G.L., Lamb, T.D., Matthews, H.R. and Murphy, R.L.W. (1989) *J. Physiol.* **416**, 215–243.
242. Dowling, J.E. and Ripps, H. (1970) *J. Gen. Physiol.* **56**, 491–520.
243. Lagnado, L. and Baylor, D.A. (1994) *Nature* **367**, 273–277.
244. Jones, G.J. (1995) *J. Physiol.* **487**, 441–451.
245. Matthews, H.R. (1996) *J. Physiol.* **490**, 1–15.
246. Matthews, H.R. (1997) *J. Gen. Physiol.* **109**, 141–146.
247. Chen, T.Y., Illing, M., Molday, L.L., Hsu, Y.T., Yau, K.-W. and Molday, R.S. (1994) *Proc. Natl Acad. Sci. USA* **91**, 11757–11761.
248. Arshavsky, V.Y., Gray-Keller, M.P. and Bownds, M.D. (1991) *J. Biol. Chem.* **266**, 18530–18537.
249. Erickson, M.A., Lagnado, L., Zozulya, S., Neubert, T.A., Stryer, L. and Baylor, D.A. (1998) *Proc. Natl Acad. Sci. USA* **95**, 6474–6479.
250. Fain, G.L., Matthews, H.R. and Cornwall, M.C. (1996) *Trends Neurosci.* **19**, 502–507.
251. Leibrock, C.S., Reuter, T. and Lamb, T.D. (1998) *Eye* **12**, 511–520.
252. Hollins, M. and Alpern, M. (1983) *J. Gen. Physiol.* **62**, 430–447.
253. Schnapf, J.L. (1983) *J. Physiol.* **343**, 147–159.
254. Baylor, D.A. (1996) *Proc. Natl Acad. Sci. USA* **90**, 560–565.